Technische Universität München
TUM School of Life Sciences

TUM

The role of gut microbiota in intestinal lipid absorption and systemic lipid metabolism

Johannes Plagge

Vollständiger Abdruck der von der TUM School of Life Sciences der Technischen Universität

München zur Erlangung eines

Doktors der Naturwissenschaften (Dr. rer. nat.)

genehmigten Dissertation.

Vorsitz: Prof. Dr. Dr. Li Deng

Prüfer*innen der Dissertation:

   1.   Priv.-Doz. Dr. Josef Ecker
   2.   Prof. Dr. Dirk Haller

Die Dissertation wurde am 21.12.2022 bei der Technischen Universität München eingereicht

und durch die TUM School of Life Sciences am 16.05.2023 angenommen.

Gewidmet allen, die mich auf meinem Weg unterstützt haben.

TABLE OF CONTENTS

LIST OF FIGURES

LIST OF TABLES

LIST OF ABBREVIATIONS

Abbreviation	Full name
ABCB4	ATP binding cassette B4 (synonym MDR2)
ABCB11	Bile salt export pump
AGR2	Anterior gradient protein 2 homolog
AIC	Akaike information criterion
AMP	Antimicrobial peptide
AMPK	AMP-activated protein kinase
APBDJ	Anomalous pancreaticobiliary ductal junction
apoA-IV	Apolipoprotein A-IV
apoB-48	Apolipoprotein B-48
apoC	Apolipoprotein C
apoE	Apolipoprotein E
ASBT	Apical sodium-dependent bile acid transporter
AUC	Area under the curve
BA	Bile acid
BAAT	Bile acid-CoA:amino acid N-acyltransferase
BAL	Bile salt-activated lipase (synonyms BSSL, CEL)
BSEP	Bile salt export pump
BSH	Bile salt hydrolase
BSSL	Bile salt stimulated lipase (synonyms BAL, CEL)
CCK	Cholecystokinin
CD36	Cluster of differentiation 36
CE	Cholesteryl ester
CEL	Carboxyl ester lipase (synonyms BAL, BSSL)
Cer	Ceramide
CFU	Colony-forming unit
CL	Cardiolipin
CM	Chylomicron
CMC	Critical micellar concentration
CONV	Conventionalized
CTα	CTP:phosphocholine cytidylyltransferase-α
CYP	Cytochrome P450
CYP27A1	Sterol 27-hydroxylase
CYP2A12	Steroid hormones 7-α-hydroxylase
CYP2C70	Cytochrome P450 2C70
CYP7A1	Cholesterol 7α-hydroxylase
CYP7B1	Cytochrome P450 7B1
CYP8B1	7-Alpha-hydroxycholest-4-en-3-one 12-alpha-hydroxylase
DG	Diglyceride
DIO	Diet-induced obesity
ELOVL6	Elongation of very long chain fatty acids protein 6
ER	Endoplasmic reticulum

Abbreviation	Full name
ERK	Extracellular-signal regulated kinase
eWAT	Epididymal white adipose tissue
FA	Fatty acid
FATP4	Fatty acid transport protein 4
FC	Free cholesterol
FFA	Free fatty acid
FFPE	Formalin fixed, paraffin embedded
FGF15	Fibroblast growth factor 15
FGFR4	FGF receptor 4
FIAF	Fasting-induced adipocyte factor
FXR	Farnesoid X receptor
GC-MS	Gas-chromatography coupled to mass spectrometry
GF	Germ-free
GIT	Gastrointestinal tract
GLP-1	Glucagon-like peptide-1
GLP-2	Glucagon-like peptide-2
GPBAR1	G-protein coupled bile acid receptor 1 (synonym TGR5)
GPR	G-protein coupled receptor
HDL	High density lipoproteins
HexCer	Hexosylceramide
HFD	High-fat diet
HYA	10-hydroxy-cis-12-octadecenoic acid
iBAT	Interscapular brown adipose tissue
IQR	Interquartile range
iWAT	Inguinal white adipose tissue
JNK	c-Jun N-terminal kinase
KO	Knock-out
LCFA	Long-chain fatty acid
LPC	Lysophosphatidylcholine
LPE	Lysophosphatidylethanolamine
LPL	Lipoprotein lipase
LRH-1	Liver receptor homolog-1
MAG	Monoacylglycerol
MCA	Muricholic acid
MDR2	Multidrug resistance protein 2 (synonym ABCB4)
MSE	Mean squared error
MTP	Microsomal triglyceride transport protein
MUC2	Mucin-2
NPC1L1	Niemann-Pick C1-like protein 1
OASIS	Cyclic AMP-responsive element-binding protein 3-like protein 1
OMM	Oligo-Mouse-Microbiota
PAS-AB	Periodic acid schiff-alcian blue
PC	Phosphatidylcholine

Abbreviation	Full name
PC O	Phosphatidylcholine-ether
PE	Phosphatidylethanolamine
PE O	Phosphatidylethanolamine-ether
PG	Phosphatidylglycerol
PL	Phospholipid
PLA_1	Phospholipase A_1
PLA_2	Phospholipase A_2
PNLIP	Pancreatic lipase
PPARγ	Peroxisome proliferator-activated receptor γ
PUFA	Polyunsaturated fatty acid
PXR	Pregnane X receptor
SCFA	Short-chain fatty acid
SD	Standard deviation
SEM	Standard error of the mean
SHP	Small heterodimer partner
SI	Small intestine
SM	Sphingomyelin
SPF	Specific-pathogen-free
TFF3	Trefoil factor 3
TG/TAG	Triglyceride
TGR5	Takeda G protein-coupled receptor 5 (synonym GPBAR1)
VDR	Vitamin D receptor
WTD	Western-type diet

ABSTRACT

The gut microbiota is known to be a key regulator of human metabolism in health and disease. Dysbiosis, the disruption and imbalance of the gut microbiome, has been associated with the body's energy balance and the development of metabolic disorders but the impact of gut microbiota on lipid absorption from the nutrition has not yet been well defined. Stable isotope labeled tracers were used in gnotobiotic mouse models to reveal that the systemic uptake of dietary fat is depending on microbial colonization. Physiology-based kinetic modeling revealed that the gut microbiota reduced the uptake of dietary fat from the gut lumen into enterocytes.

By combining lipidomics and proteomics measurements, it was discovered that gut microbiota enhance phospholipase A_1 (PLA_1) activity in the bile by increasing taurocholic acid (TCA) levels. Thereby, they cause phosphatidylcholine (PC) degradation important for micelle formation and subsequently, suppressed intestinal lipid absorption. Proteomic measurements identified carboxyl ester lipase (CEL) as the enzyme responsible for PLA_1 activity in the bile.

Conclusively, this thesis unveiled a novel metabolic interplay between gut microbes and the host to reduce dietary lipid uptake. An enzymatic phospholipase activity in the bile mediates this process. A pharmacological intervention or manipulation of the microbiome to influence biliary glycerophospholipid metabolism might therefore offer a new approach to modulate dietary fat uptake.

ZUSAMMENFASSUNG

Die Darmmikrobiota ist bekannt als ein Schlüsselregulator des menschlichen Stoffwechsels im gesunden und kranken Zustand. Dysbiose, die Störung des Darmmikrobiomgleichgewichts, wurde mit Veränderungen im Energiehaushalt des Körpers und der Entwicklung von Stoffwechselstörungen in Verbindung gebracht. Der Einfluss der Darmmikrobiota auf die Lipidaufnahme aus der Nahrung ist aber noch nicht genau definiert. In gnotobiotischen Mausmodellen wurden mit stabilen Isotopen markierte Tracer verwendet, und es konnte in dieser Arbeit gezeigt werden, dass die systemische Aufnahme von Nahrungsfett von der mikrobiellen Besiedlung abhängt. Eine Physiologie-basierte kinetische Modellierung zeigte, dass die Darmmikrobiota die Aufnahme von Nahrungsfett aus dem Darmlumen in die Enterozyten reduzierte.

Durch die Kombination von Lipidomics- und Proteomics-Messungen wurde entdeckt, dass die Darmmikrobiota die Phospholipase A_1 (PLA_1) Aktivität in der Galle durch Erhöhung der Taurocholsäure-Konzentration (TCA) verstärkt. Dadurch bewirkt sie den Abbau von Phosphatidylcholin (PC), das für die Mizellenbildung wichtig ist, und unterdrückt in der Folge die intestinale Lipidaufnahme. Proteomische Messungen identifizierten die Carboxylesterlipase (CEL) als das Enzym, das für die PLA_1-Aktivität in der Galle verantwortlich ist.

In Summe deckte diese Arbeit ein neuartiges metabolisches Zusammenspiel zwischen dem Darmmikrobiom und dem Wirt zur Verringerung der Aufnahme von Nahrungsfetten auf. Dieser Prozess wird durch eine enzymatische Phospholipase-Aktivität in der Galle vermittelt. Eine pharmakologische Intervention oder eine Manipulation des Mikrobioms zur Beeinflussung des biliären Glycerophospholipid-Stoffwechsels könnte daher einen neuen Ansatz zur Beeinflussung der Aufnahme von Nahrungsfetten darstellen.

PUBLICATIONS AND PRESENTATIONS

JOURNAL PUBLICATIONS

Under preparation:

Plagge, J.*; Zimmermann-Kogadeeva, M.*; Höring, M.; Slack, E.; Heeren, J.; Zimmermann, M.; Giansanti, P.; Basic, M.; Weiss, A. S.; Seeliger, C.; Bleich, A.; Brunner, S.; Hidrobo, M.; Stecher, B.; Coleman, O. I.; Strohmeyer A.; Klingenspor, M.; Küster, B.; Janssen, K.-P.; Haller, D.; Burkhardt, R.; Kuipers, F.; Liebisch, G.; Ecker, J. The gut microbiota limits intestinal lipid absorption by induction of host phospholipase A1 activity in bile. Revised version under preparation at *Gastroenterology*.

* These authors contributed equally to this work.

Published:

Dawczynski, C*.; **Plagge, J.***; Jahreis, G.; Liebisch, G.; Höring, M.; Seeliger, C.; Ecker, J. (2022): Dietary PUFA Preferably Modify Ethanolamine-Containing Glycerophospholipids of the Human Plasma Lipidome. In *Nutrients* 14 (15). DOI: 10.3390/nu14153055.

* These authors contributed equally to this work.

Ecker, J.; Benedetti, E.; Kindt, A. S. D.; Höring, M.; Perl, M.; Machmüller, A. C.; Sichler, A.; **Plagge, J.**; Wang, Y.; Zeissig, S.; Shevchenko, A.; Burkhardt, R.; Krumsiek, J.; Liebisch, G.; Janssen, K.-P. (2021): The Colorectal Cancer Lipidome: Identification of a Robust Tumor-Specific Lipid Species Signature. In *Gastroenterology* 161 (3), 910-923.e19. DOI: 10.1053/j.gastro.2021.05.009.

Liebisch, G.; **Plagge, J.**; Höring, M.; Seeliger, C.; Ecker, J. (2021): The effect of gut microbiota on the intestinal lipidome of mice. In *International journal of medical microbiology : IJMM* 311 (3), p. 151488. DOI: 10.1016/j.ijmm.2021.151488.

Streidl, T.; Karkossa, I.; Segura Muñoz, R. R.; Eberl, C.; Zaufel, A.; **Plagge, J.**; Schmaltz, R.; Schubert, K.; Basic, M.; Schneider, K. M.; Afify, M.; Trautwein, C.; Tolba, R.; Stecher, B.; Doden, H. L.; Ridlon, J. M.; Ecker, J.; Moustafa, T.; Bergen, M. von; Ramer-Tait, A. E.; Clavel, T. (2021): The gut bacterium *Extibacter muris* produces secondary bile acids and influences liver physiology in gnotobiotic mice. In *Gut microbes* 13 (1), pp. 1–21. DOI: 10.1080/19490976.2020.1854008.

TALKS AND POSTER PRESENTATIONS

Plagge, J.; Zimmermann-Kogadeeva, M.; […]; Ecker, J. The gut microbiota reduces intestinal lipid absorption by induction of host phospholipase A1 activity in bile. Talk at the *62nd International Conference on the Bioscience of Lipids (ICBL)* 2022 in Montréal, Canada.

Plagge, J.; Zimmermann-Kogadeeva, M.; […]; Ecker, J. The gut microbiota inhibits intestinal lipid absorption. Talk at the *61st International Conference on the Bioscience of Lipids (ICBL)* 2021 in Utrecht, Netherlands.

Plagge, J.; Liebisch, G.; […]; Ecker, J. The role of gut microbiota in intestinal lipid absorption. Poster presentation at the *12th Seeon Conference on Microbiota, Probiotics and Host* 2019 in Seeon-Seebruck, Germany.

1. INTRODUCTION

Extensive research over the last two decades has highlighted the importance of the gut microbiome as a key regulator of human metabolism in both health and disease. Dysbiosis, the disruption of microbiota composition and reduction of its diversity, has been linked to the development of common metabolic disorders such as obesity, type 2 diabetes, non-alcoholic fatty liver disease (NAFLD), and cardiovascular disease (Fan and Pedersen 2021).

The World Health Organization (WHO 2021) states that 'the fundamental cause of obesity and overweight is an energy imbalance between calories consumed and calories expended'. More than 30% of total caloric intake in adult humans comes from dietary lipids mainly consisting of triglycerides (TG, 95% of dietary fat). They are a major energy source due to their high energy density (9 kcal/g for TG) (Gupta 2019). Dietary lipid absorption is very efficient, with more than 90% of the ingested fat being resorbed into enterocytes. However, large inter-individual differences are observed, with fat excretion in stool ranging from 1.3–5.4 g/day (Hartmann et al. 1993; Hussain et al. 1994). The microbiome could be an important factor explaining these variations and serve as an attractive target for the regulation of energy accumulation from dietary fat (Jumpertz et al. 2011).

Despite that, only few studies investigating the influence of gut microbiota on the dietary fat absorption process have been published, often with conflicting results (Rabot et al. 2010; Semova et al. 2012; Martinez-Guryn et al. 2018; Kindt et al. 2018; Araújo et al. 2020). A systematic investigation of dietary lipid uptake and *in vivo* flux in dependence of gut microbial status has been lacking so far. Using state of the art stable isotope lipid tracing technologies in combination with mass spectrometric lipidomic analyses, this thesis aims to further decipher the relationship between the gut microbiota and host lipid absorption.

1.1. DIETARY LIPIDS

1.1.1. Digestion of dietary lipids

The process of dietary lipid digestion begins in the mouth catalyzed by lingual lipase in the saliva and continues in the stomach, where gastric lipase is released from chief cells in the mucosa. Both lipases hydrolyze TG to release mainly diglycerides (DG) and free fatty acids (FFA) and prefer TG with medium to short-chain-length FA. While the actions of lingual and gastric lipase are essential for dietary lipid digestion in infants, in adults, only 20–30% of dietary lipids are hydrolyzed this way (He et al. 2020; Gupta 2019).

The majority of dietary lipids is digested and taken up in the small intestine (SI) via a multi-step process (Hussain 2014). Food intake triggers the release of the gut hormone cholecystokinin (CCK) from enteroendocrine cells in the proximal duodenum, thereby promoting, among other effects, gallbladder contractions (Shaffer 2000). The bile, which is secreted into the SI from the gallbladder, aids with the

digestion of lipids: Bile acids (BA), PL and cholesterol emulsify the lipids from the diet, drastically increasing the lipid-aqueous interface area. After their solubilization, lipids can be more easily accessed and broken down by lipases (Ko et al. 2020).

The pancreas produces a variety of lipolytic enzymes as well as alkaline secretions, which help to neutralize stomach acid and provide an optimal pH environment for lipolytic enzyme activity and lipid micelle formation. TG digestion in the SI is mainly accomplished by pancreatic triacylglycerol lipase (PNLIP), breaking down TG into free fatty acids (FFA) and monoacylglycerols (MAG). Dietary PL are hydrolyzed into lysophospholipids and FFA by Phospholipase A_2 (PLA$_2$) (Gupta 2019; Ko et al. 2020). The role and importance of a third lipolytic enzyme, carboxyl ester lipase (CEL), has been debated in the literature for several decades. CEL shows a broad substrate specificity and has therefore been documented with several alternative names in the literature over time. Synonyms include cholesterol esterase, bile salt-activated or stimulated lipase (BAL or BSSL respectively), and pancreatic lysophospholipase. CEL can cleave all three ester bonds from TG to release FFA and glycerol. It is also known to digest PL and cholesteryl esters (CE) but only the latter reaction is unique to this enzyme. Therefore, it is thought that CEL acts rather as a compensatory or supplementary enzyme for the digestion of TG and PL (Hui and Howles 2002).

Above the critical micellar concentration (CMC), bile acids form heterogeneous mixed micelles incorporating the digested dietary lipids. This allows them to cross the unstirred water layer to reach the brush border of enterocytes, where the lipids are taken up (Brannon et al. 2018). The BA are released from the mixed micelles and reabsorbed in the distal ileum, where they enter the enterohepatic circulation (Gupta 2019).

1.1.2. Absorption into enterocytes

Uptake of FFA into the enterocytes occurs by two distinct processes (Figure 1). Due to the initial concentration difference across the membrane, FFA can pass through enterocyte membranes via a flip-flop mechanism. They integrate into the outer leaflet of the membrane before randomly flipping to the inner side. There, the carboxyl group gets deprotonated, which prevents flopping back of the now negatively charged FA headgroup through the hydrophobic membrane. FFA diffuse out of the inner leaflet and will be rapidly re-esterified in the cells. This helps keeping the intracellular FFA concentration low and allows for a continuous uptake via diffusion (Brannon et al. 2018; Ko et al. 2020).

The second process is a carrier-mediated lipid uptake. Several putative FA transporters have been published and controversially discussed over the years (Glatz et al. 2010; Jay et al. 2020). Among those proteins discussed are fatty acid transport protein 4 (FATP4) as well as cluster of differentiation 36 (CD36). While FATP4 was initially suggested as a major intestinal FA transport protein (Stahl et al. 1999), it was since shown that FATP4 associates to the endoplasmic reticulum (ER) instead of the plasma membrane (Milger et al. 2006). *Fatp4* knock-out (KO) in mice also showed no impact on intestinal lipid uptake (Shim et al. 2009). CD36 is an integral membrane

protein highly expressed in the SI with a broad ligand specificity. It translocates long-chain FA across the enterocyte membrane but the exact mechanism is not understood (Brannon et al. 2018; Ko et al. 2020). *Cd36* KO mice not only show impaired lipid uptake but also defects in chylomicron assembly and secretion (Drover et al. 2005; Nauli et al. 2006; Nassir et al. 2007).

The uptake process of 2-MAG, released from dietary TG besides FFA, is not well studied. One *in vitro* study in Caco-2 cells suggests a protein mediated mechanism (Ho and Storch 2001) but a passive uptake via diffusion cannot be ruled out. Another possibility is the further hydrolysis of MAG by CEL, releasing the last FA to form glycerol (Hui and Howles 2002).

Finally, lysophospholipids are absorbed via passive diffusion (Ko et al. 2020) while cholesterol is transported via the Niemann-Pick C1-like protein 1 (NPC1L1) into enterocytes (Altmann et al. 2004).

1.1.3. Lipid secretion from enterocytes

Once in the enterocytes, the chain length determines the fate of absorbed dietary FA (Figure 1). Short-chain (and to a certain degree medium-chain) FA are polar enough to be transported in the bloodstream. They are secreted into the portal vein towards the liver, bound to albumin. Long-chain FA, as well as lysophospholipids and cholesterol are targeted towards the ER, where they are re-esterified and either stored in cytosolic lipid droplets or packaged into chylomicrons (CM) for secretion into the lymphatic system (Ko et al. 2020).

CM are lipoproteins with a monolayer membrane containing mainly phosphatidyl-choline (PC) and proteins and a core storing TG and cholesterol. A sufficient PC supply from bile and to a minor part the diet is essential for the formation of CM in enterocytes. Consequently, KO mice secreting no PC in their bile show impaired CM formation (Voshol et al. 2000). Besides uptake from the gut lumen, a secondary source of PC for CM membranes is from *de novo* synthesis in enterocytes by the enzyme CTP:phosphocholine cytidylyltransferase-α (CTα). Mice lacking this enzyme in enterocytes absorb dietary fat normally when fed a chow diet but have impaired uptake on a high-fat diet (HFD) (Kennelly et al. 2018).

Pre-CM assembly begins in the rough ER, where the microsomal triglyceride transport protein (MTP) catalyzes the transfer of lipids onto apolipoprotein B48 (apoB-48). The hydrophobic core is then expanded by the addition of more TG and CE and apoA-IV is integrated. Pre-CMs are transported to the Golgi where they are glycosylated and acquire another lipoprotein, apoA-I. Nascent chylomicrons are secreted into the lymphatic system and subsequently into the blood circulation, where they acquire two additional proteins from high density lipoproteins (HDL) (Ko et al. 2020; Brannon et al. 2018).
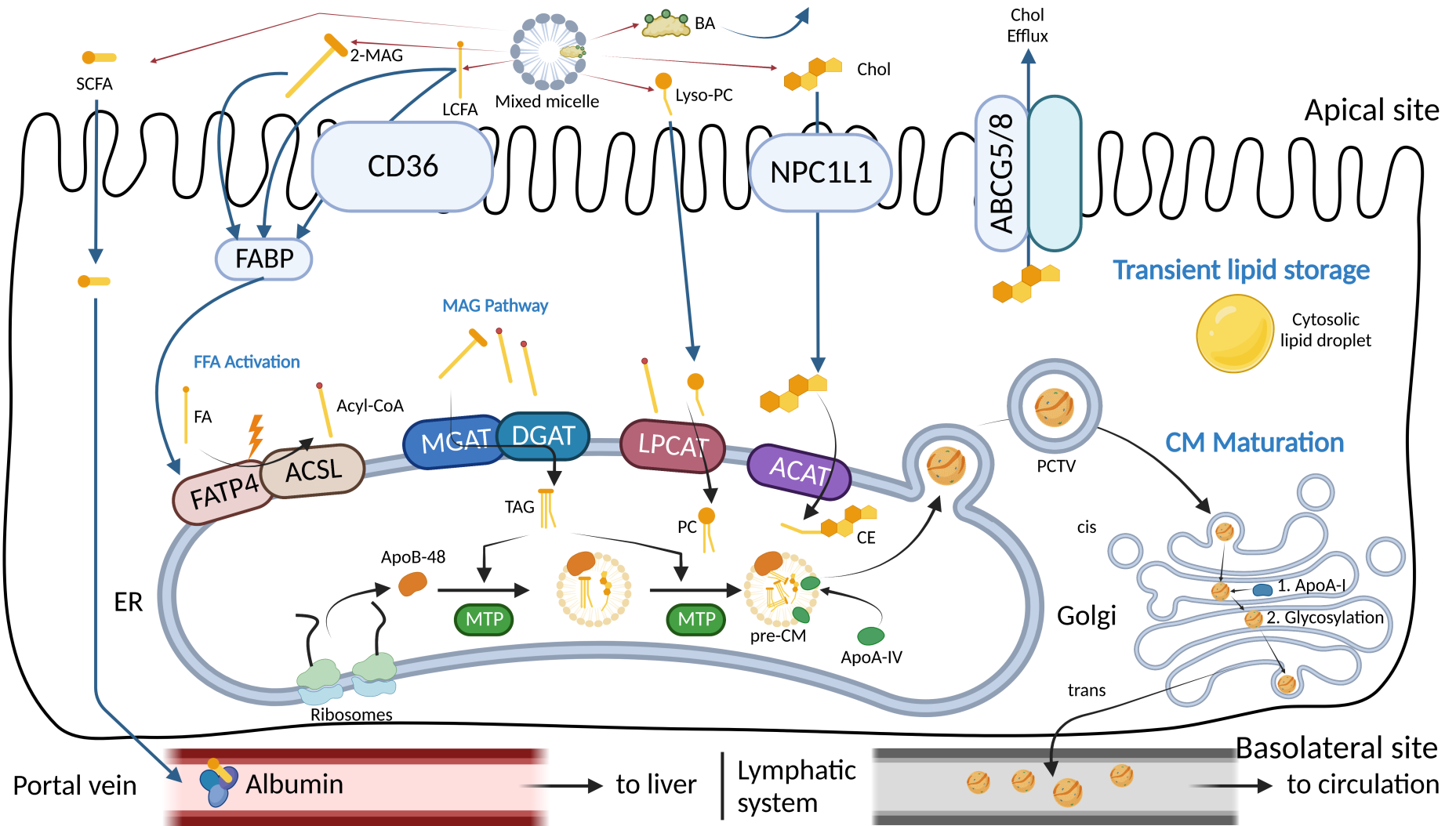
Figure 1.   Lipid uptake into enterocytes and distribution into the circulation

2-MAG: 2-Monoacylglycerol, ABCG5/8: ATP-binding cassette sub-family G member 5/8, ACAT: Acyl-coenzyme A:cholesterol acyltransferase, ACSL: Long-chain-fatty-acid--CoA ligase, Acyl-CoA: Acyl-Coenzyme A, ApoA-I: Apolipoprotein A-I, ApoA-IV: Apolipoprotein A-IV,

Figure 1 continued: ApoB-48: Apolipoprotein B-48, BA: Bile acid, CD36: Cluster of differentiation 36, CE: Cholesteryl ester, Chol: Cholesterol, CM: Chylomicron, DGAT: Diacylglycerol O-acyltransferase, ER: Endoplasmic reticulum, FA: Fatty acid, FABP: Fatty acid-binding protein, FATP4: Long-chain fatty acid transport protein 4, FFA: Free fatty acid, LCFA: Long-chain fatty acid, LPCAT: Lysophosphatidylcholine acyltransferase, Lyso-PC: Lysophosphatidylcholine, MAG: Monoacylglycerol, MGAT: Monoacylglycerol acyltransferase, MTP: Microsomal triglyceride transfer protein, NPC1L1: Niemann-Pick C1-like protein 1, PC: Phosphatidylcholine, PCTV: Pre-chylomicron transport vesicle, SCFA: Short-chain fatty acid, TAG: Triacylglycerol

Lipoprotein lipase (LPL) releases FFA from the chylomicrons for energy production or storage in various tissues. About 80% of the lipids in CMs are delivered to extrahepatic tissues. CM remnants are removed by the liver, where the remaining 20% of lipids end up. CM remnants are identified in the liver via receptors for apoE, the second lipoprotein which CM have obtained from HDL (Gupta 2019).

1.2. BILE ACIDS

1.2.1. General

Bile acids are amphipathic molecules which are synthesized in the liver from cholesterol and secreted with the bile into the SI. They serve several important roles in lipid metabolism.

First, they are crucial for the formation of mixed micelles in the SI to solubilize and aid with the digestion of dietary lipids (Aguiar Vallim et al. 2013).

Second, evidence from x-ray crystallography studies shows that bile salts bind to lipolytic digestive enzymes, altering their activity. Pancreatic PLA_2 binds BA such as CA, GCA, TCA and GCDCA, leading to both activation at low concentrations and inhibition at higher levels (Pan and Bahnson 2007). Carboxyl ester lipase (CEL) has two TCA binding sites, one close and one distal to the active site (Wang et al. 1997). The hydrolytic activity of CEL depends on bile salts, especially TCA (Fontbonne et al. 2011).

Third, they induce bile flow from hepatocytes into the canaliculi and the gallbladder (Aguiar Vallim et al. 2013).

Fourth, excess cholesterol is eliminated mainly via the conversion into BA and excretion in the feces, maintaining whole body sterol homeostasis. Besides their role in lipid metabolism, BA also activate several receptors, regulating not only their own synthesis but also whole body energy metabolism (Aguiar Vallim et al. 2013; Sayin et al. 2013; Wahlström et al. 2016).

1.2.2. Bile acid structure and synthesis

The bile acid structure is composed of four steroid rings with a convex hydrophobic face and a concave hydrophilic face with a varying number of hydroxyl groups. Their short carboxylic acid side chain can be conjugated to either glycine or taurine (Figure 2). The presence or absence and α/β-orientation of the hydroxyl groups influences both the solubility and hydrophobicity of the bile acids.
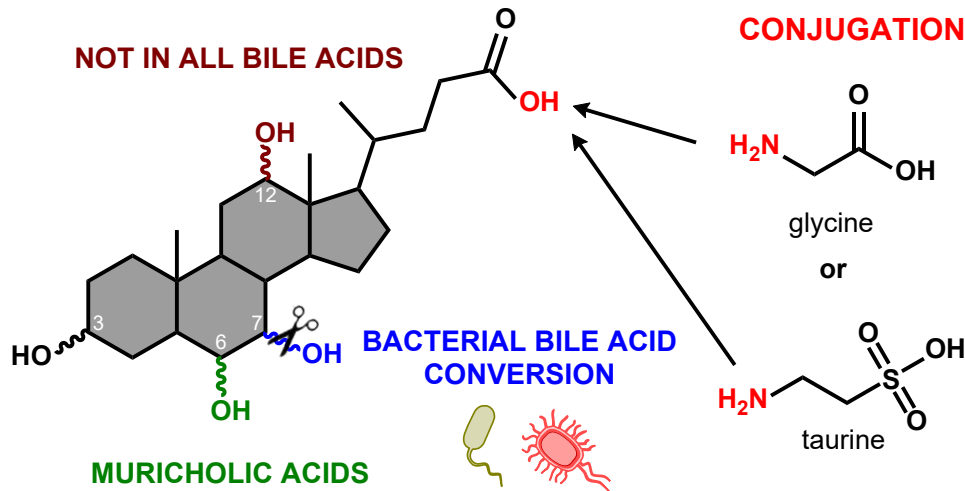
Figure 2.   General structure of bile acids
Bile acids are conjugated to either glycine or taurine. The α/β-position of the hydroxyl groups at C3, 6, 7 and 12 determines the type of bile acid. The stereochemistry of the BA structure has been simplified for better understanding.

Two pathways for BA synthesis in the liver exist: Around 75% of all BA in mice are synthesized via the classical pathway (Schwarz et al. 1996) which is initiated by the rate-limiting enzyme cholesterol 7α-hydroxylase (CYP7A1) (Figure 3). 7α-hydroxycholesterol is either converted to CDCA or CA, depending on the action of 7-α-hydroxycholest-4-en-3-one 12-α-hydroxylase (CYP8B1) to introduce the 12-hydroxy group. The alternative or acidic pathway produces CDCA and accounts for 25% of total BA synthesis in mice (Schwarz et al. 2001). It begins with cholesterol side chain oxidation by sterol-27-hydroxylase (CYP27A1) followed by oxysterol 7α-hydroxylase (CYP7B1) catalyzed steroid ring hydroxylation (Figure 3).

Primary BA profiles differ significantly between species. In humans, only CA and CDCA are synthesized in the liver, while mouse primary BA include CA and CDCA, as well as UDCA and the hydrophilic muricholic acids (MCA) (Aguiar Vallim et al. 2013). The enzyme CYP2C70 catalyzes the 6β-hydroxylation and 7α/β-epimerization to produce α–MCA and β-MCA (Figure 3) (Takahashi et al. 2016; Boer et al. 2020)

In the liver, Bile acid-CoA:amino acid N-acyltransferase (BAAT) conjugates BA to glycine or taurine in humans, while in mice, they are almost exclusively conjugated to taurine (Figure 3) (Li and Dawson 2019). Conjugation increases the BA solubility and reduces the pKa for improved micelle formation in the duodenum. Conjugated BA are then secreted into the canaliculi by bile salt export protein (BSEP, ABCB11) and stored in the gallbladder.
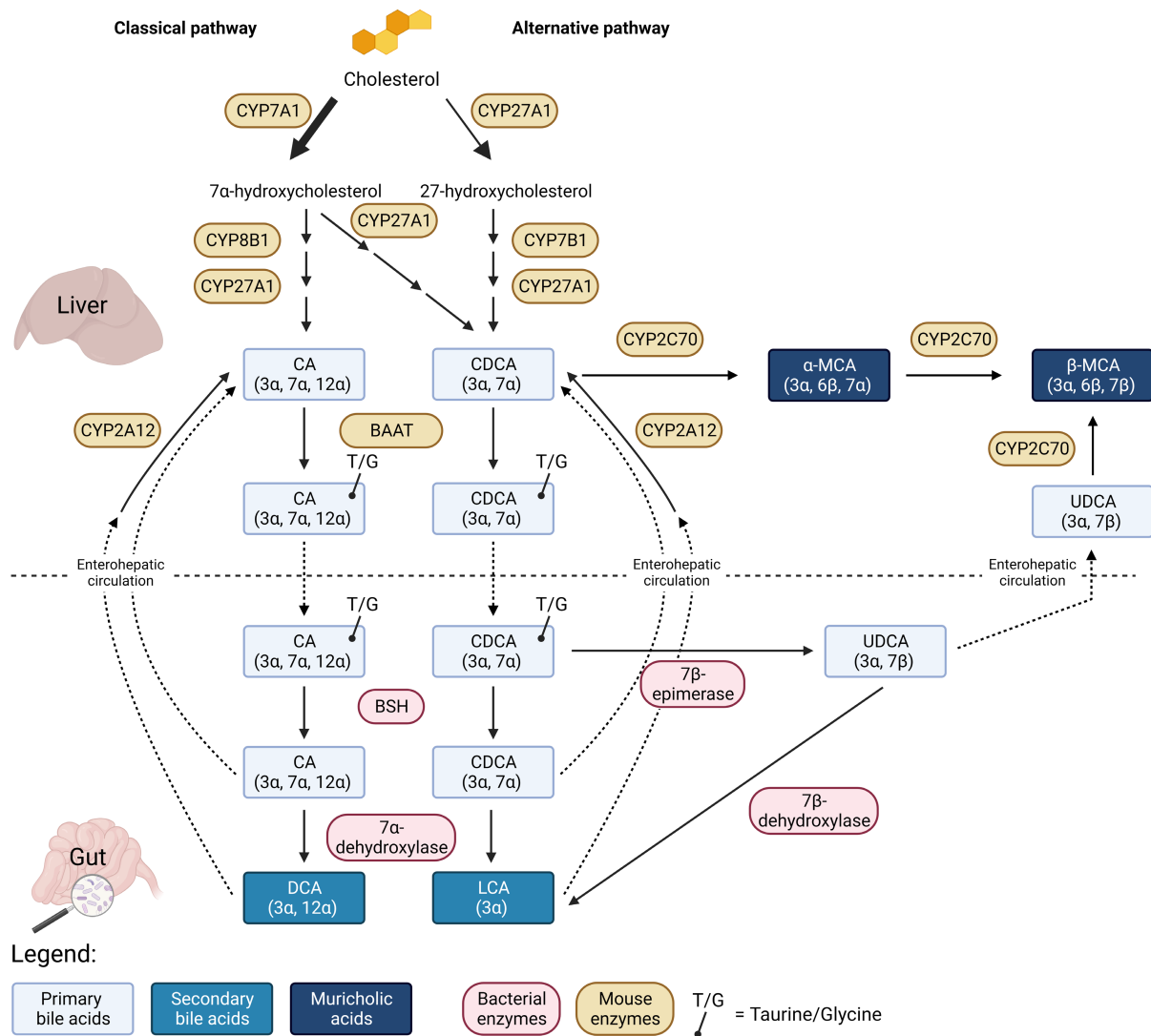
Figure 3.   Murine BA synthesis in the liver and bacterial metabolism in the gut
Only key enzymes for the synthesis of CA and CDCA from cholesterol are shown.
α-MCA: α-Muricholic acid, β-MCA: β-Muricholic acid, BAAT: Bile acid-CoA:amino acid N-acyltransferase, BSH: Bile salt hydrolase, CA: Cholic acid, CDCA: Chenodeoxycholic acid, CYP: Cytochrome P450, DCA: Deoxycholic acid, LCA: Lithocholic acid, UDCA: Ursodeoxycholic acid

1.2.3.   Metabolism of bile acids by the gut microbiota

After secretion of BA into the duodenum upon a meal ingestion, ~95% are reabsorbed in the distal ileum via the apical sodium-dependent bile acid transporter (ASBT) and returned to the liver. BA escaping reuptake into the enterohepatic circulation are deconjugated by bacterial bile salt hydrolases (BSH) and dehydroxylated at the C7 position to hydrophobic secondary BA such as DCA and LCA (Figure 3) (Aguiar Vallim et al. 2013). Other bacterial modifications include oxidation and epimerization of the 3-, 7-, and 12-hydroxy groups of BA (Ridlon et al. 2006). In mice, reabsorbed secondary BAs can be converted back to primary BAs by the action of steroid hormones 7-α-hydroxylase (CYP2A12), an enzyme which is not found in humans (Honda et al. 2020).

The absence of a gut microbiota in GF mice has more profound effects than just a lack of secondary BA: These mice have increased proportions of TβMCA and concomitantly reduced TCA levels in the liver and gallbladder bile, an overall larger BA pool, as well as enlarged gallbladders (Sayin et al. 2013). The microbiota impacts BA metabolism and synthesis via the nuclear farnesoid X receptor (FXR), downregulating key enzymes of BA synthesis such as CYP7A1 or CYP8B1 (Sayin et al. 2013; Claus et al. 2011; Li et al. 2013).

1.2.4. Bile acid signaling

BA activate three nuclear receptors, namely farnesoid X receptor (FXR), pregnane X receptor (PXR), vitamin D receptor (VDR), as well as the Takeda G protein-coupled receptor 5 (TGR5) (Aguiar Vallim et al. 2013). They thereby not only regulate their own synthesis and metabolism, but also impact whole body energy homeostasis (Wahlström et al. 2016).

Farnesoid X receptor (FXR)

BA synthesis is regulated via negative feedback inhibition through the transcription factor FXR (Sinal et al. 2000). Although found in several tissues, the expression of FXR is highest in the liver and ileum. BA activate FXR with different potencies with CDCA > DCA > LCA >> CA (Wang et al. 1999; Makishima et al. 1999; Parks et al. 1999). UDCA and MCAs were shown to rather act as FXR antagonists (Sayin et al. 2013; Mueller et al. 2015).

In the liver, FXR activation induces the expression of small heterodimer partner (SHP), binding to the liver receptor homolog-1 (LRH-1), and thereby, inhibition of *Cyp7a1* gene expression (Goodwin et al. 2000; Lu et al. 2000; Sinal et al. 2000). In the distal ileum, FXR activation by BA induces the expression of fibroblast growth factor 15 (*Fgf15, FGF19* in humans) which travels through the portal vein to the liver. There, it binds to the FGF receptor 4 (FGFR4)/β-klotho heterodimer complex and induces a JNK/ERK signaling cascade to inhibit *Cyp7a1* expression (Inagaki et al. 2005).

Studies treating WT and *Fxr* $^{-/-}$ mice with FXR agonists, as well as data from BA studies in humans indicate that FXR regulates several metabolic processes besides BA synthesis. This encompasses the metabolism of glucose and plasma lipoproteins, as well as regulation of steatosis, inflammation or bacterial growth (Aguiar Vallim et al. 2013; Wahlström et al. 2016; Molinaro et al. 2018).

Pregnane X receptor (PXR)

High PXR expression is found in the liver and intestine, as well as low levels in other tissues. PXR activation occurs not only by BA, but also xenobiotics, or pharmaceutical drugs. The secondary BA LCA and 3-keto-LCA activate this nuclear receptor, while CDCA, DCA or CA do not elicit a response (Staudinger et al. 2001). PXR activation by LCA and 3-keto-LCA, as well as by other hepatotoxic BA intermediates, induces the expression of CYP3A. This enzyme catalyzes hydroxylations of the steroid side-chain as a method of detoxification and excretion of those toxic products (Staudinger et al. 2001; Goodwin et al. 2003).

Vitamin D receptor (VDR)

VDR is expressed in various tissues like kidney and intestine, as well as in macrophages. It controls bone and calcium metabolism, immunity, cellular growth, and differentiation. As the name suggests, VDR is potently activated by 1,25-dihydroxyvitamin D3. Surprisingly, LCA and 3-keto-LCA also activate VDR, inducing their CYP3A mediated detoxification (Makishima et al. 2002). VDR signaling also alters the expression of *Cyp7a1*, although with contradicting results. It was observed that vitamin D induces VDR mediated secretion of FGF15 from enterocytes, which subsequently represses hepatic *Cyp7a1* (Schmidt et al. 2010). However, another study observed the induction of hepatic *Cyp7a1* expression upon vitamin D treatment. This was reported to occur via hepatic VDR activation and subsequent repression of *Shp* (Chow et al. 2014).

Takeda G protein-coupled receptor 5 (TGR5)

TGR5, also known as G-protein coupled bile acid receptor 1 (GPBAR1), is ubiquitously expressed in the plasma membranes of gallbladder, liver, intestinal enteroendocrine cells, skeletal muscle, or brown adipose tissue (Maruyama et al. 2006). It is activated by hydrophobic BA with LCA > DCA > CDCA > CA >> UDCA (Sato et al. 2008).

Tgr5$^{-/-}$ mice showed a decreased bile acid pool, hinting at a role of the receptor in BA homeostasis (Maruyama et al. 2006). TGR5 activation in rodent models of obesity lead to decreased obesity and insulin resistance by directly promoting thyroid hormone activity in skeletal muscle and brown adipose tissue (Watanabe et al. 2006). Another group showed that TGR5 signaling in enteroendocrine cells lead to the release of glucagon-like peptide-1 (GLP-1) and increased energy expenditure (Thomas et al. 2009).

1.3. THE GUT MICROBIOTA

1.3.1. General

The human microbiota is a complex and dynamic ecosystem encompassing members from all three domains of life (Bacteria, Archaea, Eukarya) (Donaldson et al. 2016). Bacteria outnumber the other two members by 2–3 orders of magnitude and it is estimated that the average adult man harbors 38 trillion bacterial cells with a total mass of around 0.2 kg (Sender et al. 2016). The overwhelming majority of bacteria is found in the gastrointestinal tract, where they influence host physiology, metabolism and immunity as well as breaking down dietary components, making them available to the host (Sonnenburg and Bäckhed 2016; Fan and Pedersen 2021; Koh and Bäckhed 2020). Metagenomic sequencing has revealed the immense coding potential of the gut microbiota harboring 500-fold more genes than found in our own genome (Qin et al. 2010; Li et al. 2014). Collectively, the gut bacteria and their genes are referred to as the microbiome.

1.3.2. Composition along the gastrointestinal tract

The gut microbial composition differs not only between individuals in dependence of factors such as dietary habits and environmental impacts, but also within those same individuals. Along the gastrointestinal tract (GIT), physiological conditions strongly vary, with gradients in oxygen concentration, nutrient availability, pH, BA or host digestive enzyme concentrations giving rise to unique habitats colonized by adapted bacterial species (Figure 4) (Donaldson et al. 2016; Martinez-Guryn et al. 2019).

Research regarding the small intestinal microbiota has been relatively sparse, especially in humans, due to the ethical concerns and technical difficulties in obtaining bacterial samples from healthy adults. Most research has thus been deriving relationships between the microbiome and host health and disease from fecal samples (Kastl et al. 2020). Recent publications have highlighted the importance of SI microbes for host metabolic processes and uptake of nutrients, including lipids (Martinez-Guryn et al. 2018; Araújo et al. 2020; Tazi et al. 2018).
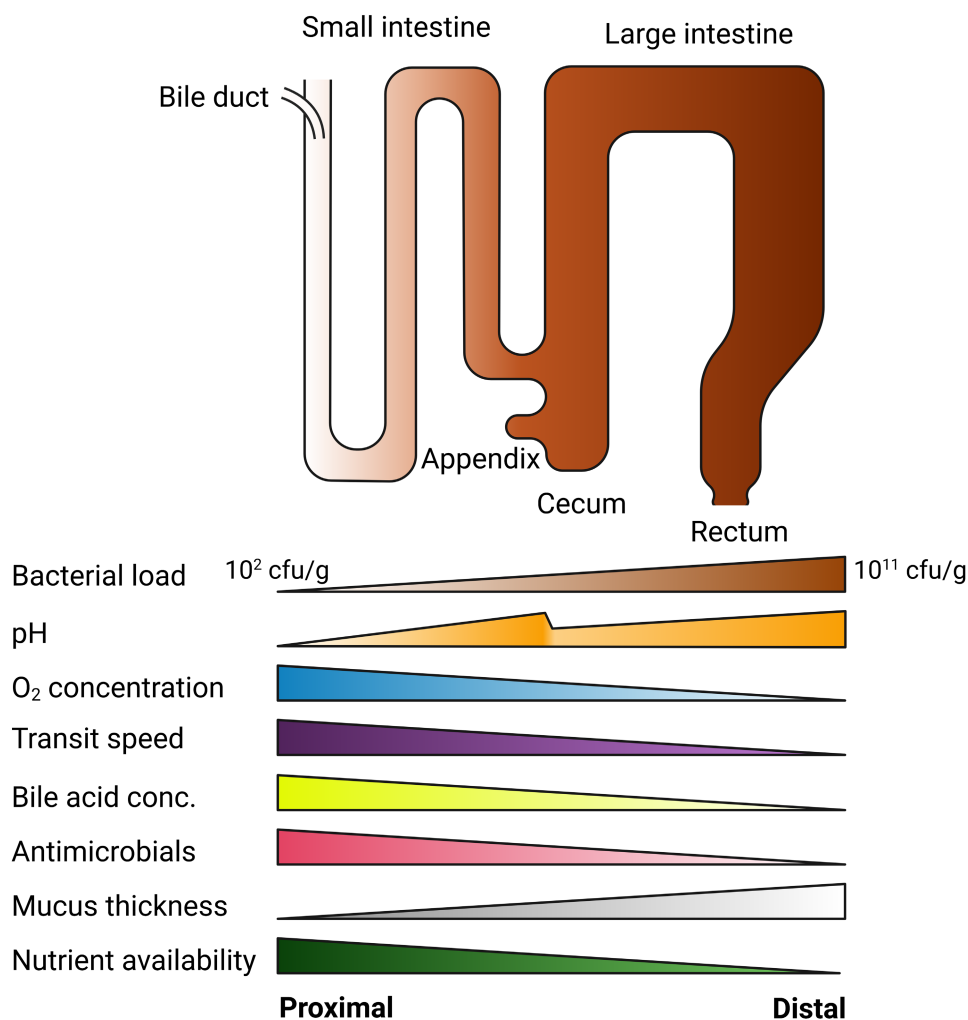
Figure 4.   Physiological conditions affecting bacterial colonization along the GIT
Illustration modified from Donaldson et al. 2016

Microbial diversity and abundance in the small intestine (SI) is relatively low compared to that of the cecum and large intestine, likely due to fast transit times of intestinal content (3–5 h) and strong mixing thereof (Szarka and Camilleri 2012). The lowest bacterial concentration is found in the duodenum with 10^1–10^3 CFU/mL (O'Hara and Shanahan 2006).

This is due to unfavorable conditions such as low pH from gastric chyme, intake of oxygen with the diet as well as high concentrations of host digestive enzymes and bile acids, stemming from pancreatic and biliary secretions. These conditions favor fast-growing facultative anaerobes with a tolerance towards the surfactant properties of BAs and antimicrobial peptides (AMP), consuming simple carbohydrates provided from the diet (Donaldson et al. 2016; Martinez-Guryn et al. 2019).

In the jejunum, bacterial concentrations increase to 10^4–10^7 CFU/mL (O'Hara and Shanahan 2006) and in humans, the major bacterial phyla include 60–80% Firmicutes, 10–25% Proteobacteria, and less than 3% Bacteroidetes and Actinobacteria (Seekatz et al. 2019). Compared to the duodenum, where dietary TG digestion by pancreatic enzymes is initiated, the jejunum is the major site for uptake of these lipids. Interestingly, the jejunal microbiota composition changes more drastically in response to high-fat diet (HFD) feeding than the cecal or stool microbiota. Transplantation of a HFD imprinted jejunal microbiota into GF mice lead to increased lipid absorption compared to controls, receiving transplants from low-fat diet fed mice (Martinez-Guryn et al. 2018).

Finally, in the ileum, bacterial concentrations reach 10^3–10^8 CFU/mL, with facultative and obligate anaerobes like Bacteroides, Clostridium, Enterobacteria, *Enterococcus*, *Lactobacillus*, and *Veillonella* colonizing this part of the SI (Zoetendal et al. 2012; Li et al. 2017)

Thanks to longer transit times >30 h (Szarka and Camilleri 2012), the large intestine harbors a much higher density and diversity of gut microbes (10^{10}–10^{12} CFU/mL) with phylas like Firmicutes and Bacteroidetes and families like Lachnospiraceae, Bacteroidaceae, and Prevotellaceae (O'Hara and Shanahan 2006). Microbes in the colon expand the metabolic capacity of the host by converting dietary substrates which escaped digestion in the SI or cannot be broken down by host enzymes. Examples include complex fibers, sugar alcohols, secondary plant metabolites, or certain proteins (Blaut 2018).

Notably, complex, non-digestible carbohydrates are fermented to produce short-chain fatty acids (SCFA) such as acetate, propionate, and butyrate at millimolar concentrations. SCFAs are rapidly absorbed in the large intestine and used in both anabolic and catabolic reactions by the host, providing ~10% of caloric input in humans (Besten et al. 2013). Butyrate is preferentially metabolized by colonocytes, while remaining SCFAs are transported to the liver via the portal vein. There, they can be metabolized or serve as building blocks for anabolic processes such as the *de novo* FA synthesis from acetate (Besten et al. 2013; Kindt et al. 2018).

1.4. IMPACT OF GUT MICROBIOTA ON LIPID ABSORPTION AND METABOLISM

1.4.1. Impact on lipid metabolism and diet induced obesity

To date, there are only a few studies that have investigated the effects of endogenous gut bacteria on lipid absorption and metabolism. One of the first studies was conducted by Bäckhed and colleagues (Bäckhed et al. 2004). They compared GF and conventional mice and concluded that a normally formed intestinal microbiota favors the absorption of monosaccharides, which induced *de novo* lipogenesis in the liver. Further, the microbiota suppressed the intestinal expression of the circulating LPL inhibitor fasting-induced adipocyte factor (*Fiaf*), increasing incorporation of TG into adipocytes. In 2007, the same group showed that germ-free animals had higher levels of phosphorylated AMP-activated protein kinase (AMPK) in skeletal muscle and liver. The increased β-oxidation protected them from diet-induced obesity (DIO) on a western-style, high-fat, sugar-rich diet (Bäckhed et al. 2007). Another study found that germ-free mice on a high-fat diet excreted significantly more dietary lipids in their feces in addition to reduced feed intake. Lower concentrations of TG and cholesterol were found in the plasma of fasted germ-free animals compared with conventionally colonized animals (Rabot et al. 2010). Regarding the protection of GF mice from DIO on a HFD, there have also been conflicting results published, showing that GF mice are not generally resistant to weight gain (Fleissner et al. 2010). The composition and fat source of the HFD was shown to also play a major role, as GF mice on a lard HFD were protected from DIO, but not on a palm oil HFD (Kübeck et al. 2016).

A first lipidomic characterization of TG and PC profiles in serum, liver and adipose tissue of conventional and germ-free mice also showed strong differences between the two groups (Velagapudi et al. 2010). In colonized mice, TG species were decreased in the serum and increased in adipose tissue and liver. The substantial increase in liver TG was likely due to increased influx of SCFA from bacterial fermentation in the colon, which could serve as building blocks for *de novo* hepatic FA synthesis. Stable isotope labeling studies using ^{13}C-acetate confirmed that this SCFA from gut microbial fiber fermentation is directly used as precursor for *de novo* FA synthesis (Kindt et al. 2018). In addition, SCFA can activate the G-protein coupled receptor GPR43, suppressing insulin signaling in adipocytes to inhibit fat accumulation and maintain metabolic homeostasis (Kimura et al. 2013).

Gut bacteria mediate the saturation and oxidation of double bonds in polyunsaturated fatty acids (PUFA) as a detoxification mechanism in the intestinal tract (Kishino et al. 2013). Like SCFA, these PUFA-derived metabolites can activate GPR to modulate host metabolism. It was shown that 10-hydroxy-cis-12-octadecenoic acid (HYA), a metabolite of bacterial linoleic acid detoxification, attenuated HFD-induced obesity via GPR40 and GPR120 and induced GLP-1 secretion (Miyamoto et al. 2019).

1.4.2. Microbial lipid metabolism in the colon

Small intestinal TG absorption is a very efficient process, with more than 90% of all dietary lipids being resorbed. Consequently, only a small portion of dietary fat reaches the large intestine. Exceptions are individuals with certain clinical conditions, such as cystic fibrosis, pancreatic insufficiency, or patients treated with anti-obesity drugs such as Orlistat, which limit dietary fat absorption (Hoyles and Wallace 2010).

Besides dietary TG, the host itself and commensal bacteria also contribute to the lipid pool in the large intestine. Desquamation of the intestinal epithelium and intestinal secretions are rich in cholesterol and phospholipids. Gut bacteria contribute phospho- and sphingolipids, SCFA and branched-chain FA as fermentation byproducts. It is estimated that 50–75% of all lipids excreted in human feces are of bacterial origin (Chen et al. 1998).

Large intestinal bacteria could hydrolyze dietary TG which escaped digestion by the host. A microbial TG lipase activity *in vitro* has for example been described for some members of the *Coriobacteriaceae* family (Just 2017). Additionally, intestinal bacteria possess phospholipase C activity and can digest phospholipids to 1,2-*sn*-diacylglycerols (DG) (Morotomi et al. 1990). These DG can act as secondary messengers which stimulate protein kinase C, a regulator of cell growth. DG at concentrations found in feces were able to induce mitogenesis in colon adenoma and carcinoma cell cultures, hinting at a link between high-fat diets, colorectal cancer, and the gut microbiota (Friedman et al. 1989).

1.4.3. Microbial influence on lipid absorption in the small intestine

Several studies established the impact of the gut microbiota on host lipid metabolism and physiology in the context of high-fat diet induced obesity (chapter 1.4.1). However, they left open whether the observed effects were caused by an influence of the gut microbiome on exogenous lipid absorption or metabolism, or the endogenous synthesis and metabolism of lipids in the liver. Using FA coupled to fluorescent probes (Semova et al. 2012), lipid uptake in the small intestine could be directly tracked to investigate alterations in response to the gut microbiota. In zebrafish, gut microbial colonization stimulated uptake of BODIPY-labeled lipids into epithelial lipid droplets and peripheral tissues but no mechanistic details were presented (Semova et al. 2012). A study treating rats with antibiotics established that the gut microbiota activates mucosal mast cells, contributing to fat-induced intestinal permeability (Sato et al. 2016). Production of apolipoproteins and secretion of chylomicrons from enterocytes was also increased in control vs. antibiotics treated rats. Using radiolabeled lipids, one study showed that the colonization of GF mice with a jejunal microbiota from HFD-fed SPF mice increased lipid absorption (Martinez-Guryn et al. 2018).

While these studies showed an increase in lipid absorption upon colonization of the GI tract, studies focusing on the role of individual bacterial species as opposed to the complex intestinal microbiota came up with contradictory results. The fermentation products L-lactate and acetate from *Lacticaseibacillus paracasei* and *Escherichia coli* were shown to impede chylomicron secretion, inducing either the storage or oxidation of FA in mouse enterocytes (Tazi et al. 2018; Araújo et al. 2020). In contrast, conditioned medium from *Clostridium bifermentans* induced the expression of enzymes required for TG re-esterification and lipid uptake in small intestinal organoid cultures (Martinez-Guryn et al. 2018).

1.5. RESEARCH OBJECTIVES

In light of the current obesity epidemic, the role of the gut microbiota in influencing host lipid metabolism and fat intake from the diet is only starting to emerge. Studies using different animal models and a variety of high-fat diets of differing composition have elucidated important metabolic pathways which are under microbial control. Still, these studies have partly produced conflicting results and a systematic investigation of dietary lipid uptake and *in vivo* flux with respect to gut microbial status has not been conducted so far.

The current thesis aims to establish differences in dietary lipid absorption and metabolism in GF and colonized mice under physiological conditions with a regular chow diet. Stable isotope labeled lipids will be supplied via oral gavage and tissues collected over a 6 h time course to obtain kinetics of lipid uptake and metabolism. State of the art high-resolution mass spectrometry (HR-MS) and gas-chromatography coupled to mass spectrometry (GC-MS) will be used to quantify label uptake into blood and peripheral tissues and to track integration of the labeled FA into different lipid classes. Mice colonized with minimal microbial consortia will be employed to help establish the role of particular microbial species in the regulation process.

Understanding the role of gut microbiota on the mechanistic level could open up new doors for treating disorders which are driven by an excess intake of calories in the form of fat.

2. MATERIALS AND METHODS

2.1. MATERIALS

Table 1. Biological samples

Resource	Source	Identifier
Human bile sample	This work; Department of Surgery, Technical University of Munich (TUM), Munich	N/A
Mouse tissue and fluid samples	This work	N/A

Table 2. Chemicals

Reagent	Source	Identifier
PC 15:0/18:1[D7]	Avanti Polar Lipids	Cat# 791637C
Glyceryl Tri(hexadecanoate-d31)	CDN Isotopes	Cat# D-5213
Hexadecanoic-15,15,16,16,16-d5 Acid	CDN Isotopes	Cat# D-5397
Evans Blue	Sigma Aldrich	Cat# E2129
1-Palmitoyl-2-Linoleoyl-sn-Glycero-3-Phosphatidylcholine	Larodan	Cat# 37-1622-5
Trypsin Gold Mass Spectrometry Grade	Promega	Cat# V5280
Taurocholic acid	Sigma Aldrich	Cat# T4009

Table 3. Commercial assays

Resource	Source	Identifier
S-Trap™ micro MS sample prep kit	Protifi	Cat# K02-micro-10
RNEasy Mini Kit	Qiagen	Cat# 74106
QIAshredder homogenizer	Qiagen	Cat# 79656
FastStart Essential DNA Probes Master	Roche	Cat# 06402682001
LightCycler 480 Universal Probe Library System	Roche	N/A
NucleoSpin gDNA clean-up kit	Macherey-Nagel	Cat# 740230.250
NucleoSpin RNA II kit	Macherey-Nagel	Cat# NZ74095550
Moloney murine leukemia virus reverse transcriptase Point Mutant Synthesis System	Promega	N/A
AMV Reverse Transcriptase	Promega	Cat# M5108

Table 4. Experimental model organisms

Resource	Source	Identifier
Mouse: C57BL/6JZtm (GF, OMM[12], OMM[11], SPF colonized)	Central Animal Facility (Hannover Medical School, Hanover, Germany)	N/A
Mouse: *Cyp2c70* KO	Jörg Heeren and Folkert Kuipers collaboration (Boer et al. 2021)	N/A

Table 5. Oligonucleotides

Resource	Source	Identifier
Primers for qPCR of bacterial 16S rRNA genes	Brugiroux et al. 2016	N/A
Cluster of differentiation 36 (*Cd36*) fw: 5'-CAATCAAAAGGGAAGTTGTCCTTGA-3' rev: 5'-CTGTCTGTACACAGTGGTGCC-3'	This work	ENSMUST00000169095
Solute carrier family 27 Member 4 (*Slc27a4/Fatp4*) fw: 5'-GCACAGCAGGTATTATCGTATGG-3' rev: 5'-TGCTGAGTGGTAGAGGGGGA-3'	This work	ENSMUST00000080065
Glyceraldehyde-3-Phosphate Dehydrogenase (*Gapdh*) fw: 5'-CGCCTGGAGAAACCTGCC-3' rev: 5'-AGCCGTATTCATTGTCATACCAGG-3'	This work	ENSMUST00000117757
Glyceraldehyde-3-Phosphate Dehydrogenase (*Gapdh*) fw: 5'-TCCACTCATGGCAAATTCAA-3' rev: 5'-TTTGATGTTAGTGGGGTCTCG-3'	This work	UPL probe #9
Trefoil factor 3 (*Tff3*) fw: 5'-GTAACAACCGTGGCTGCTG-3' rev: 5'-GAGCCTGGACAGCTTCAAAA-3'	This work	UPL probe #109
Cyclic AMP-responsive element-binding protein 3-like protein 1 (*Oasis*) fw: 5'-GATGGAGGACACCACTCAAGA-3' rev: 5'-CCATGATGGAGCACAGCTT-3'	This work	UPL probe #81
Mucin-2 (*Muc2*) fw: 5'-GCAGTACAAGAACCGGAGT-3' rev: 5'-GGTCTGGAGTCCTCGAA-3'	This work	UPL probe #66
Anterior gradient protein 2 homolog (*Agr2*) fw: 5'-TGCTGAACATAAAGAAATCCAGAA-3' rev: 5'-CAGGAGAAAGGTGCTTGTCA-3'	This work	UPL probe #53

2.2. DATA AND SOFTWARE

Table 6. Deposited data

Resource	Source	Identifier
Raw and analyzed lipidomics data	This work	N/A
Bile proteomics data	This work	ProteomeXchange: PXD033894
Liver transcriptomics data	Kindt et al. 2018	ArrayExpress: E-MTAB-6079
Liver proteomics data	Kindt et al. 2018	ProteomeXchange: PXD010412

Table 7. Software and algorithms

Resource	Source	Identifier
MatLab 2019b SimBiology Toolbox	MathWorks	https://www.mathworks.com/products/simbiology.html
Code related to the physiology-based kinetic multi-compartment modeling	This work	https://github.com/mszimmermann/Microbiome_effect_on_lipid_metabolism
MaxQuant (version 1.6.10.43)	Cox and Mann 2008	https://www.maxquant.org/maxquant/
Perseus (v. 1.6.13.0)	Tyanova et al. 2016	https://www.maxquant.org/perseus/
UniprotKB database	The UniProt Consortium	https://www.uniprot.org
Human Protein Atlas	Uhlén et al. 2015	http://www.proteinatlas.org/
OriginPro 2021 (v. 9.8.0.200)	OriginLab Corporation	https://www.originlab.com/2021
LightCycler® 480 Software 1.5.1	Roche	N/A
Excel 2016	Microsoft Corporation	N/A
GCMSsolution v. 4.45	Shimadzu Corporation	N/A
ChemDraw Professional 19.0	Perkin Elmer	https://perkinelmerinformatics.com/products/research/chemdraw/
BioRender	BioRender	https://biorender.com/

2.3. MISCELLANEOUS

Table 8. Miscellaneous

Resource	Source	Identifier
Protein LoBind tubes	Eppendorf	Cat# 0030108.132
50 kGy gamma-irradiated feed	Ssniff	Cat# V1124-927
Autoclaved feed	Ssniff	Cat# V1124-300
TissueLyser LT	Qiagen	N/A
FastPrep-24 homogenizer	MP Biomedicals	N/A
Lightcycler 96	Roche	N/A
Lightcycler LC 480	Roche	N/A
Agilent 2100 Bioanalyzer	Agilent Technologies	N/A
NanoDrop spectrophotometer	Thermo Fisher Scientific	N/A
Leica TP1020 Tissue Processor	Leica	N/A
Leica EG1150C Cold Plate	Leica	N/A
Digital microscope M8	PreciPoint	N/A
Q Exactive Orbitrap HF-X mass spectrometer	Thermo Fisher Scientific	N/A
Vanquish Pump	Thermo Fisher Scientific	N/A
15 cm Acclaim PepMap 100 C18 column (2 µm particle size, 1 mm ID)	Thermo Fisher Scientific	Cat# 164711
Shimadzu 2010 GC-MS system	Shimadzu Corp.	N/A
BPX70 column (10 m length, 0.10 mm diameter, 0.20 µm film thickness)	Trajan Scientific	Cat# 054600

2.4. EXPERIMENTAL MODEL AND SUBJECT DETAILS

2.4.1. Mouse housing

GF, gnotobiotic (OMM^{12} and OMM^{11} colonized) and SPF C57BL/6JZtm mice were obtained from the Central Animal Facility of the Hannover Medical School (Hanover, Germany) in cooperation with Marijana Basic. Breeding of GF and gnotobiotic animals was performed in plastic film isolators (Metall+Plastik GmbH, Radolfzell-Stahringen, Germany) located in a room with a controlled environment (20–22 °C, 50–55% humidity) and 12 h light/dark cycles. GF and gnotobiotic mice received pelleted 50 kGy gamma-irradiated feed (V1124-927, Ssniff Spezialdiäten GmbH, Germany) and autoclaved water *ad libitum*. SPF mice were housed in individually ventilated cages (XJ Edge, Allentown) in a room with a controlled environment (20–22 °C, 50–55% humidity) and 12 h light/dark cycles. SPF mice received pelleted 50 kGy gamma-irradiated feed (V1124-927, Ssniff) and chlorinated water *ad libitum*. Routine microbiological monitoring did not reveal any evidence of infection with common murine pathogens in SPF animals or contaminants in gnotobiotic animals (Mähler Convenor et al. 2014; Basic et al. 2021).

Cyp2c70 $^{-/-}$ mice and littermate controls were obtained through a collaboration with Jörg Heeren. They were raised in the animal facility of the University Medical Center Hamburg-Eppendorf (Hamburg, Germany) at room temperature (22 °C) and held at a 12 h light/dark cycle with *ad libitum* access to standard laboratory chow diet and water.

All mouse experiments were performed according to the relevant ethical guidelines and were approved by the local institution in charge (Regierung von Oberbayern, approval number 55.2-1-54-2532-192-2016, ROB-55.2-2532.Vet_02-21-124). Adult male and female mice were used for the experiments and their age is noted under the respective method details subheading. Animals were randomly assigned to the experimental groups.

2.4.2. Human bile samples

Samples were obtained from a female patient (38 years) undergoing gall bladder removal (cholecystectomy), in the absence of malignant disease, in 2021 at the Department of Surgery (Klaus-Peter Janssen), Technical University of Munich (TUM), Munich. Samples were immediately shock-frozen in liquid nitrogen, following established bio banking protocols and in accordance with local and national ethical and legal standards for data protection (Ethics Committee of the Faculty of Medicine, TUM, #1926/07; #5428/12).

2.5. METHOD DETAILS

2.5.1. Stable isotope tracing of lipid uptake and flux in mice

To prepare the stable isotope labeled lipid gavages, for each gavage, 10 µmol FA 16:0[D5] (Hexadecanoic-15,15,16,16,16-d_5 Acid) and 3.33 µmol TG (16:0[D31])$_3$ (Glyceryl Tri(hexadecanoate-d_{31})) (both from CDN isotopes) were weighed into separate glass tubes. Per gavage to prepare, 100 µL of isooctane:isopropanol 3:1 (v:v) were added into both of the glass tubes. The tube containing FA 16:0[D5] was sonicated at 37 °C until the FA completely dissolved, and all liquid was transferred into the second tube containing the incompletely dissolved TG (16:0[D31])$_3$. The tube now containing both lipids was sonicated at 37 °C until the TG (16:0[D31])$_3$ dissolved. Per gavage, 200 µL of the prepared solution was aliquoted into 1.5 mL tubes and evaporated to dryness using a vacuum concentrator (Jouan RC 10.10). Per tube, 100 µL of olive oil (Rewe Beste Wahl) were added and the gavages were stored at 4 °C until use. Before gavaging the labels, they were sonicated at 37 °C for 30 min and checked to be clear of any precipitated labeled lipids.

For the lipid uptake experiments, 10–16-week old GF, OMM[12], OMM[11] and SPF C57BL/6JZtm mice were starved for 2 h before oral gavage of 100 µL of olive oil containing the labeled lipids. After 1, 2 and 6 h, mice were sacrificed by CO_2 asphyxiation, tissues were collected as outlined below, snap frozen in liquid nitrogen and stored at −80 °C.

For the experiment investigating the impact of PC supplementation on lipid uptake, SPF mice were starved for 2 h before oral gavage of labeled lipids in olive oil, either with or without added 0.1 µmol of 1-Palmitoyl-2-Linoleoyl-sn-Glycero-3-Phosphatidylcholine (PC 34:2, Larodan). After 1 h, mice were sacrificed by CO_2 asphyxiation.

2.5.2. Plasma, bile, tissue and gut content collection

EDTA plasma was collected from the heart by centrifugation (10 min, 1,500 × g, 4 °C). The liver was perfused with saline solution (0.9% NaCl) to remove blood and the left lobe was sampled. Bile was collected directly from the gallbladder using an insulin syringe. Beginning at the base of the stomach, the small intestine was divided as follows: The first 8 cm - duodenum, the last 8 cm - ileum and the middle part - jejunum. The large intestine was collected in one piece. Gut content of the sections was sampled, and the intestinal tissues were rinsed thoroughly with saline solution to remove residual oral gavage lipids. Inguinal and epididymal white adipose tissue (iWAT and eWAT) as well as interscapular brown adipose tissue (iBAT) were collected. All samples were snap frozen in liquid nitrogen and stored at −80 °C.

2.5.3. Experimental quantification of gastric flow

8–19-week old GF, OMM[12] and SPF C57BL/6JZtm mice were starved for 2 h before receiving an oral gavage of 100 µL of olive oil containing 50 mg/mL Evans Blue (Sigma-Aldrich). After 12.5 min, mice were sacrificed by CO_2 asphyxiation, the intestinal system was removed and the distance from the base of the stomach to the blue dye front in the small intestine was measured. Distances were normalized to the total lengths of the small intestines

2.5.4. Physiology-based kinetic multi-compartment modelling

The multi-compartment kinetic model of fatty acid metabolism in the mouse was developed together with Michael Zimmermann and Maria Zimmermann-Kogadeeva (EMBL, Heidelberg). It contained 11 compartments (duodenum, jejunum, ileum and colon lumen, duodenum, jejunum, ileum and colon tissue, plasma, liver and fat tissue). One additional compartment (small_intestine_gi) was used as reservoir for the initial fatty acid abundance. The serum compartment incorporated processes occurring in all other body parts apart from the gastrointestinal tract (GIT), liver and fat tissue. Labeled fatty acid administration was modelled as an input to the small_intestine_gi compartment of the initial amount of D. Label propagation through the body was driven by the flow of gastrointestinal material in different GIT sections and lumen:tissue and tissue:serum diffusion and absorption coefficients. Model parameters and equations are provided in the GitHub Repository (see Table 7 for link). All equations were defined for fatty acid amounts. Parameters for FA 16:0[D5] and FA 16:0[D31] were assumed to be the same and were fitted simultaneously to the data from both fatty acid measurements. For the parameter fitting, fatty acid concentrations were converted into amounts using estimated compartment volumes provided in Supplemental Table 1. The model was created using the MatLab 2019b SimBiology Toolbox (MathWorks).

To assess model improvement when each of the model parameters is set to be mouse group-specific, a general model with six parameters was built, which included equations for FA 16:0[D5] and FA 16:0[D31] from each mouse group, and parameters were fitted to the data profiles from the three mouse groups simultaneously. Next, each of the six parameters was defined as mouse-group specific, and the equations containing this parameter for each mouse group were changed accordingly. For each of the modified models, mean squared error, Akaike information criterion (AIC), and Bayesian information criterion (BIC) were recorded. The model with the largest negative change of the AIC was considered the best improvement compared to the general model.

2.5.5. Quantitative PCR of bacterial 16S rRNA genes

The quantitative PCR of bacterial 16S rRNA genes was performed in collaboration with the lab of Bärbel Stecher (Max von Pettenkofer-Institut, LMU Munich). gDNA extraction using a phenol-chloroform based protocol was performed as described previously (Herp et al. 2019). Fecal pellet or intestinal content was weighed and resuspended in 500 µL extraction buffer (200 mM Tris-HCl, 200 mM NaCl, 20 mM

EDTA in ddH$_2$O, pH 8, autoclaved), 210 µL 20% SDS and 500 µL phenol:chloroform:isoamylalcohol (25:24:1, pH 7.9). 0.1 mm-diameter zirconia/silica beads (Roth) were added and bacteria were lysed with a bead beater (TissueLyser LT, Qiagen) for 4 min at 50 Hz. After centrifugation (14,000 × g, 5 min, RT), the aqueous phase was transferred into a new tube, 500 µL phenol:chloroform:isoamylalcohol (25:24:1, pH 7.9) were added and again spun down. The resulting aqueous phase was gently mixed with 1 mL 96% ethanol and 50 µL of 3 M sodium acetate by inverting. After centrifugation (30 min, 14,000 × g, 4 °C), the supernatant was discarded and the gDNA pellet was washed with 500 µL ice-cold 70% ethanol and again centrifuged (14,000 × g, 4 °C; 15 min). The resulting gDNA pellet was resuspended in 150 µL Tris-HCl, pH 8. Subsequently, gDNA was purified using the NucleoSpin gDNA clean-up kit (Macherey-Nagel) and stored at −20 °C.

Quantitative PCR was performed as described previously (Brugiroux et al. 2016). As template, 2.5 µL of gDNA diluted to 2 ng/µL were used. Strain-specific 16S rRNA primers and hydrolysis probes were used for amplification (Lightcycler 96, Roche). The FastStart Essential DNA Probes Master (Roche) was used for the reactions. Standard curves using linearized plasmids containing the 16S rRNA gene sequence of the individual strains were used for absolute quantification of 16S rRNA gene copy numbers of individual strains. The readout of 16S rRNA copies per 5 ng gDNA was normalized to the individual sample weight to determine 16S rRNA copies per 1 g intestinal content (absolute abundance).

2.5.6. RNA isolation from intestinal tissue and qPCR analysis

Frozen tissue samples were ground under liquid nitrogen using a mortar and pestle and total RNA was extracted using QIAshredder columns and the RNEasy Mini Kit (both Qiagen). The purity and integrity of the RNA were assessed using the Agilent 2100 Bioanalyzer (Agilent Technologies). For real-time PCR, 1 µg RNA was transcribed into cDNA using the Reverse Transcription System from Promega. Real-time quantitative RT-PCR analysis was performed using the Light Cycler LC 480 (Roche). The following primer were used: Cluster of differentiation 36 (*Cd36*; fw: 5'-CAATCAAAAGGGAAGTTGTCCTTGA-3'; rev: 5'-CTGTCTGTACACAGTGGTGCC-3'), Solute carrier family 27 Member 4 (*Slc27a4/Fatp4*; fw: 5'-GCACAGCAGGTATTATCGTATGG-3'; rev: 5'-TGCTGAGTGGTAGAGGGGGA-3'). Glyceraldehyde-3-Phosphate Dehydrogenase, used as reference gene (*Gapdh*; fw: 5'-CGCCTGGAGAAACCTGCC-3'; rev: 5'-AGCCGTATTCATTGTCATACCAGG-3'). Quantification relative to GF mouse tissue was carried out using LightCycler® 480 Software 1.5.1 (Roche) and the $2^{-\Delta\Delta C_T}$ Method (Livak and Schmittgen 2001; Langmann et al. 2006).

2.5.7. Gene expression analysis of goblet cell markers by qPCR

RNA of total intestinal tissue was isolated according to the manufacturer's instructions (NucleoSpin RNA II kit, Macherey-Nagel) and measured by NanoDrop spectro-photometer (Thermo Fisher Scientific). Complementary DNA was synthesized from 500 ng RNA using random hexamers and Moloney murine leukemia virus reverse transcriptase Point Mutant Synthesis System (Promega, Madison, WI). Quantification was performed using the LightCycler 480 Universal Probe Library System (Roche). Calculations by the $2^{-\Delta\Delta C_T}$ method (Livak and Schmittgen 2001) were normalized to GAPDH (UPL probe #9) as housekeeper. Primer sequences and respective probes are listed in Table 5.

2.5.8. Mucin-filled goblet cell determination by AB/PAS staining

Intestinal tissue was processed as Swiss Rolls, fixed in 10% phosphate-buffered formalin for 24 h, dehydrated (Leica TP1020), and embedded in paraffin (McCormick; Leica EG1150C).

For AB/PAS staining, Swiss roll sections (3 µm thick) were deparaffinized and rehydrated before staining with alcian blue solution for acidic mucins (1% (v/v) in 3% acetic acid, pH 2.5, 10 min), treated with periodic acid solution (0.5% (v/v), 5 min) and co-stained with Schiff's reagent for neutral mucins (10 min). Nuclei were counterstained with hematoxylin, before dehydrating and mounting the tissue sections. The number of mucin-filled goblet cells was counted in five separate areas per Swiss roll, for a total of 50–55 crypts, and was calculated as total number of mucin-filled goblet cells per 100 µm^2. Images were acquired by the digital microscope M8 (PreciPoint, Freising, Germany).

2.5.9. Adherent mucus thickness measurement

For the adhering mucus thickness measurements, dissected but still longitudinally unopened intestinal tubes were rolled to form a closed "Swiss roll" and fixed in Carnoy solution overnight (60% dry MeOH, 30% dry chloroform, 10% acetic acid). Dehydration of samples was performed by washes in dry MeOH (2 times, 30 min each), 100% EtOH (20 and 15 min), xylene/100% EtOH (1:1) (5 min), and xylene (2 times, 5 min each). Dehydrated colonic tissue was submerged in melted paraffin for 20 min and embedded. Samples were cut at 3 µm thickness and stained for AB (without PAS) as described in chapter 2.5.8 above.

The adherent mucus thickness was measured in three separate locations on one villus, for a total of 50 villi. The average for each villus was calculated and represented graphically. Images were acquired by the digital microscope M8 (PreciPoint, Freising, Germany). All mucus characterizations (chapters 2.5.7, 2.5.8, 2.5.9) were performed in collaboration with Olivia Coleman (Department of Nutrition and Immunology, TUM, Freising).

2.5.10. Bile proteomics

Sample preparation

12–26 week old C57BL/6 mice were fasted for 2 h, sacrificed and bile samples were collected by direct puncture of the gallbladder using an insulin syringe. Samples were immediately frozen in liquid nitrogen and stored at –80 °C until further use. Bile from 6 mice was pooled. Human bile was obtained from the Department of Surgery, Technical University of Munich (TUM) as described in chapter 2.4.2 and stored at –80 °C.

Bile proteins were purified and digested on-column using the S-Trap™ micro MS sample prep kit (Protifi) according to the manufacturer's protocol with minor adjustments. Protein LoBind tubes (Eppendorf) were used to reduce protein loss during the purification/digestion. In brief, 11.5 µL of human bile or 30 µL of mouse bile were mixed 1:1 with 2 × lysis buffer (10% SDS, 100 mM TEAB, pH 8.5) and vortexed. Reductant (120 mM TCEP) was added to the bile/lysis buffer mixture at a ratio of 1:23 and the samples were incubated at 55 °C for 15 min at 300 rpm. Alkylation of disulfides was performed by adding the alkylator (500 mM MMTS in isopropanol) at a ratio of 1:23 based on the initial sample/lysis buffer volume and incubating at RT for 10 min and 300 rpm. Acidifier (27.5% aqueous phosphoric acid) was added at a 1:10 ratio to the sample and vortexed. 6 × the volume of binding/wash buffer (100 mM TEAB in 90% methanol) was added to the sample and mixed. Samples were loaded onto the S-Trap column and trapped by centrifugation at 10,000 × g for 30 sec. Trapped proteins were washed 4 × with 150 µL of binding/wash buffer at 10,000 × g for 30 sec, followed by a final centrifugation at 10,000 × g for 1 min to dry the column. For protein digestion, Trypsin Gold Mass Spectrometry Grade (Promega) was resuspended at 1 µg/µL in 50 mM acetic acid (MS grade), aliquoted and stored at –80 °C. 2 µg of the resuspended Trypsin Gold was diluted in digestion buffer (50 mM TEAB) for a final volume of 20 µL and added to the S-Trap column. Columns were incubated overnight at 37 °C in a water bath without shaking. Peptides were eluted in three steps, by adding 40 µL of elution buffer 1 (50 mM TEAB), elution buffer 2 (0.2% MS grade formic acid) and elution buffer 3 (50% MS grade acetonitrile), each followed by a centrifugation step at 10,000 × g for 1 min. Pooled eluates were dried down at RT in a vacuum concentrator (RC 10.10, Jouan) and resuspended in 0.1% formic acid (MS grade) for LC-MS/MS analysis.

Proteomics

Proteomics measurements were performed in collaboration with Piero Giansanti (BayBioMS, MRI, Munich). All samples were analyzed on a µLC-MS/MS system using a modified Vanquish pump coupled to a Q Exactive Orbitrap HF-X mass spectrometer (both Thermo Fisher Scientific). Chromatographic separation was performed via direct sample injection (1–15 µL) onto the head of a 15 cm Acclaim PepMap 100 C18 column (2 µm particle size, 1 mm ID, Thermo Fisher Scientific) at a flow rate of 50 µL/min (Bian et al. 2020). Solvent A was 0.1% FA, 3% DMSO in water, and solvent B was 0.1% FA, 3% DMSO in ACN. Samples were separated with a linear gradient of 3% to 28% B in

30 min, and the total analysis time was 32 min. The IonMax source was used to acquire the data with HESI-II probe depth at "position A".

The mass spectrometer was operated in positive ion mode using an electrospray voltage of 3.5 kV, capillary temperature of 325 °C and vaporizer temperature of 125 °C. The flow rates of sheath gas, aux gas and sweep gas were set to 32, 5, and 0, respectively. A data-dependent acquisition method was used, which automatically switched between MS and MS/MS. Survey full-scan MS spectra were recorded in the orbitrap at a resolution of 60,000 at m/z 200 and an AGC target value of 3e6 with a maximum injection time (maxIT) of 50 ms. The MS1 mass range was set to 360–1300. The isolation width was set to 1.3 m/z, and the first mass was fixed at 100 m/z. After the survey scan, the 12 most abundant precursors passing the intensity threshold of 9.1e4 were selected for HCD fragmentation, and MS2 spectra were recorded in the orbitrap with an AGC target value of 1e5 and maxIT of 22 ms. The normalized collision energy was set to 28. MS1 and MS2 spectra were acquired in profile and centroid mode, respectively. The dynamic exclusion value was set to 15 s.

Data processing and analysis
Raw data files were processed with MaxQuant (version 1.6.10.43) using the default parameters (Cox and Mann 2008). Spectra were searched against the UniProtKB database (Mus musculus, UP000000589, 55,431 entries downloaded on 12.2019, or Homo sapiens, UP000005640, 79,071 entries downloaded on 02.2021). Enzyme specificity was set to trypsin and up to 2 missed cleavages were allowed. Cysteine carbamidomethylation was set as a fixed modification while protein N-term acetylation and methionine oxidation were selected as variable modifications. Precursor tolerance was set to 5 ppm, and fragment ion tolerance to 20 ppm. For label-free quantification, the iBAQ quantification was enabled along with the match-between-runs feature, using default parameters. Results were adjusted to 1% false discovery rate at protein and peptide levels. Identifications were filtered to remove contaminants and decoy hits using Perseus (v. 1.6.13.0) (Tyanova et al. 2016) before any subsequent analysis.

To identify bile proteins of putative pancreatic origin, the dataset was compared to 65 human proteins classified as "enriched in pancreas tissue" by the Human Protein Atlas (proteinatlas.org) (Uhlén et al. 2015).

2.5.11. Phospholipase activity assay
10–14 week old C57BL/6 mice were fasted for 2 h, sacrificed and bile samples were collected by direct puncture of the gallbladder using an insulin syringe. Samples were immediately frozen in liquid nitrogen and stored at −80 °C until further use. As a negative control, proteins in bile were denatured by heat (95 °C, 15 min, 700 rpm, 1% SDS) and then centrifuged (16,100 × g, 4 °C, 5 min). To determine the effect of TCA concentration on PLA activity, 1 mM and 5 mM of TCA where dissolved in the bile samples beforehand. The phospholipase substrate PC 15:0/18:1[D7] (1 mg/mL in chloroform, Avanti Polar Lipids) was evaporated in reaction tubes using a vacuum concentrator (RC 10.10, Jouan) and tubes were pre-warmed at 37 °C. Baseline

samples before the addition of bile to the substrate were drawn, diluted 1:100 in ddH$_2$O and frozen in liquid nitrogen. To start the reactions, bile was added to the evaporated substrate and vortexed for 30 sec to dissolve it in the bile samples. The final substrate concentration in the bile was set to 10 nmol/µL. Samples were incubated at 37 °C and 700 rpm. At the respective time points, samples were drawn, diluted 1:100 in ddH$_2$O and frozen immediately in liquid nitrogen to quench the reactions.

2.5.12. Total fatty acid analysis

Sample preparation

For the FA quantification in liver, lung, intestinal and fat tissues, 20–60 mg of the frozen samples were aliquoted into 2 mL screw cap tubes (Sarstedt) prefilled with 0.7 g of ceramic beads (1.4 mm diameter, Bertin Technologies). Cold tissue extraction solution (MeOH:ddH$_2$O 1:1, 1% SDS) was added to a final concentration of 0.05 mg/µL. Samples were homogenized using a FastPrep-24 homogenizer (MP Biomedicals) with the following settings: 1 × 30 sec, 6 m/s. Gut contents were transferred into 2 mL screw cap tubes (Sarstedt) prefilled with 0.7 g of ceramic beads (1.4 mm diameter, Bertin Technologies). 1 mL of cold 70% isopropanol was added. Samples were homogenized using a FastPrep-24 homogenizer (MP Biomedicals) with the following settings: 1 × 30 sec, 6 m/s. Using cut-off pipette tips, 200 µL of the homogenized gut contents were transferred into new tubes and the samples were evaporated to dryness using a vacuum concentrator (RC 10.10, Jouan) to determine the dry weight concentration. All samples were adjusted to a final concentration of 2 mg dry weight/mL with 70% isopropanol before measurement.

GC-MS analysis

For liver, lung and intestinal tissues, 20 µL of the tissue extraction solutions (= 1 mg tissue equivalent) were used for the fatty acid derivatization. For fat tissues, 4 µL (= 0.2 mg tissue equivalent) were used. For plasma analysis, 10 µL were used directly in the reaction. Bile was diluted 1:100 in ddH$_2$O and 20 µL of the dilutions were used. For gut content measurements, 125 µL of the gut contents in 70% isopropanol (= 0.2 mg dry weight equivalent) were used. Fatty acid methyl esters (FAMEs) were generated by acetyl chloride and methanol treatment and extracted with hexane as previously described (Ecker et al. 2012). Total FA analysis was carried out using a Shimadzu 2010 GC-MS system. FAMEs were separated on a BPX70 column (10 m length, 0.10 mm diameter, 0.20 µm film thickness) from SGE using helium as the carrier gas. The initial oven temperature was 50 °C and was programed to increase at 40 °C/min to 155 °C, 6 °C/min to 210 °C, and finally 15 °C/min to 250 °C. The FA species and their positional and cis/trans isomers were characterized in scan mode and quantified by single ion monitoring to detect specific fragments of saturated and unsaturated FAs (saturated, m/z 74; mono-unsaturated, m/z 55; di-unsaturated, m/z 67; poly-unsaturated, m/z 79). Isotopically labeled FA species were quantified by single ion monitoring of their respective molecular ions using the calibration curves of the unlabeled species. The internal standard was non-naturally occurring C21:0 iso.

2.5.13. Bile acid analysis

Bile acids measurements were performed in collaboration with Sabrina Krautbauer and Gerhard Liebisch (Institute of Clinical Chemistry and Laboratory Medicine, University Hospital Regensburg). Bile acids were quantified by liquid chromatography tandem mass spectrometry (LC-MS/MS) according to the principle described previously (Krautbauer et al. 2016) with some modifications to cover also muricholic acids and their conjugates. In brief, LC separation was performed with a Kinetex® 2.6 µm Biphenyl 50 × 2.1 mm column (Phenomenex, Torrance, CA, USA), water as solvent A and methanol as solvent B both containing 0.1% ammonium hydroxide (25%) and 10 mmol/L ammonium acetate. A gradient elution started with 15% B and a linear increase to 51% B until 0.1 min, followed by an increase to 61% B until 4.0 min and further to 74% B at 5.2 min. The column was washed from 5.3 to 6.0 min with 100% B and re-equilibrated at 15% B for 1 min. For most of the analytes stable isotope labeled internal standards were added prior to acetonitrile precipitation. Bile samples corresponding to 100 nL were subjected to analysis. β- and ω-Muricholic acid peaks could not be resolved and the sum of both bile acids was determined instead.

2.5.14. Lipidomics

Lipidomics measurements were performed in collaboration with Marcus Höring and Gerhard Liebisch (Institute of Clinical Chemistry and Laboratory Medicine, University Hospital Regensburg). Samples were subjected to lipid extraction in presence of internal standards as described previously (Höring et al. 2021). The following lipid species were added as internal standards: PC 14:0/14:0, PC 22:0/22:0, PE 14:0/14:0, PE 20:0/20:0 (di-phytanoyl), PS 14:0/14:0, PS 20:0/20:0 (di-phytanoyl), PI 17:0/17:0, LPC 13:0, LPC 19:0, LPE 13:0, SM 18:1;O2/12:0, Cer 18:1;O2/14:0, Cer 18:1;O2/17:0, GlcCer 18:1;O2/12:0, GlcCer 18:1;O2/17:0, D7-FC, CE 17:0, CE 22:0, TG 51:0, TG 57:0, DG 28:0 and DG 40:0. The following sample amounts were used: 10 µl plasma, tissue homogenates representing a wet weight of 2 mg, bile 100 nL (or 500 nL for phospholipase activity assays). Dried chloroform residues were dissolved in either in 10 mM ammonium acetate in methanol/chloroform (3:1, v/v) (for low mass resolution tandem mass spectrometry) or chloroform/methanol/2-propanol (1:2:4 v/v/v) with 7.5 mM ammonium formate (for high resolution mass spectrometry).

Quantification of lipids was performed by direct flow injection analysis (FIA) using a triple quadrupole mass spectrometer (FIA-MS/MS; QQQ triple quadrupole) and a hybrid quadrupole-Orbitrap mass spectrometer (FIA-FTMS; high mass resolution). FIA-MS/MS was carried out in positive ion mode using the analytical setup and strategy described previously (Liebisch et al. 2004). The fragment ions of m/z 184 and m/z 264 were used for lysophosphatidylcholine (LPC) (Liebisch et al. 2004) and sphingosine-based ceramides (Cer)/hexosylceramides (HexCer) (Liebisch et al. 1999), respectively. The following neutral losses were applied: Phosphatidylethanolamine (PE), m/z 141; phosphatidylserine (PS), m/z 185; phosphatidylglycerol (PG), m/z 189; phosphatidylinositol (PI), m/z 277 (Matyash et al. 2008). PE-based plasmalogens

(PE P) were analyzed according to the principles described by Zemski-Berry (Zemski Berry and Murphy 2004). Quantification was achieved by calibration lines generated by addition of naturally occurring lipid species to the respective sample matrix. Calibration lines were generated for the following naturally occurring species: PC 34:1, 36:2, 38:4, 40:0 and PC O-16:0/20:4; SM 18:1;O2/16:0, 18:1, 18:0; LPC 16:0, 18:1, 18:0; PE 34:1, 36:2, 38:4, 40:6 and PE P-16:0/20:4; PS 34:1, 36:2, 38:4, 40:6; Cer 18:1;O2/16:0, 18:0, 20:0, 24:1, 24:0; FC, CE 16:0,18:2,18:1,18:0. The FIA-FTMS setup was described in detail previously (Höring et al. 2021). Triglycerides (TG), diglycerides (DG) and cholesteryl ester (CE) were recorded in positive ion mode FTMS in range m/z 500–1000 for 1 min with a maximum injection time (IT) of 200 ms, an automated gain control (AGC) of 1×10^6, three microscans and a target resolution of 140,000 (at m/z 200). Phosphatidylcholine (PC), sphingomyelin (SM) were measured in range m/z 520-960. Multiplexed acquisition (MSX) was used for the $[M+NH_4]^+$ of free cholesterol (FC) (m/z 404.39) and D7-cholesterol (m/z 411.43) 0.5 min acquisition time, with a normalized collision energy of 10%, an IT of 100 ms, AGC of 1×10^5, isolation window of 1 Da, and a target resolution of 140,000 (Höring et al. 2019).

Data were processed as described previously (Höring et al. 2021). The extracted data were exported to Microsoft Excel 2016 and further processed by self-programmed Macros. FIA-FTMS quantification was performed by multiplication of the spiked IS amount with analyte-to-IS ratio. Labeled complex lipids were analyzed at the respective accurate m/z and quantified using the respective internal standard. Lipid species were annotated according to the latest proposal for shorthand notation of lipid structures that are derived from mass spectrometry (Liebisch et al. 2020). For QQQ analysis, glycerophospholipid species annotation was based on the assumption of even numbered carbon chains only. Cer and HexCer species annotation assumes that a sphingoid base with two hydroxyl groups is present.

2.5.15. Quantification and statistical analysis

All statistical parameters, including the number of replicates (n) and the type of tests used, can be found in the figure legends. Statistical analyses were performed using OriginPro 2021 and Microsoft Excel 2016 software. Results were considered to be significant for $p < 0.05$ where p represents either the uncorrected or FDR corrected p-value. For labeled and unlabeled lipid time profile comparison, area under the curve (AUC) was calculated as the sum of mean values measured at each time point. Statistical significance of the difference between time profiles in the three mouse groups was assessed with repeated measured ANOVA analysis (fitrm function in MatLab 2019b). P-values were adjusted for multiple hypotheses testing with Benjamini-Hochberg procedure (mafdr function in MatLab 2019b with ('bhfdr', 1) parameter). For volcano plots (Figure 21D, E), lipid species concentrations from all measured lipid classes were included in the analysis. Missing values were replaced by 1/5 of the smallest non-zero value of each lipid species. All data were $\log_2$ transformed, averages and $\log_2$ fold changes were calculated and statistical significance was determined by unpaired t-tests with unequal variance. FDR

correction by the Benjamini-Hochberg procedure was applied to the p-value cut-offs (FDR 5%). Sample sizes were estimated according to previous experience. Samples were removed as outliers due to obvious technical problems or after performing Grubbs' test for outliers.

2.5.16. BioRender

The following figures were fully or partially created with BioRender.com: Figure 1, Figure 3, Figure 5, Figure 24, Figure 26, and Figure 34.

3. RESULTS

3.1. IMPACT OF THE GUT MICROBIOTA ON DIETARY LIPID UPTAKE AND METABOLISM

To investigate the impact of gut microbial colonization on dietary lipid absorption and metabolism *in vivo*, a stable-isotope labeling approach using three differentially colonized mouse models was employed (Figure 5): Besides germ-free (GF) mice harboring no microbiota, and specific-pathogen-free (SPF) mice with a natural microbial diversity, mice colonized with the Oligo-Mouse-Microbiota (OMM[12]) consortium were also included in the experiments.
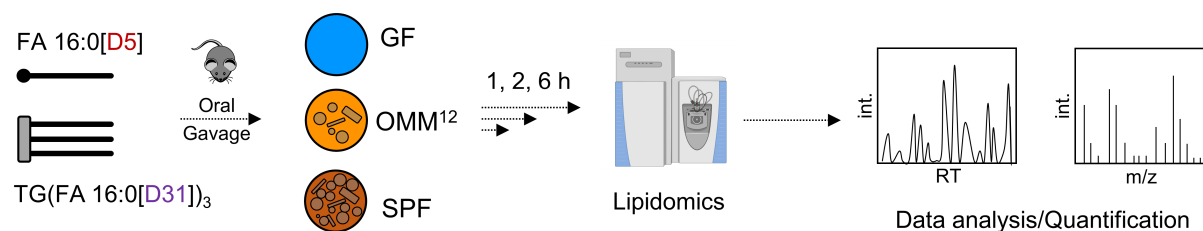

Figure 5. **Experimental setup to quantify dietary lipid uptake into peripheral tissues in the different mouse models**

OMM[12] mice are stably colonized with a minimal consortium of 12 bacterial strains encompassing members of the major bacterial phyla in the murine gut including Bacteroidetes and Firmicutes (Brugiroux et al. 2016). Certain confounding factors of the SPF model such as the natural microbial variability or the differences in housing conditions compared to GF mice are negated in the OMM[12] model. Still, the OMM[12] consortium cannot recapitulate the full functional spectrum of an SPF microbiota. For example, bacterial species capable of secondary bile acid production are absent in this model (Studer et al. 2016) and cecal size is not completely normalized to that of SPF mice. Therefore, OMM[12] colonization should be considered an intermediary model between GF and SPF mice.

Mice from all three groups were starved for 2 h and then orally gavaged with an equimolar mixture (based on FFA content) of deuterium-labeled palmitic acid (FA 16:0[D5]) and tripalmitin (TG (16:0[D31])$_3$). Absorption and metabolism of D5/D31 labeled FA in plasma, liver, fat tissues, intestinal tissues and contents was quantified after 1, 2, and 6 h using gas-chromatography coupled to mass-spectrometry (GC-MS). Integration of the labeled FA into different lipid species was measured using high resolution mass spectrometry (HR-MS).

3.1.1. Lipid uptake into plasma and WAT is reduced in colonized mice

Uptake of the labeled FA into plasma was significantly reduced in colonized mice compared to GF mice after 1 h, with a peak in plasma concentrations occurring after 1–2 h (Figure 6A). Area under the curve (AUC) calculations in plasma showed ~1.5-fold higher amounts in OMM[12] vs. SPF mice and ~2.3–2.7-fold higher amounts in GF vs. SPF mice.
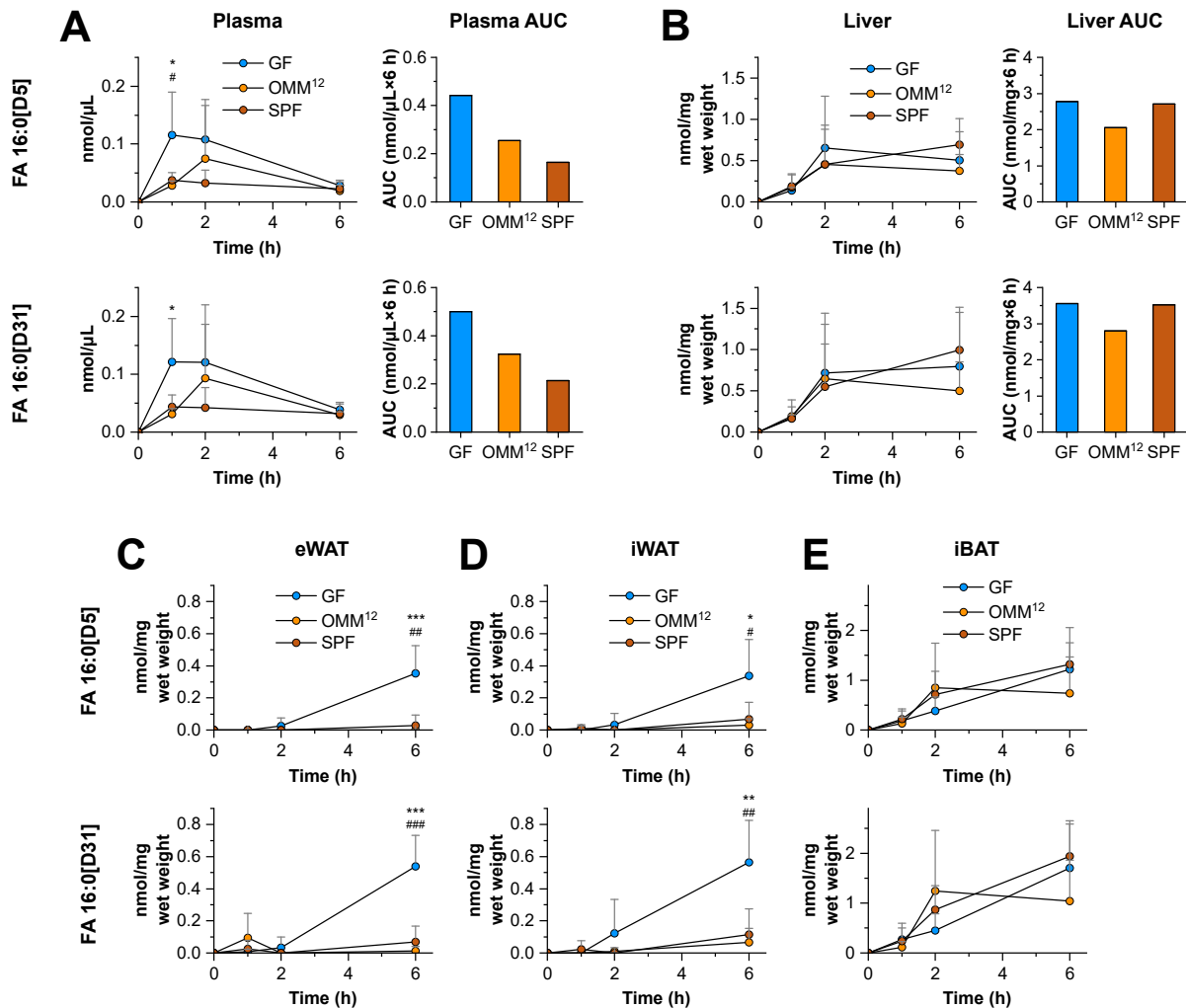
Figure 6. The gut microbiota reduces systemic lipid uptake in plasma and white adipose tissue

Concentrations of FA 16:0[D5] and FA 16:0[D31] in plasma (A), liver (B), eWAT (C), iWAT (D), and iBAT (E) at 1, 2, and 6 h post-gavage. Area under the curve (AUC) is calculated for plasma (A) and liver (B). Data are shown as mean ± SD of n = 4–5 per time point. */#/$p < 0.05, **/##/$$p < 0.01, ***/###/$$$p < 0.001 after one-way ANOVA with Tukey post-hoc test. * GF vs. OMM[12], # GF vs. SPF, $ OMM[12] vs. SPF.

Labeled FA concentrations in the liver (Figure 6B) increased over the 6 h time course, but with no significant differences between the groups and the AUCs.

In line with the observations in plasma, uptake of deuterated palmitic acid into epididymal and inguinal white adipose tissues (eWAT, iWAT) was also significantly increased in GF vs. colonized mice, with the labeled FA reaching the adipose tissues

after 6 h (Figure 6C–D). Interestingly, interscapular brown adipose tissue (iBAT) showed a much faster and higher accumulation of the labeled FA, independent of mouse colonization, underlining the functional differences between white and brown adipose tissue (Figure 6E).
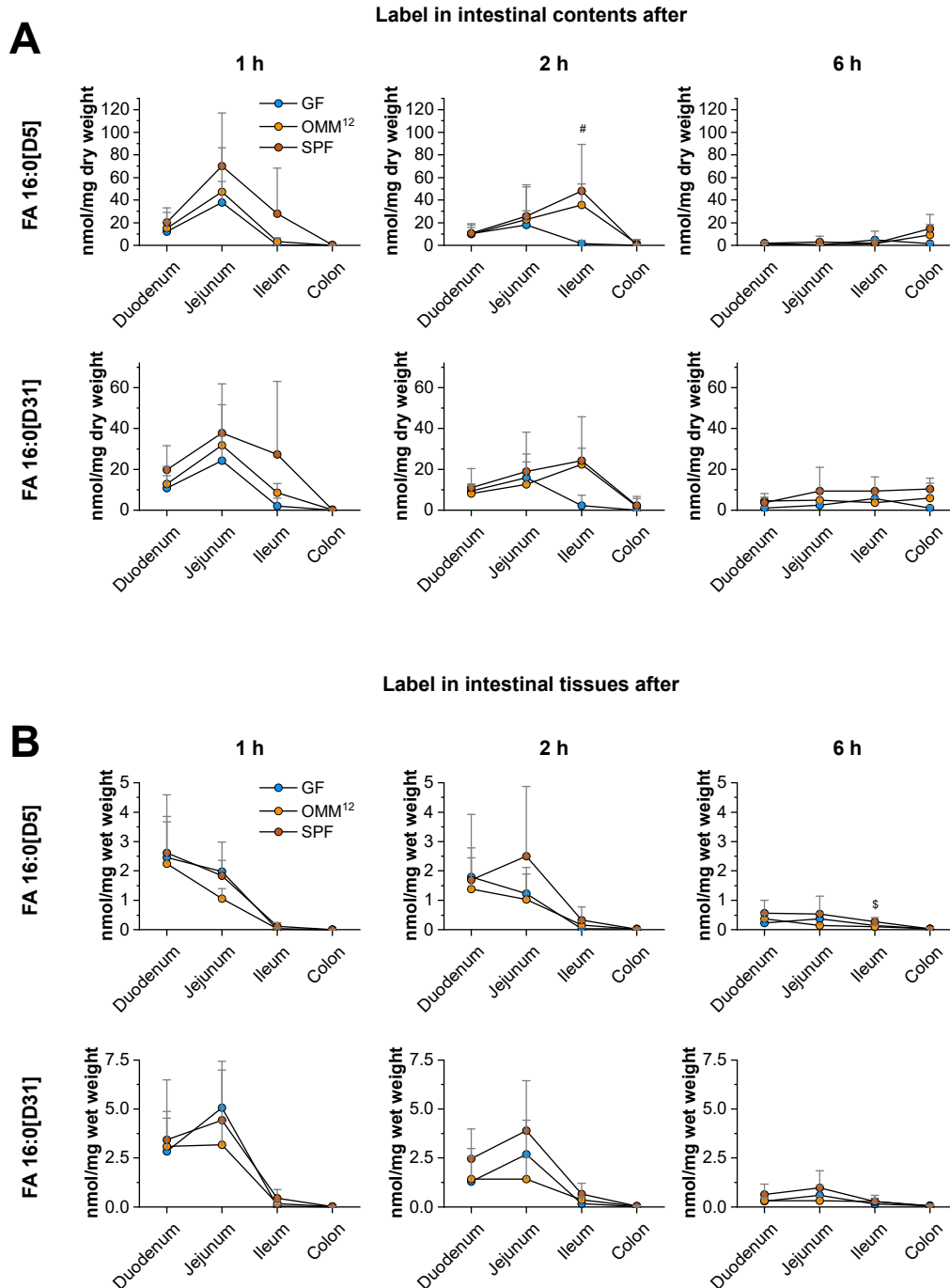
Figure 7.   Distribution of labeled FA in intestinal tissue and content sections after the lipid gavage
Concentrations of FA 16:0[D5] and FA 16:0[D31] in intestinal contents (A) and intestinal tissue sections (B) after 1, 2, and 6 h. Data are shown as mean ± SD of n = 4–5 per gut section. */#/$p < 0.05 after one-way ANOVA with Tukey post-hoc test. * GF vs. OMM[12], # GF vs. SPF, $ OMM[12] vs. SPF.

Concentrations of the free fatty acid FA 16:0[D5] and FA 16:0[D31] released from TG (16:0[D31])$_3$ were comparable in the analyzed tissues and showed the same patterns depending on the microbiota. This indicated that the hydrolysis of TG by PNLIP, which is a requirement for FA 16:0[D31] but not for FA 16:0[D5] uptake, was not altered by microbial colonization status.

In agreement with the reduced uptake in plasma and white adipose tissue of colonized mice (Figure 6A, C, D), intestinal contents and tissues of those mice exhibited higher label concentrations (Figure 7A, B). Especially the contents of more distal segments like ileum and colon showed increased concentrations of FA 16:0[D5] and [D31], with significantly more FA in the ileal content of SPF vs. GF mice after 2 h (Figure 7A). This was likely due to the lower uptake of lipids in the proximal segments of the SI in colonized mice, allowing them to reach the ileum and colon. In contrast, labeled FA in GF mice were mostly absorbed before reaching the ileum. The observed concentration distribution of labeled FA 16:0 along the SI tissue sections (Figure 7B) confirmed that the duodenum and jejunum act as the major sites of lipid absorption, in contrast to the ileum. These data are in good accordance with observations from another study, showing that in WT SPF mice, the highest label concentrations are found in the proximal 50% of the SI 2 h after an olive oil gavage containing radiolabeled triolein (Wang et al. 2016).

3.1.2. Elongation of labeled FA 16:0[D5/31] is observed in most tissues

The fatty acid elongase ELOVL6 catalyzes the first and rate-limiting step of long-chain fatty acid elongation, converting FA 16:0[D5/D31] into the 18-carbon fatty acid FA 18:0[D5/31]. These elongation products were detected in plasma and liver (Figure 8A, B), as well as in iBAT, SI gut contents and intestinal tissues (Supplemental Figure 1A–C).

No elongation products could be detected in WAT and colon content, either due to their very low concentrations or because of them only appearing at later time points than 6 h.
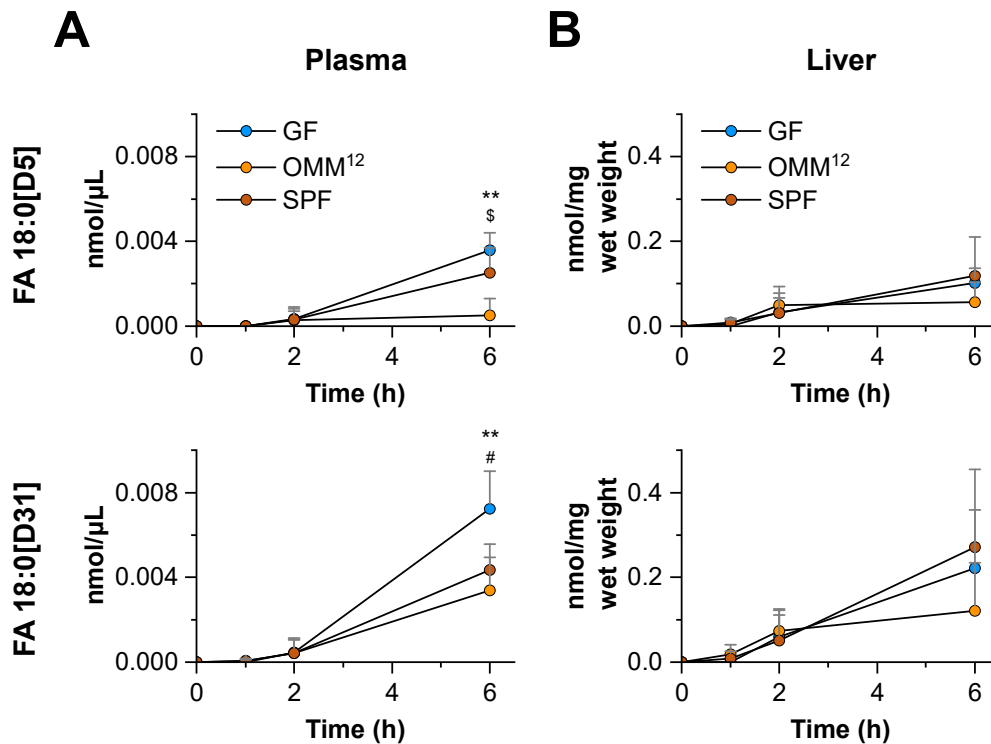
Figure 8. Elongated FA 18:0[D5/31] detected in plasma and liver after the oral lipid gavage

Concentrations of FA 18:0[D5] and FA 18:0[D31] in plasma (A) and liver (B), at 1, 2, and 6 h post-gavage. Data are shown as mean ± SD of n = 4–5 per time point. */#/$p < 0.05, **/##/$$p < 0.01 after one-way ANOVA with Tukey post-hoc test. * GF vs. OMM[12], # GF vs. SPF, $ OMM[12] vs. SPF.

3.1.3. Dietary FA are integrated into TG and PC species of plasma, liver, WAT and intestinal tissues

To reveal into which lipid species the stable isotope tracers FA 16:0[D5/31] are integrated, we performed a quantitative lipidome analysis using HR-MS. A total of 436 unique lipid species were detected (Figure 9). The measurements revealed that the labeled FA were integrated into TG and PC species in plasma, liver, and intestinal tissues, as well as in TG species in adipose tissues (Figure 9, Figure 10A–C). Due to a systematic peak overlap and insufficient resolving power of the mass spectrometer, the D5 labeled TG and PC species could not be accurately quantified and have been omitted from this analysis. Only D31 labeled species are shown.

Figure 9.   Heat map showing differences in lipid species and classes in the analyzed tissues between GF, OMM[12] and SPF mice
Depicted are AUC fold changes from the 6 h time course of the experiment after oral gavage of the stable isotope labeled lipids for GF vs. OMM[12] and GF vs. SPF (n =4–5). Lipid species are sorted by lipid class, the number of analyzed lipid species per class is indicated in brackets. Only fold-changes for lipid species passing the threshold of p-value < 0.1 after repeated ANOVA measures are shown in color. The figure was prepared in collaboration with Maria Zimmermann-Kogadeeva (EMBL, Heidelberg).

In plasma (Figure 10A), the majority of labeled FA was integrated into TG species, peaking after 1–2 h and resembling the uptake curve of total labeled FA (Figure 6A). A minor part also began to arise in PC species after 2–6 h (Figure 10A). In both cases, significantly less labeled lipid species were found in the colonized mice compared to GF. The different time courses for integration into TG vs. PC species are reflecting the canonical path of absorbed dietary lipids: After uptake into enterocytes, FFA are re-esterified as TG and secreted into the circulation packaged into CM, peaking in the plasma after the meal ingestion. LPL then releases FFA from those TG in peripheral tissues, making them available for the integration in other lipid species like PC. It is plausible that the labeled PC appearing in the plasma after 2–6 h could originate from the liver, which would secrete PC as part of the membranes of hepatically produced lipoproteins. Fittingly, the plots of total PC[D31] in plasma and liver showed a strong similarity (Figure 10A, B).

Figure 10. Quantitative lipidome analysis reveals the integration of labeled FA into TG and PC species of plasma, liver and adipose tissue
Sum of all TG and PC species harboring one FA 16:0[D31] moiety, denoted as total TG[D31] and total PC[D31], in plasma (A), liver (B), and adipose tissue (C) at 1, 2, and 6 h post-gavage. Data are shown as mean ± SD of n = 4–5 per time point. */#/$p < 0.05, **/##/$$p < 0.01 after one-way ANOVA with Tukey post-hoc test. * GF vs. OMM[12], # GF vs. SPF, $ OMM[12] vs. SPF.
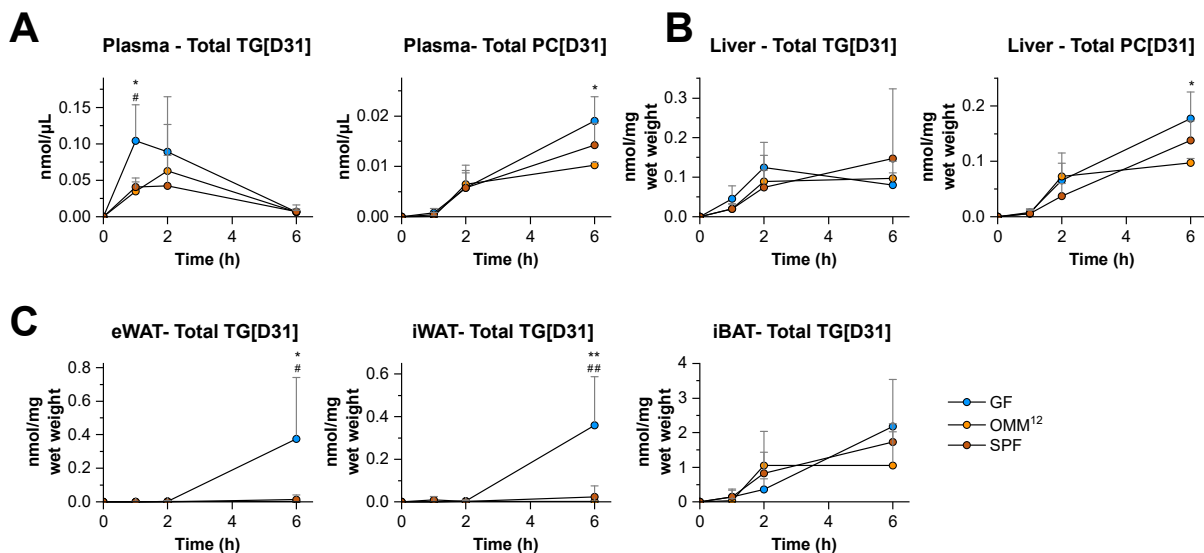
In liver tissue (Figure 10B), no strong differences between the label integration into TG vs. PC could be observed and only TG[D31] species were detected in the adipose tissues (Figure 10C). This was not surprising, granted that TG are by far the dominating lipid subclass in both WAT and BAT (Hoene et al. 2014).

In conclusion, these data show that the gut microbiota alters both luminal and systemic contents of stable isotope labeled FA by reducing uptake of dietary lipids into the circulation. In most of the measurements, labeled lipid concentrations in OMM[12] mice were found to be between that of GF and SPF mice. This again confirms the role of the OMM[12] bacterial consortium as an "intermediary model" between the germ-free state and the native microbial ecosystem.

3.2. THE MICROBIOTA LIMITS ABSORPTION FROM THE LUMEN INTO INTESTINAL TISSUE

To pinpoint the step of the dietary lipid uptake process which is altered by the gut microbiota, a physiology-based kinetic multi-compartment model of *in vivo* FA flux and metabolism was set up in collaboration with Maria Zimmermann-Kogadeeva and Michael Zimmermann (EMBL, Heidelberg) (Zimmermann et al. 2019). The model consisted of 11 compartments (intestinal lumen and tissues, plasma, liver, fat tissues) for which time dependent FA 16:0[D5] and FA 16:0[D31] concentrations were available (Figure 11A). Concentrations were converted into absolute amounts using estimated compartment volumes (Supplemental Table 1). Six model parameters were defined to describe the lipid flux between the compartments: k_{p1} and k_{p2} representing the gastrointestinal flow in the small and large intestine, k_{abs} describing the FA absorption from the lumen into the epithelium and further into blood, k_{hep} and k_{stor} for FA

distribution from blood into liver and adipose tissues, as well as k_e for transport into all other tissues. First, a basic model with six parameters was build, assuming no microbiome impact on the flux parameters. Parameters for FA 16:0[D5] and FA 16:0[D31] were assumed to be the same. The model was therefore fit to the combined data from all three mouse groups for both FA 16:0[D5] and [D31] simultaneously.
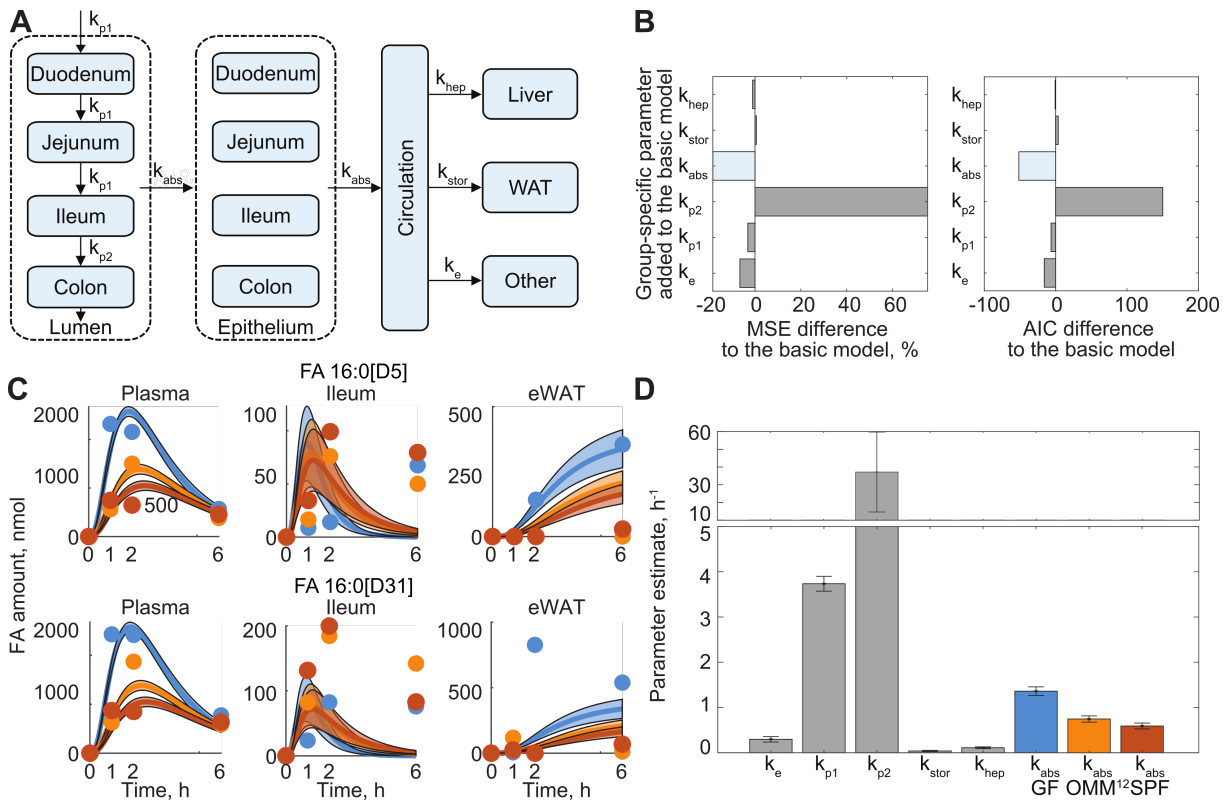
Figure 11. A physiology-based kinetic multi-compartment model shows that the gut microbiota limits intestinal lipid absorption from the lumen

(A) Model scheme showing the 11 different compartments and 6 parameters k_i describing the lipid flux between the compartments.

(B) Improvement of the mouse group-specific models over the basic model was measured using mean squared error (MSE) reduction and Akaike information criterion (AIC) difference. For each of the group-specific models, one of the six parameters k_i was set to be microbiome dependent, i.e. was further subdivided into three parameters k_i GF, k_i OMM[12] and k_i SPF. The parameter for which the group-specific model best outperforms the basic model is highlighted in light blue.

(C) Fit of the best group-specific model (with microbiome specific k_{abs} parameter) to the FA amounts in plasma, ileum tissue and eWAT over time. The model was fitted to data from all three mouse groups (GF, OMM[12], SPF) for both FA 16:0[D5] and [D31] simultaneously.

(D) Parameter estimates for the best group-specific model. The microbiome specific k_{abs} parameters are colored.

The figure was prepared in collaboration with Maria Zimmermann-Kogadeeva (EMBL, Heidelberg).

To then elucidate the impact of the microbiome on the FA flux between host compartments, one by one, each of the six model parameters was further subdivided into three microbiome specific parameters. The parameters were then fit to the same data as for the basic model (Figure 11B). Comparing the six group-specific models, the most substantial model improvement was achieved by setting the intestinal

absorption parameter k_{abs} as microbiome specific (mean squared error reduction > 20%, Akaike information criterion difference > 50 compared to the basic model).

The k_{abs} group-specific model was able to accurately predict the kinetics of FA 16:0[D5] and [D31] flux in most tissues (Figure 11C). Confirming our observations from GC-MS based total FA analysis (Figure 6A), the intestinal absorption coefficient k_{abs} was twofold higher in GF than in OMM[12] or SPF mice (Figure 11D).

In summary, the kinetic multi-compartment model revealed that the microbiota reduces FA absorption from intestinal lumen into enterocytes, leading to the observed differences in FA profiles across tissues in the three mouse groups.

3.3. THE ROLE OF INDIVIDUAL BACTERIAL SPECIES IN INFLUENCING LIPID UPTAKE

While colonization with the complex SPF microbiota reduced absorption of the stable isotope tracers the most, the OMM[12] minimal microbial consortium showed an attenuated effect between that of GF and SPF mice (Figure 6, Figure 7). These findings raised the interesting question of the contribution of individual bacterial species to the observed phenotype. By adding or removing single bacterial species from the OMM[12] consortium, such effects can be conveniently studied. *Akkermansia muciniphila*, a gram-negative, mucin degrading bacterium from the phylum of Verrucomicrobia, was selected as a showcase for further experiments.

A. muciniphila is part of the OMM[12] consortium and was chosen because its abundance was inversely associated with overweight, obesity, plasma lipid levels and lipid storage (Cani and Vos 2017; Depommier et al. 2019). Furthermore, *A. muciniphila* was reported to be the major colonizer in the small intestine of OMM[12] mice, with an average relative abundance of ~64% as determined by 16S rRNA amplicon sequencing (Wyss et al. 2019).

To study the role of *A. muciniphila* in reducing dietary lipid uptake in the setting of the OMM[12] consortium, mice were stably colonized with the remaining 11 bacterial species, forming the newly created OMM[11] consortium. OMM[11] mice were generated by Marijana Basic (MHH, Hanover). Then, stable-isotope lipid tracing experiments comparing GF, OMM[11] and OMM[12] mice were carried out.

3.3.1. *A. muciniphila* is consistently colonizing OMM[12] mouse small intestine and is absent in OMM[11] mice

To confirm if *A. muciniphila* was consistently colonizing in the SI of the OMM[12] mice, and to analyze changes in absolute bacterial abundances upon removal of *A. muciniphila* in OMM[11] mice, bacterial abundances in intestinal contents of OMM[11] and OMM[12] mice were quantified by qPCR in collaboration with Anna Weiß and Bärbel Stecher (Max von Pettenkofer-Institut, LMU Munich). *A. muciniphila* was found in all colon contents, as well as in most duodenum, jejunum and ileum contents of OMM[12] mice (Figure 12), albeit at lower relative abundances than those reported in the literature (Wyss et al. 2019). Its non-detection in some of the OMM[12] samples is likely

due to difficulties in collecting enough bacterial material for the analysis, corroborated by the low copy numbers in those samples. Especially the proximal SI has a relatively low bacterial abundance compared to ileum and colon, making the reliable collection of bacterial material challenging. As expected, no *A. muciniphila* was detected in any of the OMM[11] samples.
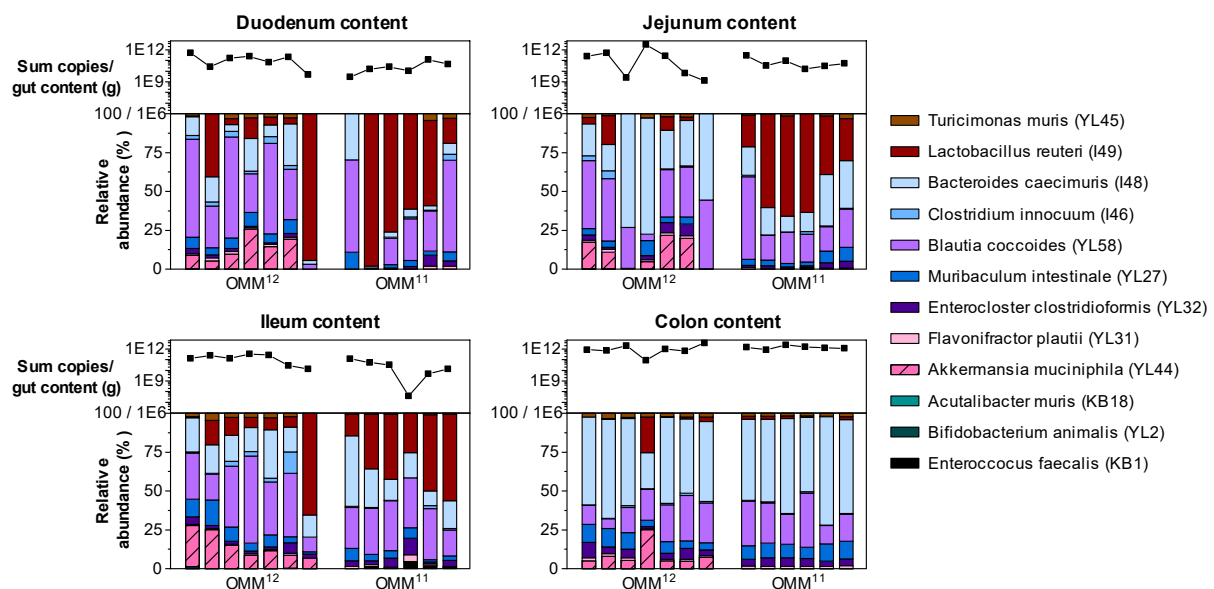
Figure 12. Gut microbial load and composition in the intestinal segments of OMM[12] vs. OMM[11] mice
Microbial composition (lower panel parts) and total abundance (upper panel parts) was determined by qPCR of 16S rRNA genes of n = 6–7 per group. *A. muciniphila* is highlighted by hatching.

3.3.2. Removal of *A. muciniphila* from the OMM[12] consortium drives lipid absorption closer to a GF phenotype

GF, OMM[11] and OMM[12] mice were gavaged with FA 16:0[D5] and FA 16:0[D31] to investigate potential differences in lipid absorption after removal of *A. muciniphila* from the consortium. 1 h after tracer administration, FA uptake into plasma and liver was significantly reduced in colonized mice compared to GF in agreement with the previous experiment in GF, OMM[12] and SPF mice (Figure 6). In addition, lipid uptake showed a trend of GF > OMM[11] > OMM[12], suggesting that the removal of *A. muciniphila* from OMM[12] drives lipid uptake more towards the GF phenotype.
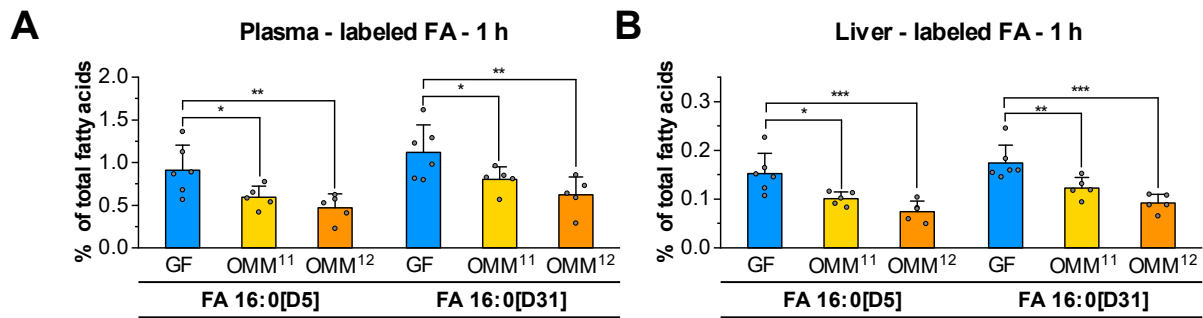
Figure 13. Reduced uptake of labeled lipids in plasma and liver of OMM[11] and OMM[12] mice compared to GF
FA 16:0[D5] and FA 16:0[D31] contents in plasma (A) and liver (B) of GF, OMM[11] and OMM[12] mice 1 h after the oral lipid gavage. Data are shown as mean ± SD of n = 5–6. *$p < 0.05$, **$p < 0.01$, ***$p < 0.001$ after one-way ANOVA with Fisher LSD post-hoc test.

3.3.3. Individual and total bacterial abundances are not altered in intestinal contents of OMM[11] vs. OMM[12] mice

Alterations not only in relative but also in absolute bacterial abundances after removal of *A. muciniphila* might explain the observed trend towards higher lipid absorption in OMM[11] vs. OMM[12] mice (Figure 13).

Therefore, individual species abundances as well as the total bacterial load in intestinal segments of OMM[11] and OMM[12] mice were determined by qPCR (Figure 14). However, significant alterations could neither be observed in individual (Figure 14A) nor total bacterial abundances (Figure 14B). The space left by *A. muciniphila* appeared to stay unoccupied, with no other species increasing their abundance in OMM[11] mice. This could be expected, given that *A. muciniphila* grows in the very specific mucin niche, which could not be easily occupied by other bacterial species.

Whether the increased lipid absorption in OMM[11] mice compared to OMM[12] is explained due to a mechanism unique to *A. muciniphila* or whether the same effect could also be replicated by removing other species, is not yet clear. In future experiments, stepwise removal of more species from the OMM[11] consortium might reveal if this translates into a gradual increase in lipid absorption towards GF levels. Since SPF mice have an even greater bacterial richness and absorb less dietary lipids than OMM[12] mice, a relationship between these two factors is plausible.

All in all, observations from the OMM[11] model confirm that (A) the gut microbiota reduces dietary lipid uptake compared to GF mice and (B) this effect can be modulated by changing the bacterial composition.
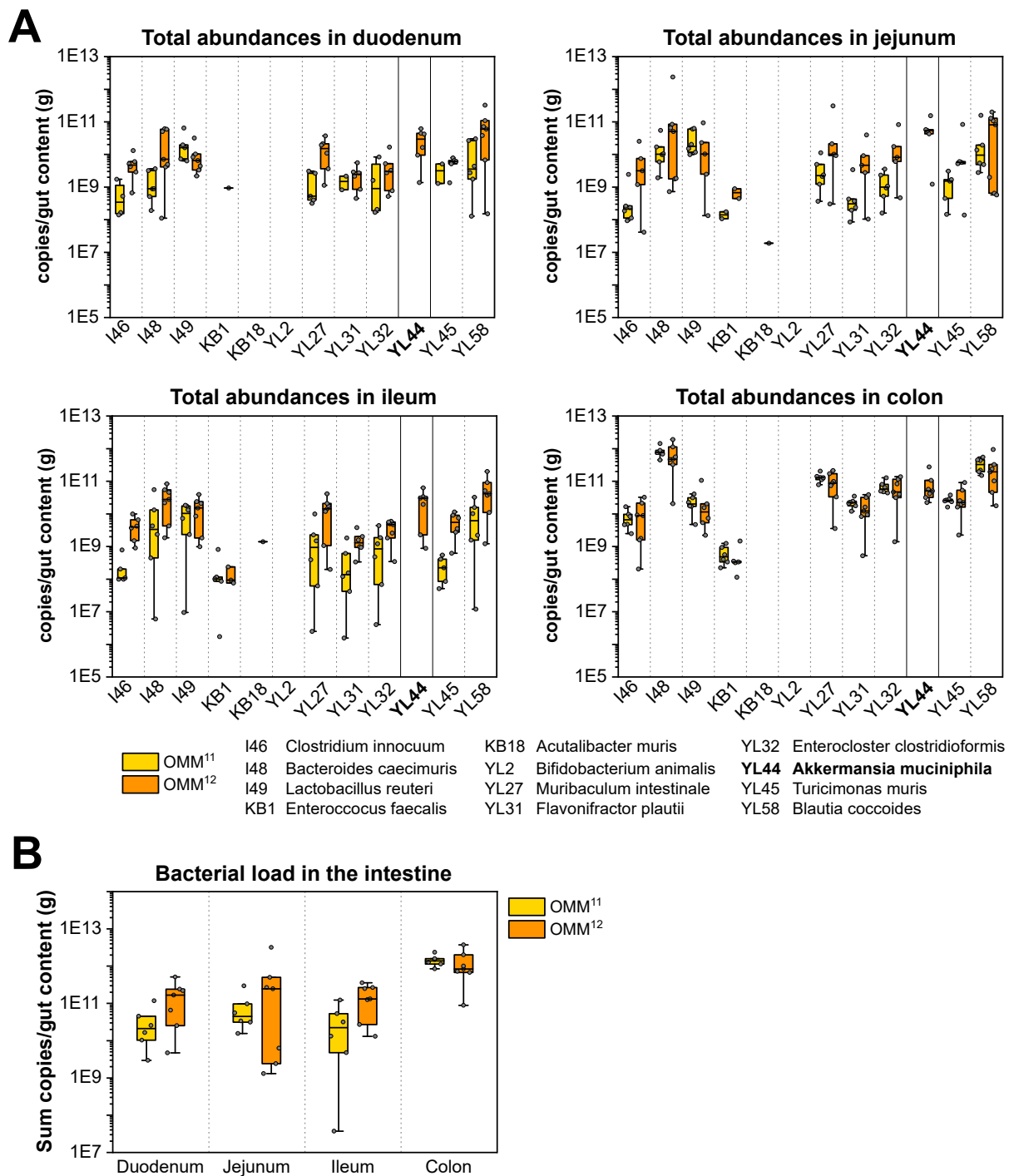
Figure 14. Individual and total bacterial abundances are not altered in intestinal contents of OMM[11] vs. OMM[12] mice

Quantification of individual bacterial abundances (A) as well as total bacterial abundance (B) in the intestinal sections of OMM[11] and OMM[12] colonized mice by qPCR of 16S rRNA genes of n = 6–7 per group. *Akkermansia muciniphila* (YL44) is highlighted in (A). Whiskers are drawn within the 1.5 interquartile range (IQR) value. No significant differences between OMM[11] and OMM[12] after two-sided t-test with unequal variance and Benjamini-Hochberg FDR correction (A) or Mann–Whitney *U* test (B).

3.4. POTENTIAL MECHANISMS FOR GUT MICROBIAL REDUCTION OF LIPID UPTAKE

The physiology-based kinetic multi-compartment modeling showed that the gut microbiota affects intestinal lipid absorption by reducing uptake from the gut lumen into enterocytes. Therefore, processes related to this first step of lipid resorption (Figure 15) were further investigated to elucidate a gut microbial mechanism of action.

A potential alteration of pancreatic lipase activity by the gut microbiota (Figure 15A) could already be excluded as discussed earlier (chapter 3.1.1). Thus, the focus was set on studying microbial influences on the gastrointestinal flow (B), FA transporter expression (C), the mucus layer (D) and bile contents relevant for dietary lipid emulsification (E).
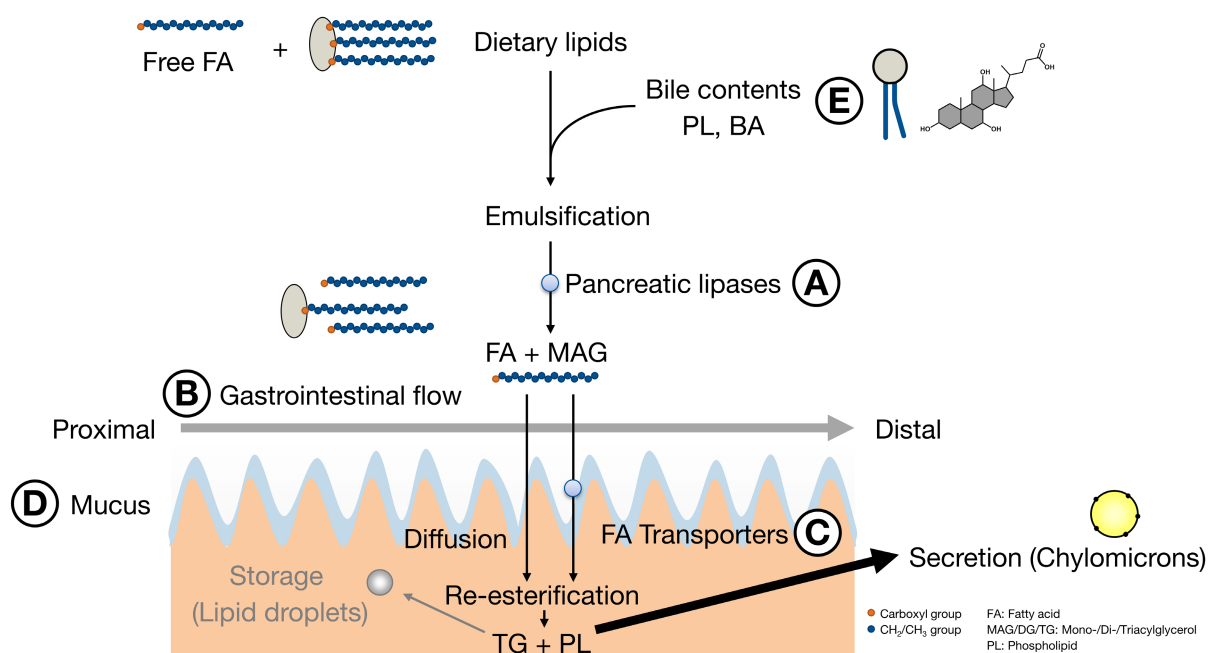
Figure 15. Steps of the lipid uptake process potentially altered by the gut microbiota
(A) Pancreatic lipase activity, (B) Gastrointestinal flow, (C) FA transporter expression, (D) Mucus layer, (E) Bile contents relevant for dietary lipid emulsification.

3.4.1. The gastric flow is not altered by the microbiota

Intestinal motility and the associated transit time in the gastrointestinal tract are important physiological factors that influence the extent to which nutrients from food can be digested and absorbed. It was reported that the intestinal transit speed was reduced in GF mice compared to mice with a normal intestinal microbiome (Abrams and Bishop 1967). Studies in rats revealed a reduction in myoelectric activity, causal for the prolonged transit time in GF mice (Husebye et al. 1992, 1994). However, in two recent publications studying the impact of microbiota on lipid absorption, the authors did not see any significant effects of the intestinal microbiome on SI transit time (Sato et al. 2016; Martinez-Guryn et al. 2018). Considering these contradictory data, the gastrointestinal flow under the experimental conditions of the stable isotope lipid gavage (Figure 5) was determined (Figure 16).

**Evans blue -
SI transit - 12.5 min**
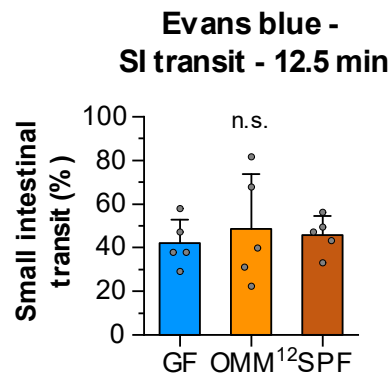
Figure 16. Gastric flow in the small intestine of GF, OMM¹² and SPF mice
Gastric flow was determined by gavaging mice with the non-absorbable Evans Blue dye (50 mg/mL) suspended in 100 µL of olive oil. Shown is the percentage of the total SI length which was colored 12.5 min post-gavage. Data are shown as mean ± SD of n = 5. n.s. = not significant by one-way ANOVA with Tukey post-hoc test.

No significant differences were observed between the gastric flow in GF, OMM¹² and SPF mice. The dye front passed ~40–50% of the small intestine within 12.5 min. In agreement with these findings, when the k_{p1} parameter representing small intestinal label propagation was set to be group-specific in the kinetic multi-compartment model (Figure 11B), only a marginal model improvement was achieved (MSE error reduction ~3%, AIC difference ~6 compared to the basic model).

Thus, the microbiota does not alter gastric flow under the experimental conditions of the oral lipid gavage and does therefore not influence dietary lipid uptake via this mechanism.

3.4.2. Expression of FA transporters did not change 1 h after the stable-isotope lipid gavage

Transport of dietary lipids into enterocytes can occur either by passive diffusion or via a protein-mediated transport as discussed in chapter 1.1.2. To answer the question whether the gut microbiota alters the expression of putative FA transporters, the mRNA expression levels of *Cd36* and *Fatp4* were determined in SI sections after 1 h and 2 h of labeled lipid gavage (Figure 17).
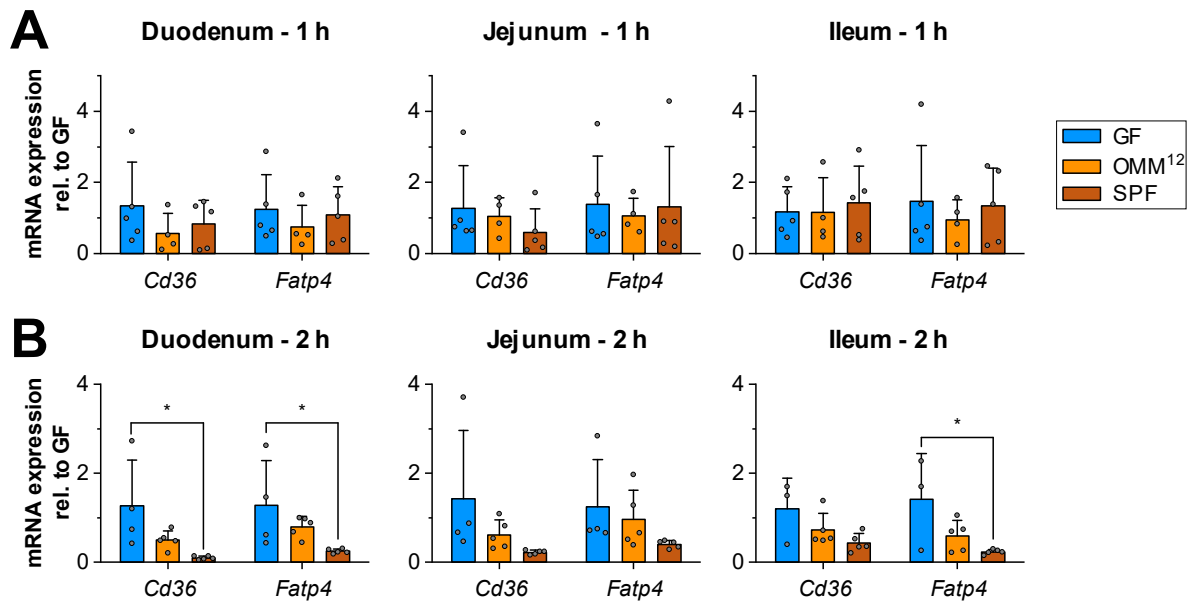
Figure 17. mRNA expression of the FA transporters *Cd36* and *Fatp4* in the small intestine of mice 1 h and 2 h post-gavage of the labeled lipids

Expression levels were determined by qPCR and are shown relative to the expression in GF animals (n = 3–5). *$p < 0.05$ by one-way ANOVA with Tukey post-hoc test.

Expression of *Cd36* and *Fatp4* was not changed after 1 h (Figure 17A), whereas FA transporter expression was significantly reduced in SPF colonized vs. GF mice after 2 h in duodenum and ileum, with the same trend in jejunum (Figure 17B).

It has been described in the literature, that intestinal FA transporter levels are altered upon dietary lipid consumption. *Cd36* expression is increased via the gut hormones glucagon-like peptide-2 (GLP-2) (Hsieh et al. 2009), CCK (Demenis et al. 2017) as well as secretin (Sekar and Chow 2014). Further, both *Cd36* and *Fatp4* expression is under the control of peroxisome proliferator-activated receptor γ (PPARγ) (Li et al. 2022), which is activated by lipids. Therefore, the higher lipid absorption in GF mice might upregulate FA transporter expression 2 h after the lipid gavage (Figure 17B).

Of note, the importance of active FA transport for dietary lipid uptake is still controversially discussed in the literature (see chapter 1.1.2). One recent publication even found that FA do not need active protein transporters to cross the enterocyte membrane and are instead taken up solely by passive diffusion (Jay et al. 2020). Additionally, the *Cd36* and *Fatp4* expression changes were only observed 2 h after the lipid gavage. However, the majority of stable isotope labeled lipids reached the circulation 1 h after the gavage (Figure 6A).

Overall, although the expression of FA transporters changed after 2 h depending on gut microbial colonization, it is likely a reaction to the already increased lipid uptake in GF vs. SPF mice. In the fasted state and up to 1 h after the lipid bolus, no changes in expression were observed. Therefore, and given the controversial role of FA transporters in the literature, these findings do not explain the microbial impact on dietary lipid uptake.

3.4.3. Adherent mucus thickness in the jejunum of GF mice is reduced

Intestinal mucus secreted by goblet cells forms a dense polymeric network and acts as an important barrier and first line of defense in the gut. It protects the host against infiltration by pathogenic bacteria, toxins, and digestive enzymes. At the same time, mucus in the SI has to be permeable enough for digestive products to pass through (Herath et al. 2020). While small molecules such as amino acids or monosaccharides could easily pass the mucosal barrier for resorption into enterocytes, dietary lipid droplets and mixed micelles are significantly larger, at 1–3 µm and 3–6 nm diameter, respectively (Gupta 2019). The mucus might therefore pose a physical barrier, slowing down dietary lipid uptake from the micelles which have to pass through it to reach the brush border.

Differences in mucus properties and thickness between colonized and GF mice could therefore be one reason for altered lipid absorption. Consequently, mucus and goblet cells in GF, OMM[11], OMM[12] and SPF mice were characterized in collaboration with Olivia Coleman (Department of Nutrition and Immunology, TUM, Freising) to unveil possible differences.

Gene expression analysis of early (*Tff3*), intermediate (*Oasis*) and mature (*Muc2*, *Agr2*) goblet cell markers was performed by qPCR (Figure 18). In the jejunum, OMM[12] mice showed significantly higher expression of the early and intermediate goblet cell markers *Tff3* and *Oasis* compared to SPF and GF. Ileal expression of *Tff3*, *Muc2* and *Agr2* was increased in SPF mice compared to the other groups. Finally, *Oasis* expression in the colon of OMM[12] mice was significantly reduced vs. GF.

In summary, the goblet cell differentiation markers in intestinal sections of the different mouse models showed no consistent microbiota-dependent changes.
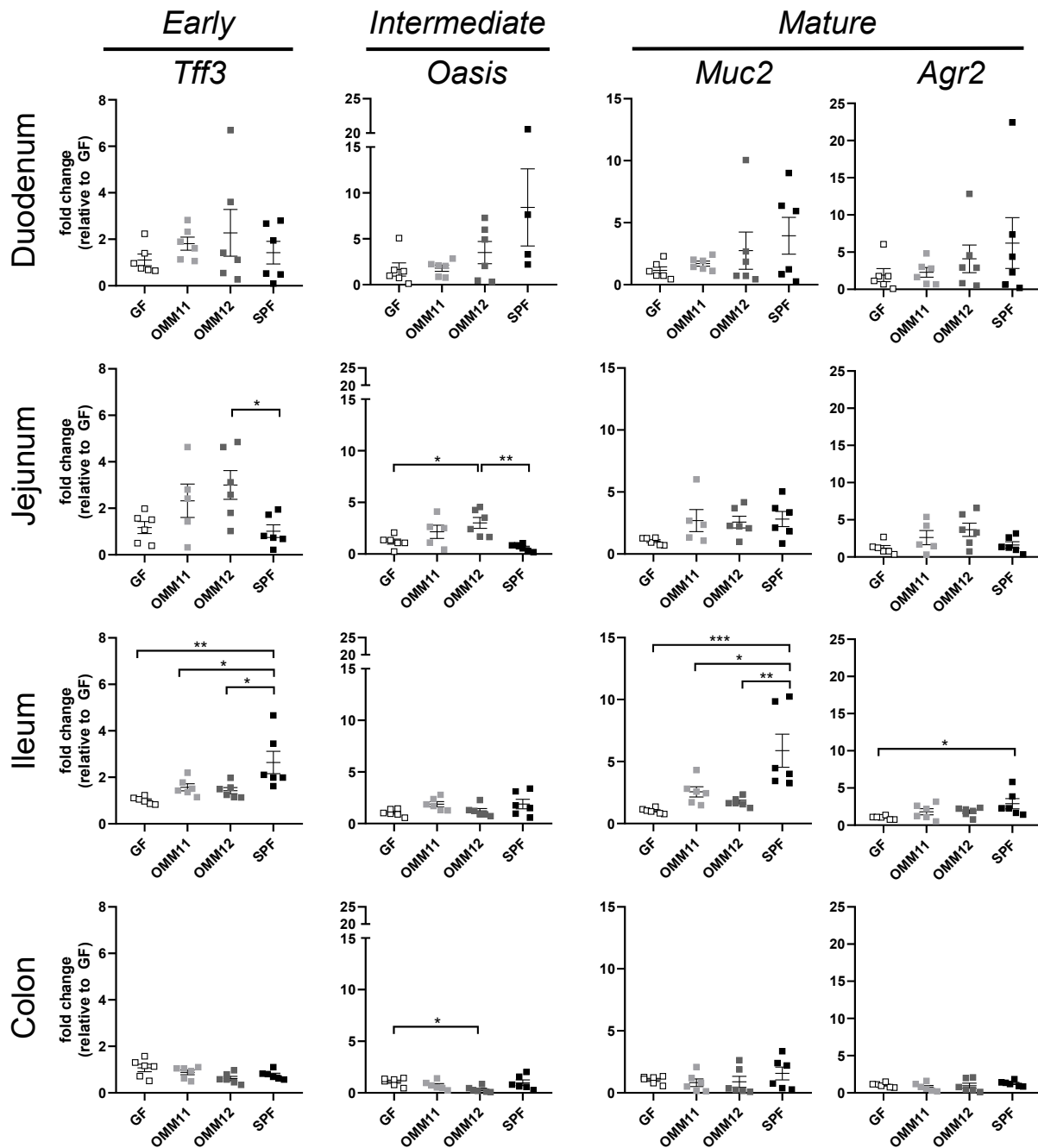
Figure 18. Gene expression analysis of goblet cell markers along the GIT
mRNA expression of *Tff3* (early goblet cell marker), *Oasis* (intermediate goblet cell marker), and *Muc2* and *Agr2* (mature goblet cell marker) are shown for the different gastrointestinal tract compartments. Data are shown as mean ± SEM of $n = 6$. $^*p < 0.05$, $^{**}p < 0.01$, $^{***}p < 0.001$ after one-way ANOVA with Tukey post-hoc test.

Next, the number of mucin-filled goblet cells per 100 µm^2 was determined in formalin fixed, paraffin embedded (FFPE) intestinal sections by periodic acid schiff-alcian blue (PAS-AB) staining (Figure 19).
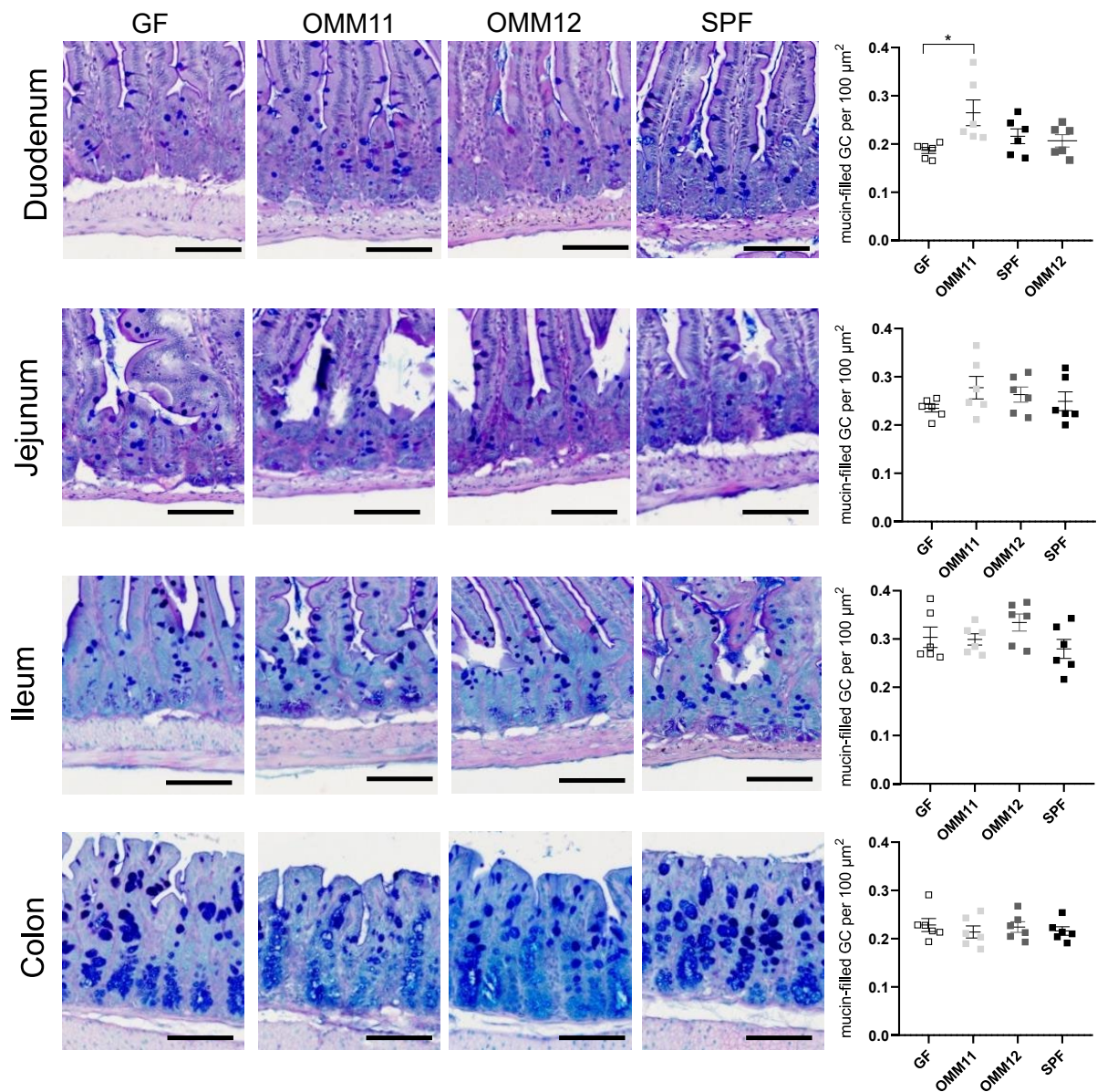
Figure 19. Mucin-filled goblet cell analysis in intestinal sections
Representative images (scale bar: 100 µm) and quantification of mucin-filled goblet cells across each colonization group in the individual intestinal compartments. Data are shown as mean ± SEM of n = 6. *p < 0.05 after one-way ANOVA with Tukey post-hoc test.

The number of mucin-filled goblet cells was not significantly different between colonization groups in the different intestinal sections, except in the duodenum of OMM[11] vs. GF mice due to two samples with very high goblet cell numbers (Figure 19). Longitudinally, the number of mucin-filled goblet cells in all mouse groups increased from duodenum to jejunum, where it reached its highest number, before dropping again in the ileum and colon (Supplemental Figure 2).

In conclusion, different gut microbial colonizations did not alter the numbers of mucin-filled goblet cells per 100 µm^2.

Studies have shown that microbial colonization and stimulation of colonic explants with bacterial products stimulates mucus secretion and thickness (Petersson et al. 2011). To see if colonization in the different mouse models also increased small intestinal mucus thickness, AB stained Carnoy-fixed sections were used to measure adherent mucus layer thickness (Figure 20).
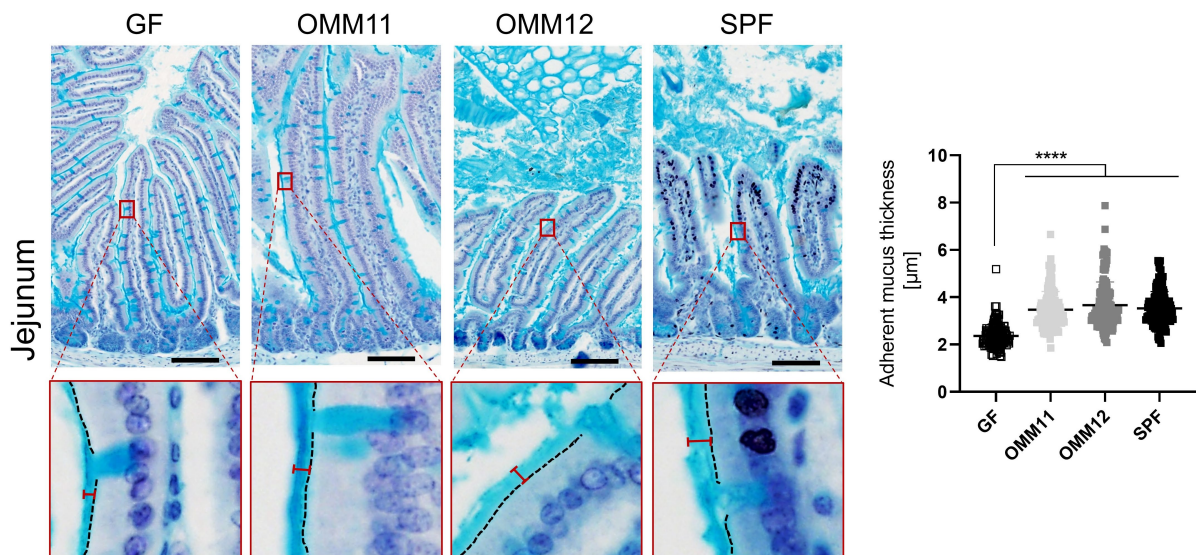
Figure 20. Measurement of adherent mucus thickness in the jejunum of Carnoy-fixed tissue

Representative images (scale bar: 100 µm) and adherent mucus thickness determined from n = 3 biological replicates shown as mean ± SEM. For each replicate, mucus thickness was measured for 50 villi. For each villus, distance was measured at three different positions and averaged. ****$p < 0.0001$ after one-way ANOVA with Tukey post-hoc test.

The average thickness of the jejunal mucus layer was 2.4 µm in GF mice, but significantly thicker in the three colonized mouse groups (3.5–3.7 µm), a ~50% increase (Figure 20). Colonization with the minimal microbial consortia OMM[11] and OMM[12] was sufficient to restore the mucus layer to the same thickness as with the SPF microbiota.

The mucus thickness determined in Carnoy-fixed tissue of colonized mice is ~70-fold lower than the 250 µm reported from jejunal tissue explants (Ermund et al. 2013). This shrinking of the mucus was expected as part of the fixation process and should impact all groups equally.

Differences in SI mucus between GF and colonized mice have been described in the literature (Johansson et al. 2015). While colonic mucus thickness was slightly reduced in GF mice, the ileal mucus was ~38% thicker in GF mice compared to conventionalized (CONV) ones. One major difference observed was that ileal mucus could more easily be detached in CONV mice compared to GF, with 86% vs. 22% of the ileal mucus aspirable, respectively.

While the data from Carnoy-fixed intestinal sections (Figure 20) show a microbial effect on the mucus layer, inferences to the actual biophysical properties and thickness *in vivo* would require additional studies using SI tissue explants. In addition, no changes in mucus thickness between the different colonized mouse groups were observed, despite a higher lipid absorption in OMM[12] vs. SPF mice. Therefore, mucus thickness cannot sufficiently explain the microbial impact on dietary fat uptake.

Passage of lipid emulsion droplets to the brush border of enterocytes does not only depend on thickness, composition and density of the mucus layer itself, but also on the biophysical properties of the emulsions. It was shown that the presence of surfactants like PC and bile salts was required for lipid emulsion droplets to penetrate mucus *ex vivo* (Macierzanka et al. 2011). Since the bile is the main source of those surfactants, crucial to the lipid digestion process, bile lipid composition in the different mouse models upon gavage of the stable isotope labeled tracers was investigated next.

3.4.4. The gut microbiota alters biliary glycerophospholipid levels

To ask if the biliary lipid composition is altered in colonized vs. GF mice, impacting dietary lipid uptake, the bile lipidome of GF, OMM[12] and SPF mice was analyzed by HR-MS (Figure 21). Bile from the 6 h time point of the oral lipid gavage experiment was analyzed as it most closely resembles the composition of fasted bile in a filled gallbladder.

The lipid profile of gallbladder bile in GF, OMM[12] and SPF mice was dominated by phosphatidylcholine (PC) and lysophosphatidylcholine (LPC) making up > 85% of all lipids, followed by 8–12% of free cholesterol (FC). Minor amounts of phosphatidylethanolamine (PE) and lysophosphatidylethanolamine (LPE) were also present at ~2–3% (Figure 21A). Significant differences in the glycerophospholipid and lysoglycerophospholipid composition in dependence of microbial status were observed. While GF mouse bile primarily contained PC (64% of total lipids), LPC was the dominating lipid class in SPF mouse bile (58% of total lipids). OMM[12] mouse bile contained equal amounts of both PC and LPC (~44% each). This translated into drastically altered PC/LPC ratios (Figure 21B) which were also recapitulated in the second dataset (see chapter 3.3.2) from GF, OMM[11] and OMM[12] mice (Figure 21C). A comprehensive analysis of individual lipid species in the bile of GF vs. OMM[12] or SPF mice (Figure 21D, E; Supplemental Figure 3A) was performed. It showed significant changes in LPC species containing unsaturated FA such as LPC 18:1, LPC 18:2, LPC 20:4 and LPC 22:6, being causal for the altered PC/LPC ratios. Meanwhile, PC lipid species levels were not significantly altered. In the GF, OMM[11], OMM[12] mouse cohort (Supplemental Figure 3B) those findings could be reproduced, with levels of unsaturated LPC, especially LPC 18:2, increasing with gut microbial diversity.
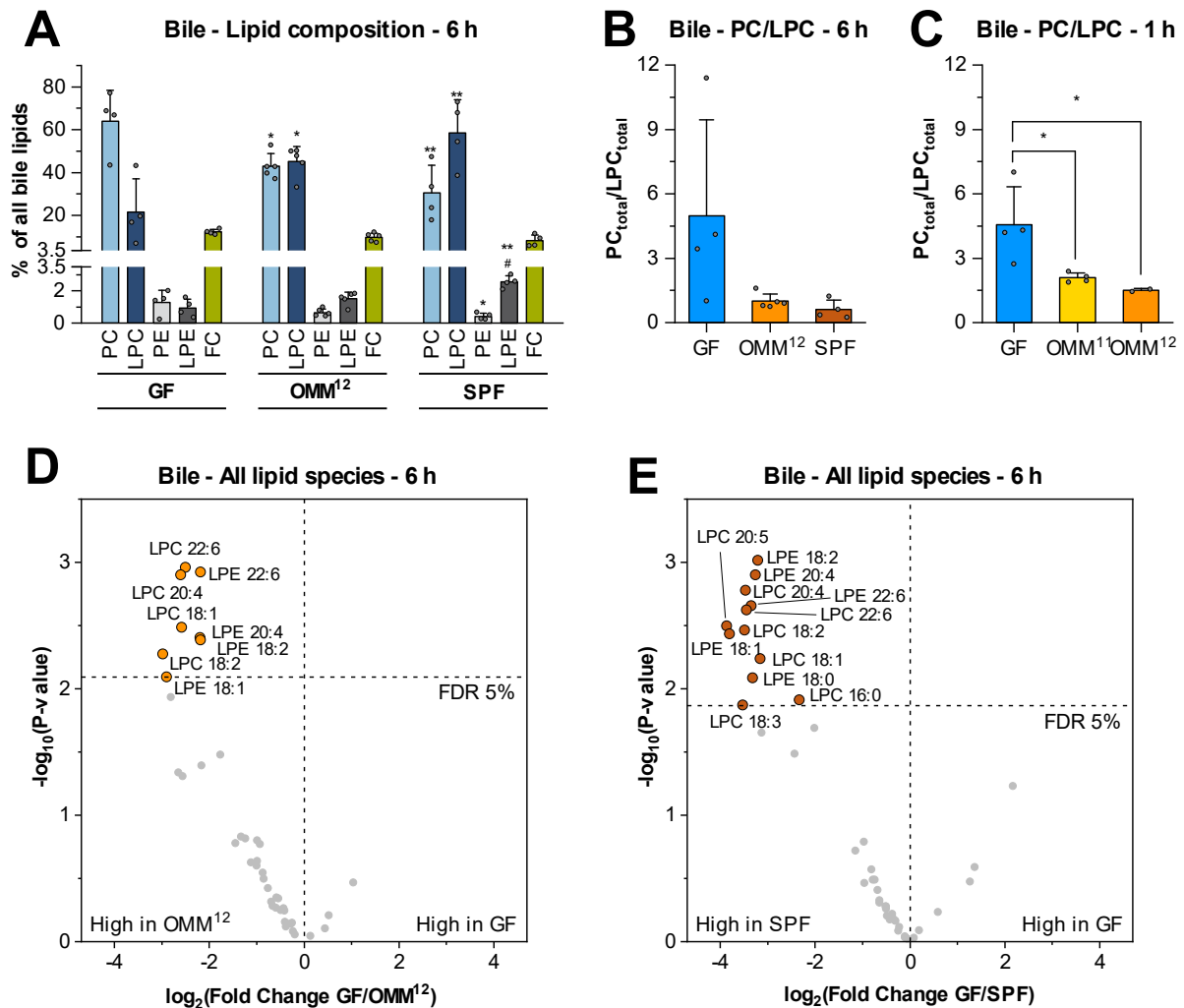
Figure 21. Biliary glycerophospholipid composition is altered in dependence of microbial status

(A)   Lipid class composition of GF, OMM[12] and SPF bile at 6 h post-lipid gavage. Data are shown as mean $\pm$ SD of n = 4–5. */#p < 0.05, **/##p < 0.01 after one-way ANOVA with Tukey post-hoc test. Significance compared to GF (*) or OMM[12] (#) mice.

(B)   Total PC/LPC ratio of GF, OMM[12] and SPF bile at 6 h post-lipid gavage. Data are shown as mean $\pm$ SD of n = 4–5. No significant differences after one-way ANOVA with Tukey post-hoc test.

(C)   Total PC/LPC ratio of GF, OMM[11] and OMM[12] bile at 1 h post-lipid gavage. Data are shown as mean $\pm$ SD of n = 2–4. *p < 0.05 after one-way ANOVA with Tukey post-hoc test.

(D–E)   Volcano plots showing log$_2$ fold changes of different lipid species concentrations in the bile of GF vs. OMM[12] animals (D) or SPF animals (E) 6 h post-lipid gavage after a total lipidome analysis. Significantly different lipid species after two-sided t-test with unequal variance and Benjamini-Hochberg FDR correction at 5% are colored. (n = 4–5 per group)

3.4.5. Biliary phospholipid levels altered by gut microbiota are linked to dietary lipid uptake

To ask whether biliary phospholipids can be linked to dietary lipid uptake, the total LPC concentration and the PC/LPC ratio in the bile of GF, OMM[11] and OMM[12] mice was correlated with the concentrations of labeled FA 16:0[D5] and FA 16:0[D31] in plasma (Figure 22A, B).
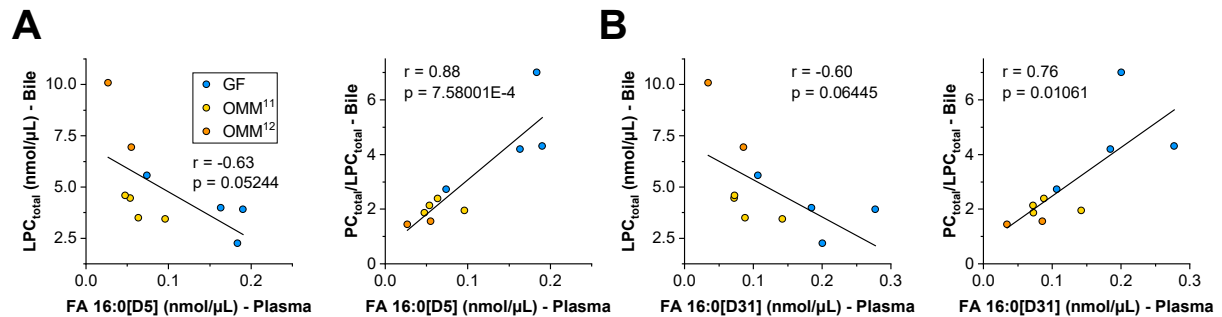
Figure 22. Correlation of biliary LPC levels and PC/LPC with uptake of FA 16:0[D5] (A) and FA 16:0[D31] (B) in the plasma of GF, OMM[11] and OMM[12] mice
Data from n = 2–4 is shown 1 h of lipid tracer administration. Pearson correlation coefficients r as well as p-values are indicated.

PC/LPC showed a significant correlation with labeled FA uptake (Pearson correlation coefficient 0.76–0.88), while LPC concentrations were negatively correlated with lipid uptake.

To demonstrate that the alteration of biliary PC/LPC as performed by the gut microbiota directly influences dietary lipid uptake, gut luminal PC contents were manipulated and the effect on dietary lipid uptake quantified. SPF mice received an oral stable isotope lipid gavage either with or without 100 nmol of PC 34:2, the major PC species in bile (Figure 23).
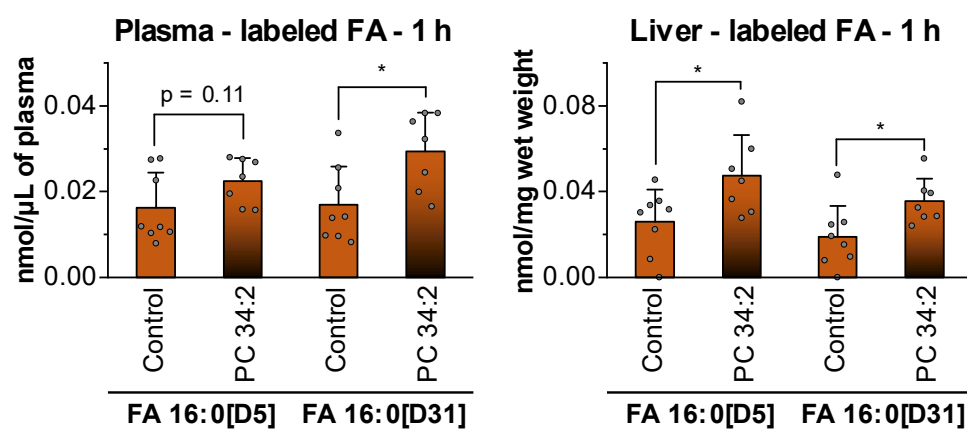
Figure 23. Increasing luminal PC boosts uptake of labeled FA 16:0 into plasma and liver
Concentrations of FA 16:0[D5] and FA 16:0[D31] were determined in plasma and liver 1 h after supplying SPF mice with the labeled lipids with or without 100 nmol of PC 34:2 via oral gavage. Data are shown as mean ± SD of n = 7–8. *p < 0.05 after two-sided t-test with unequal variance.

After 1 h, uptake of FA 16:0[D5] and [D31] in the plasma and liver of mice with PC 34:2 supplementation was ~1.4–1.9-fold elevated compared to controls.

Taken together, these data suggest that gut microbial presence reduces the PC to LPC ratio in the bile which in turn decreases dietary lipid uptake in the intestine, and that the extent of this effect depends on the microbiota composition and diversity.

3.5. MECHANISTIC DETAILS OF BILIARY PC AND LPC MANIPULATION BY THE GUT MICROBIOTA

Biliary phospholipids are synthesized in the liver and secreted into bile canaliculi draining into the bile duct before reaching the gallbladder. The gut microbiome might alter biliary PC/LPC ratios already in the liver by inducing hepatic phospholipases converting PC to LPC (Figure 24A).

The enzyme ATP binding cassette B4 (ABCB4, also known as MDR2) (Figure 24B) is essential for phospholipid secretion into bile, flopping PC across the canalicular membrane of hepatocytes (Smit et al. 1993). Whether ABCB4 could also transport hepatic LPC into bile canaliculi is unclear. *In vitro* studies showed that LPC 16:0 in contrast to PC species actually inhibited ABCB4 (Prescher et al. 2020).

Another possibility could be phospholipase activity occurring in the gallbladder itself (Figure 24C). Phospholipase A_1 and A_2 (PLA_1/PLA_2) activity in human bile has been observed before, albeit in pathological contexts such as bacterial infections (Nakano et al. 1988), cholesterol stone formation (Shoda et al. 1997) and anomalous pancreaticobiliary ductal junction (APBDJ) (Shimada et al. 1991).
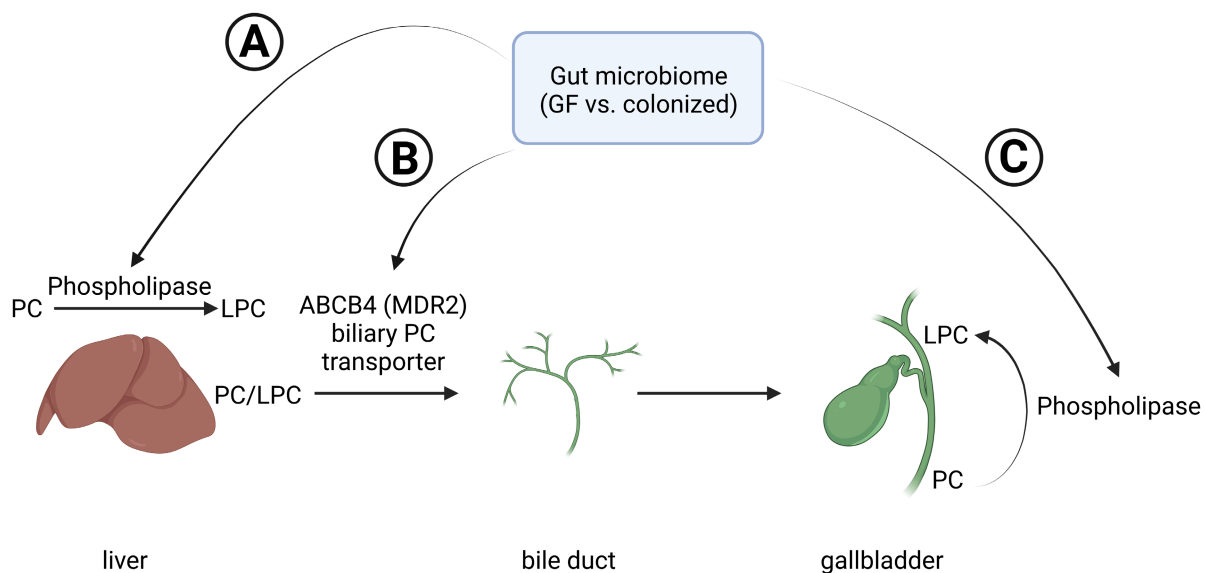

Figure 24. Potential modes of influence of the gut microbiome on biliary phospholipid secretion
(A) Influence on hepatic phospholipase activity, as well as PC and LPC levels. (B) Influence on the biliary PC transporter ABCB4 (MDR2), essential for exporting PC from the liver into the bile duct. (C) Influence on phospholipases which might degrade PC in the gallbladder bile.

3.5.1. The gut microbiota does neither alter hepatic PC/LPC contents nor biliary PC exporter expression

To investigate if the reduced PC/LPC ratios in the bile of colonized mice are due to higher PC to LPC conversion in the liver and subsequent secretion of LPC into the bile duct, total hepatic LPC and PC/LPC were measured by HR-MS (Figure 25A).
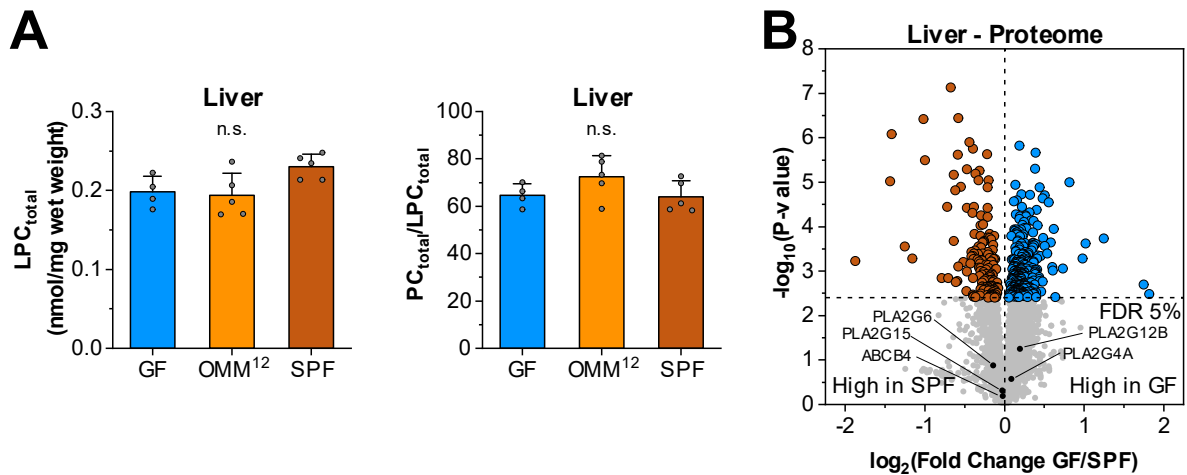
Figure 25. Liver PC/LPC contents and protein levels of hepatic phospholipases and PC exporters.
(A) LPC concentrations and PC/LPC in the liver of GF, OMM[12] and SPF mice 6 h after the oral lipid gavage. Data are shown as mean ± SD of n = 4–5. n.s. = not significant after one-way ANOVA with Tukey post-hoc test.
(B) Volcano plot showing $\log_2$ fold changes of proteins in the liver of GF vs. SPF mice from a full proteome analysis (n = 5 per group). Significance was tested via two-sided t-test with unequal variance and Benjamini-Hochberg FDR correction at 5%. The dataset was published previously (Kindt et al. 2018). Proteins with known phospholipase activity at the *sn*-1 or *sn*-2 position as well as the PC exporter ABCB4 are highlighted in black.

Neither total LPC levels nor the total PC/LPC ratio was significantly altered in the liver of GF vs. OMM[12] vs. SPF mice. LPC was generally only found at very low concentrations in the liver (~0.2 nmol/mg wet weight), with the ratio of PC/LPC being as high as 70:1. In comparison, biliary PC/LPC was found to be much lower in the range of ~0.6–4.5:1 (Figure 21B, C). In agreement with the unaltered hepatic LPC content and PC/LPC ratio, a full proteome analysis of GF vs. SPF livers showed no significant fold changes in the expression of phospholipases capable of degrading PC to LPC (Figure 25B). The expression of the PC exporter ABCB4 was also unaltered in the proteome dataset.

In a nutshell, these data do not corroborate the idea that the degradation of biliary PC to LPC occurs before secretion of phospholipids into the bile canaliculi.

3.5.2. PC is enzymatically hydrolyzed to LPC at the *sn*-1 position in bile

To test if enzymatic activity occurred directly in the gallbladder bile of GF vs. colonized mice, a novel *ex vivo* bile phospholipase assay was developed. Pooled bile samples were incubated at 37 °C with 10 nmol/μL of the substrate PC 15:0/18:1[D7] (equivalent to the average total amount of PC detect in SPF mouse bile) (Figure 26A).
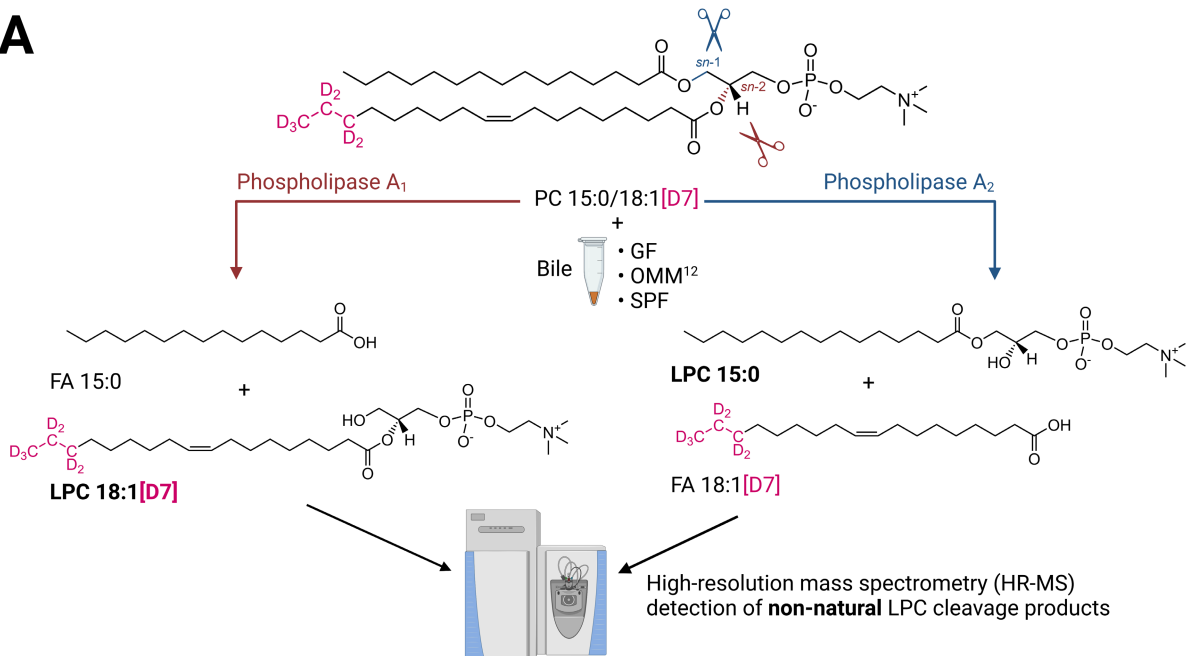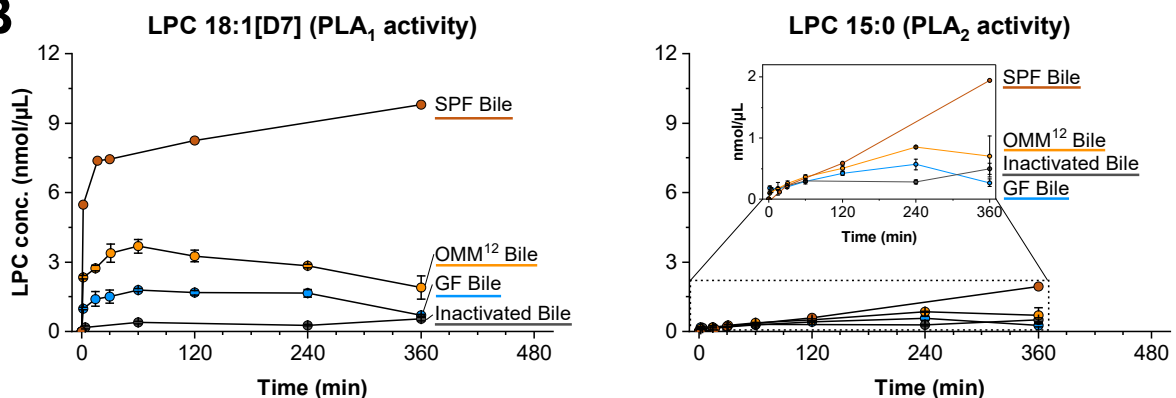
Figure 26. Phospholipase activity in bile is microbiome dependent and preferentially freeing FA at the *sn*-1 position of PC

(A) Experimental setup to analyze PLA₁ and PLA₂ activity in bile via the detection of the cleavage products LPC 18:1[D7] and LPC 15:0 by HR-MS.

(B) LPC 18:1[D7] and LPC 15:0 levels after incubation of the substrate PC 15:0/18:1[D7] for 2–360 min with GF, OMM¹² and SPF mouse bile. GF bile was incubated for 15 min at 95 °C to quench any enzyme activity and used as negative control (Inactivated Bile). Bile from n = 3–4 mice per group was pooled for the experiment and samples were drawn, extracted, and measured 1–3 times per time point.

Over the time course of 2–360 min, the reaction products of phospholipase A_1 and A_2 activity (PLA$_{1/2}$), LPC 18:1[D7] and LPC 15:0, respectively, were quantified by HR-MS (Figure 26B). Substantial PLA$_1$ activity was observed with more than 40% of the substrate being already hydrolyzed in SPF mouse bile after 2 min. In contrast, concentrations of LPC 15:0 liberated by PLA$_2$ remained close to baseline.

Most importantly, biliary PLA$_1$ activity was microbiome dependent, with LPC 18:1[D7] concentrations being ~4-fold higher in SPF and ~2-fold higher in OMM[12] bile compared to GF.

Heat-inactivated GF bile (grey traces) showed no cleavage of the PC substrate, confirming that the conversion of PC to LPC is enzyme dependent and not due to unspecific hydrolysis of the substrate in bile.

These data show that the microbiome alters PC/LPC levels in the bile by induction of PLA$_1$ activity in the gallbladder, which in consequence impacts dietary lipid uptake when bile is secreted into the small intestine to aid with fat digestion.

3.5.3. Bile proteomics shows the presence of carboxyl ester lipase, an enzyme with known phospholipase activity

To discover potential enzymes in the bile of GF, OMM[12] and SPF mice capable of metabolizing PC to LPC, a full proteome analysis of the bile samples was performed using liquid chromatography (LC) coupled to high resolution (HR) tandem mass spectrometry (MS/MS) in cooperation with Piero Giansanti (BayBioMS, MRI, Munich) (Figure 27).

A total of 393–737 proteins were detected in mouse bile. Surprisingly, neither phospholipase A_1 (PLA$_1$) nor enzymes from the phospholipase A_2 (PLA$_2$) family were found in the bile samples. However, carboxyl ester lipase (CEL), an enzyme with a broad substrate specificity including phospholipase activity (Hui and Howles 2002), was detected in all mouse bile samples. It was ranked among the 20 most abundant proteins and found at similar levels in GF, OMM[12] and SPF bile (iBAQ intensity 9.25–9.73). CEL was also detected in human bile, albeit at lower concentrations.

According to current knowledge, the main site of CEL synthesis in the body is the pancreas, from where it is normally secreted with the pancreatic juice into the small intestine to support lipid digestion (Hui and Howles 2002). Besides CEL, several other proteins of specifically pancreatic origin such as PNLIP or carboxypeptidases were found to be highly enriched in the bile proteomics datasets (Figure 27, blue dots). This suggests that CEL in bile is of pancreatic origin, reaching the gallbladder via reflux of pancreatic juice into the biliary duct.

Together, the proteomic analysis of bile samples revealed a surprisingly high number of proteins, showing the potential for further, yet unidentified enzymatic reactions. CEL, a highly expressed enzyme with described phospholipase activity in the literature, was identified as the sole candidate to explain the observed PLA$_1$ activity in bile (Figure 26).
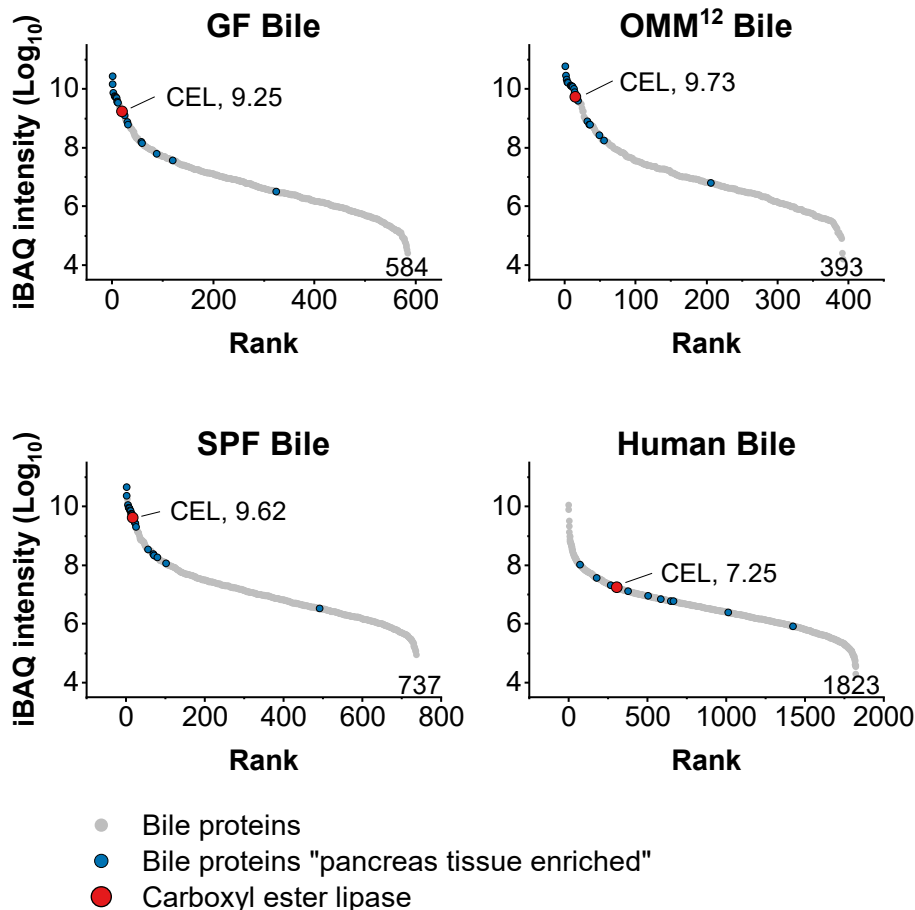
Figure 27. Proteome analysis of GF, OMM^{12}, SPF, and human bile
The rank order of all proteins is shown. The total number of detected proteins per group is noted in the bottom right corner of the panels. CEL is highlighted in red with the respective iBAQ intensity next to it. Proteins which are classified as "enriched in pancreas tissue" according to the Human Protein Atlas (proteinatlas.org) are indicated in blue. Bile samples were pooled from 1–6 bile samples per group for proteomic analysis.

3.5.4. Biliary PLA$_1$ activity is stimulated by taurocholic acid in a microbiota-dependent manner

The hydrolytic activity of CEL requires the presence of bile acids (BA) containing 3α,7α-hydroxy groups such as taurocholic acid (Wang et al. 1997; Fontbonne et al. 2011). Since the bile acid profiles of GF and SPF animals differ markedly (Sayin et al. 2013), this could pose a mechanism for microbial regulation of CEL activity. Consequently, BA in GF, OMM^{12} and SPF mouse bile were quantified using liquid chromatography coupled to tandem mass spectrometry (LC-MS/MS) to investigate a link between BA profiles and CEL activation.

Total BA concentrations in GF and SPF mouse bile were not significantly different but higher than in OMM^{12} mouse bile (Figure 28A). The profiles showed striking differences between the three mouse groups (Figure 28B, Supplemental Figure 4): While GF bile was dominated by Tauro-β/ω-muricholic acid (Tβ/ωMCA), SPF bile mainly contained Taurocholic acid (TCA) (Figure 28D).
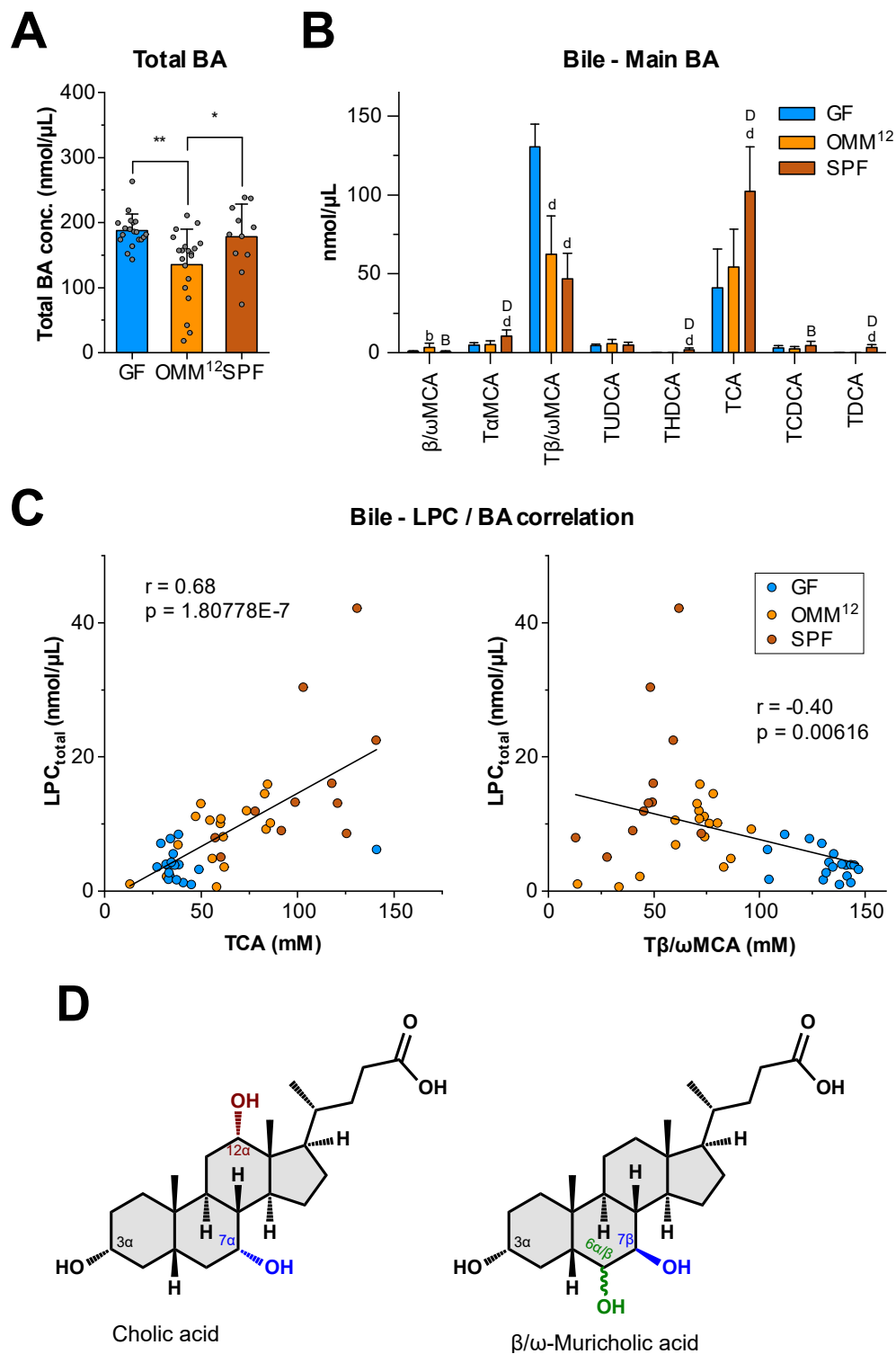
Figure 28. Bile acid profiles in GF, OMM[12] and SPF mouse bile and correlation with biliary LPC concentrations

(A) Total BA concentrations in the bile of GF, OMM[12] and SPF mice. Data from all time points of the experiment were pooled. Data are shown as mean ± SD of n = 11–20. *p < 0.05, **p < 0.01 after one-way ANOVA with Tukey post-hoc test.

(B) Concentrations of the main bile acids in GF, OMM[12] and SPF mouse bile. Only BA with an average contribution of > 1% are shown as mean ± SD of n = 11–20. a/A p < 0.05, b/B p < 0.01, c/C p < 0.001, d/D p < 0.0001 after one-way ANOVA with Tukey post-hoc test and Benjamini-Hochberg FDR correction. SPF vs. GF (a, b, c, d) or OMM[12] (A, B, C, D). For full names of BA see Supplemental Table 2.

Figure 28 continued:
(C) Correlation of biliary LPC with TCA or Tβ/ωMCA concentrations in GF, OMM[12] and SPF mice. Data from all time points of the experiment is shown. (n = 11–18 per group). Pearson correlation coefficients r and p-values are indicated.
(D) Molecular structure of unconjugated cholic acid and β/ω-muricholic acid. In mice, these BA are mainly conjugated to taurine.

OMM[12] mouse bile showed a composition between GF and SPF, with similar levels of both Tβ/ωMCA and TCA. Like in GF bile, no secondary BA were detected in OMM[12] bile. This was expected and is owed to the fact that none of the 12 bacterial strains of the consortium can perform 7α/β-dehydroxylations of the sterol backbone (Studer et al. 2016).

Total LPC concentrations in bile showed a significant positive correlation with TCA (3α,7α-OH), but not with Tβ/ωMCA (3α,7β-OH), strongly suggesting the activation of biliary CEL by TCA (Figure 28C). To provide further evidence, *ex vivo*, GF mouse bile was supplemented with different amounts of TCA and phospholipase activity was measured. TCA dose dependently elevated PLA_1-mediated generation of LPC 18:1[D7] from the substrate PC 15:0/18:1[D7] in GF bile. 5 mM TCA supplementation increased LPC levels by ~35–50% (Figure 29). As observed before (Figure 26B), no PLA_2 activity above baseline was detected.

GF Bile + TCA - PLA Assay
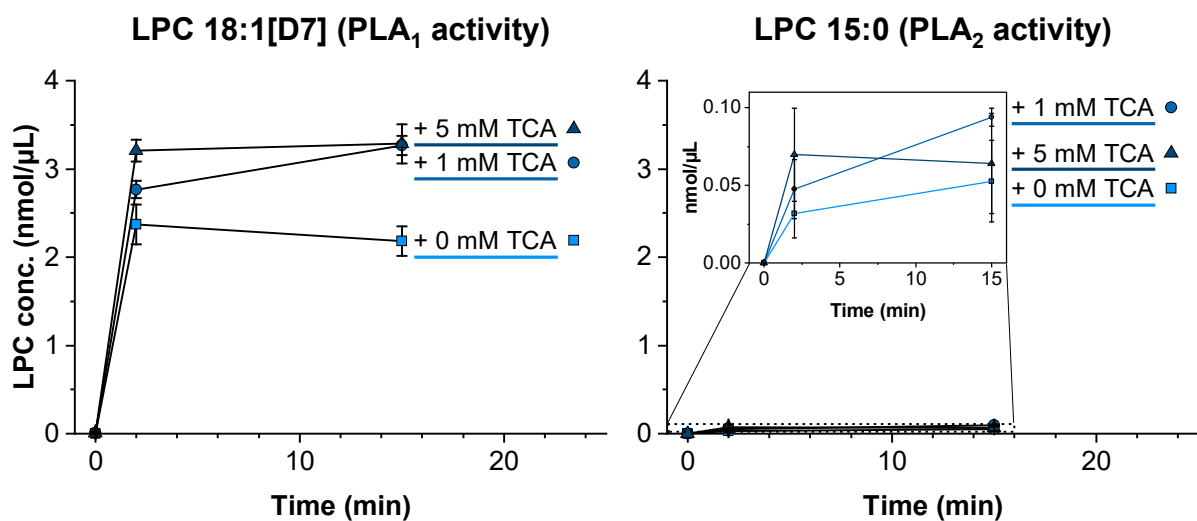
Figure 29. TCA supplementation of GF bile increases PLA_1 activity in a dose dependent manner
LPC 18:1[D7] (PLA_1) and LPC 15:0 (PLA_2) concentrations after incubation of GF bile with the substrate PC 15:0/18:1[D7] without or with 1–5 mM TCA for 2–15 min. Bile from n = 2 mice was pooled for the experiment and spiked with the different TCA concentrations. Samples were extracted and measured 3 times per time point and condition. Shown as mean ± SD.

Taken together, these data implicate microbial alterations of bile TCA levels in the regulation of biliary PLA_1 activity, causing differing PC/LPC ratios in GF vs. colonized animals.

3.5.5. Gut microbiota might increase TCA levels by inducing *Cyp8b1* expression

The gut microbial impact on hepatic bile acid synthesis has been known for quite a while (Wostmann 1973; Sayin et al. 2013). Still the question of how gut bacteria alter hepatic enzymes to specifically increase TCA levels, while reducing Tβ/ωMCA synthesis (Figure 28B), remains insufficiently explained. One study (Sayin et al. 2013) found that the gut microbiota increases FXR-FGF15 signaling in the intestine by creating a pool of more hydrophobic BAs, which are potent FXR activators (Wang et al. 1999; Makishima et al. 1999; Parks et al. 1999). In turn, this reduces the hepatic expression of *Cyp7a1* and overall BA levels in colonized animals (Sayin et al. 2013). The expression and activity of CYP8B1, the key enzyme for 12α-hydroxylation to form TCA (Gåfvels et al. 1999), was however not altered in their data.

In a study by another group comparing GF and conventional animals, only minimal changes in FXR and downstream signaling targets were observed (Selwyn et al. 2015). Enzymes for BA synthesis were actually down regulated in the livers of GF mice in this study, contrasting the previous findings by Sayin *et al*.

Still, a differential regulation of key BA synthesis enzymes by the gut microbiota is the most plausible explanation for the observed differences in TCA levels, crucial for altering biliary PLA_1 activity and PC/LPC. A previously published transcriptome and proteome dataset (Kindt et al. 2018) of GF vs. SPF livers was therefore investigated to check for differential expression of BA synthesis enzymes (Figure 30).
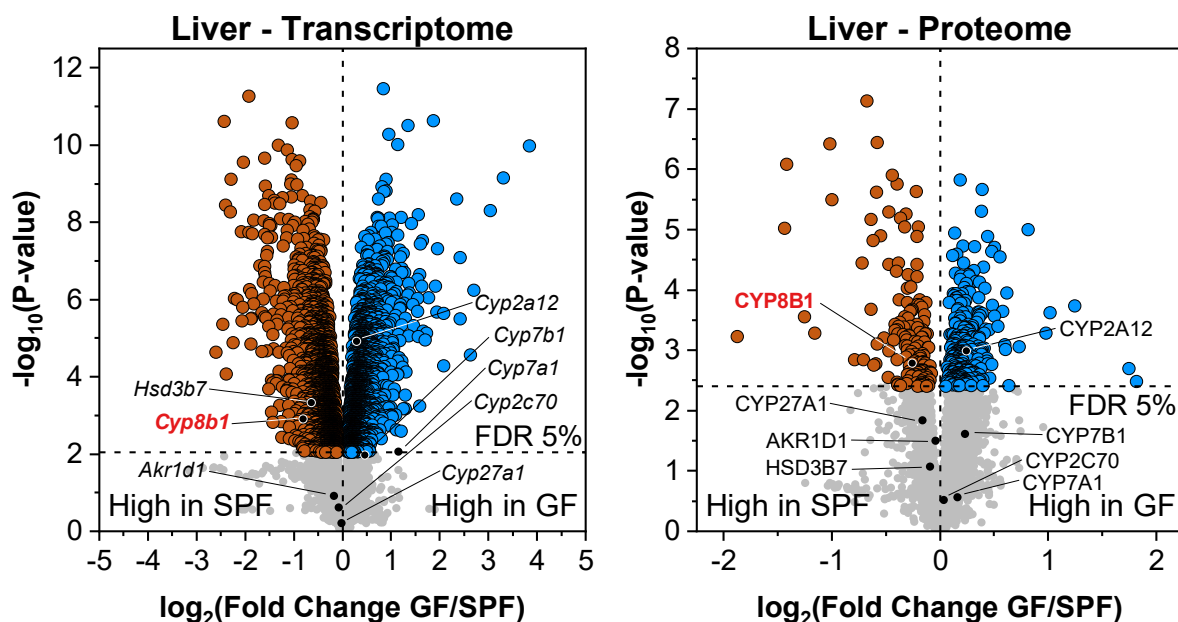
Figure 30. Transcriptomic and proteomic analysis of BA synthesis enzymes in GF and SPF livers

Volcano plot showing log_2 fold changes of transcripts (n = 6) and proteins (n = 5) in the liver of GF vs. SPF mice after a full proteome/transcriptome analysis. Benjamini-Hochberg FDR correction at 5% was used to determine the significance cut-off. The dataset was published previously (Kindt et al. 2018). Enzymes involved in BA synthesis are highlighted as black dots. CYP8B1 is additionally labeled in red.

75% of all BA in the liver are synthesized via the classical pathway (Schwarz et al. 1996), while the acidic pathway produces around 25% (Schwarz et al. 2001) (Figure 3). The acidic pathway mainly produces CDCA, which is the precursor for MCA synthesis in mice. CYP27A1 and CYP7B1, the key enzymes of this pathway, were not altered at the protein or transcript level between GF and SPF mice (Figure 30).

As observed before (Sayin et al. 2013) *Cyp7a1* gene expression was significantly higher in GF animals.

CYP8B1 is the key enzyme in determining the final BA product in the classical pathway, producing CA over CDCA. It was found to be significantly increased at both transcript and protein level in SPF mice, which have higher biliary TCA levels (Figure 30). Surprisingly, CYP2C70, catalyzing the formation of MCAs from CDCA, was unaltered between GF and SPF livers.

Taken together these data suggest that the gut microbiota increases TCA and decreases MCA levels in SPF bile by inducing *Cyp8b1* rather than increasing CDCA production via the acidic pathway or boosting MCA synthesis by CYP2C70. Whether the bacterial regulation might occur via FXR signaling or for example via other BA receptors such as TGR5, VDR or PXR, remains to be elucidated.

3.5.6. *Cyp2c70$^{-/-}$* mice lacking muricholic acids show altered PC/LPC levels and PLA$_1$ activity in bile

To substantiate that biliary PC/LPC depends on BA levels and TCA in particular, mice with a KO in the Cytochrome P450 2c70 (*Cyp2c70*) gene were investigated. CYP2C70 is the enzyme responsible for the generation of muricholic acids (MCA) in mice, hydroxylating the C6 position of the sterol backbone (Takahashi et al. 2016). *Cyp2c70$^{-/-}$* mice are devoid of any MCAs, leading to a generally more human-like and hydrophobic BA profile. In consequence, the MCA precursor CDCA accumulates in *Cyp2c70$^{-/-}$* mouse bile, while TCA levels are lowered in those mice due to reduced expression of CYP8B1, the key enzyme in CA synthesis (Honda et al. 2020).

To answer if the altered BA profiles in *Cyp2c70$^{-/-}$* mice change bile lipid composition and PLA$_1$ activity, bile and liver samples from *Cyp2c70$^{-/-}$* mice (Boer et al. 2021) were characterized by LC-MS/MS. The mice were kindly provided by Jörg Heeren (Department of Biochemistry and Molecular Cell Biology, University Medical Center Hamburg-Eppendorf).

Total BA concentration in bile of KO mice was significantly reduced (Figure 31A). This effect was due to the more than 50% reduced hepatic expression of *Cyp7a1* and *Cyp8b1* (Honda et al. 2020). Surprisingly, the absence of muricholic acids, being strong FXR antagonist (Sayin et al. 2013), and instead the accumulation of the potent FXR ligand CDCA in Cyp2c70$^{-/-}$ mice did not further increase FXR activation (Honda et al. 2020). It was instead suggested that increased levels of unconjugated CDCA in *Cyp2c70$^{-/-}$* mice induce the expression of inflammatory cytokines in Kupffer cells, causing activation of the MAPK-JNK pathway and consequently reduction of *Cyp7a1* and *Cyp8b1* expression (Miyake et al. 2000; Jahan and Chiang 2005; Li et al. 2006).
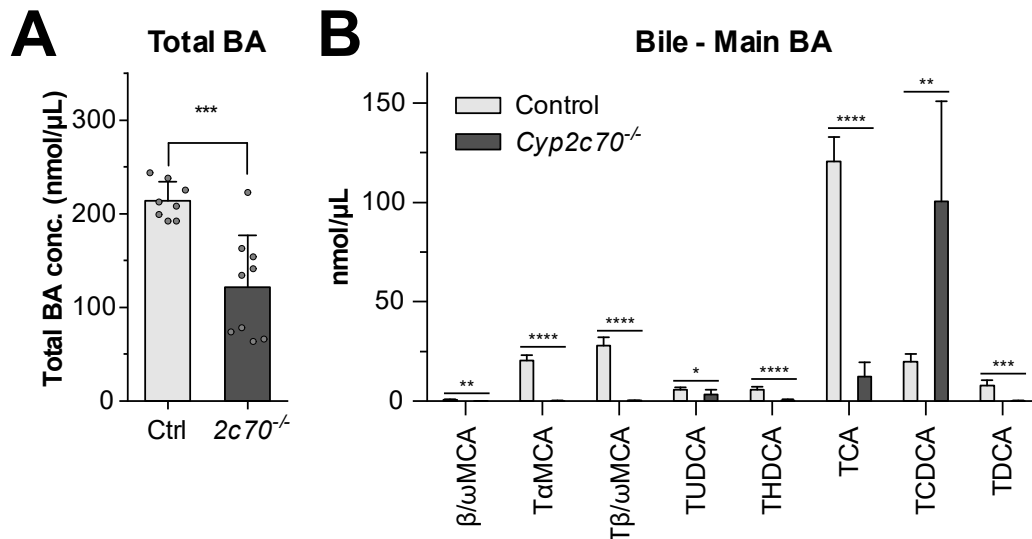
Figure 31. Total BA concentrations and BA profiles in *Cyp2c70*⁻ⁱ⁻ and control mouse bile
(A) Total BA concentrations in *Cyp2c70*⁻ⁱ⁻ and control bile. Data are shown as mean ± SD of n = 8–9. ***p < 0.001 after two-sided t-test with unequal variance.
(B) Bile acid levels in bile of *Cyp2c70*⁻ⁱ⁻ mice and controls, shown are only BA with an average contribution > 1%. Data are shown as mean ± SD of n = 8–9. *p < 0.05, **p < 0.01, ***p < 0.001, ****p < 0.0001 after two-sided t-test with unequal variance and Benjamini-Hochberg FDR correction. For full names of BA see Supplemental Table 2.

BA profiles from gallbladder bile of KO vs. control mice showed the expected absence of MCAs, as well as a 90% reduction of TCA levels and concomitant 5-fold increase in TCDCA (Figure 31B, Supplemental Figure 5).

An analysis of the bile lipidome in *Cyp2c70*⁻ⁱ⁻ mice revealed unchanged PC and PE levels, but significantly reduced concentrations of LPC and LPE by 70 and 50%, respectively (Figure 32A). Consequently, the PC/LPC ratio in KO animals increased. This change was again driven by the reduction of unsaturated LPC species such as LPC 18:1, LPC 18:2, LPC 20:4 and LPC 22:6 (Supplemental Figure 6).
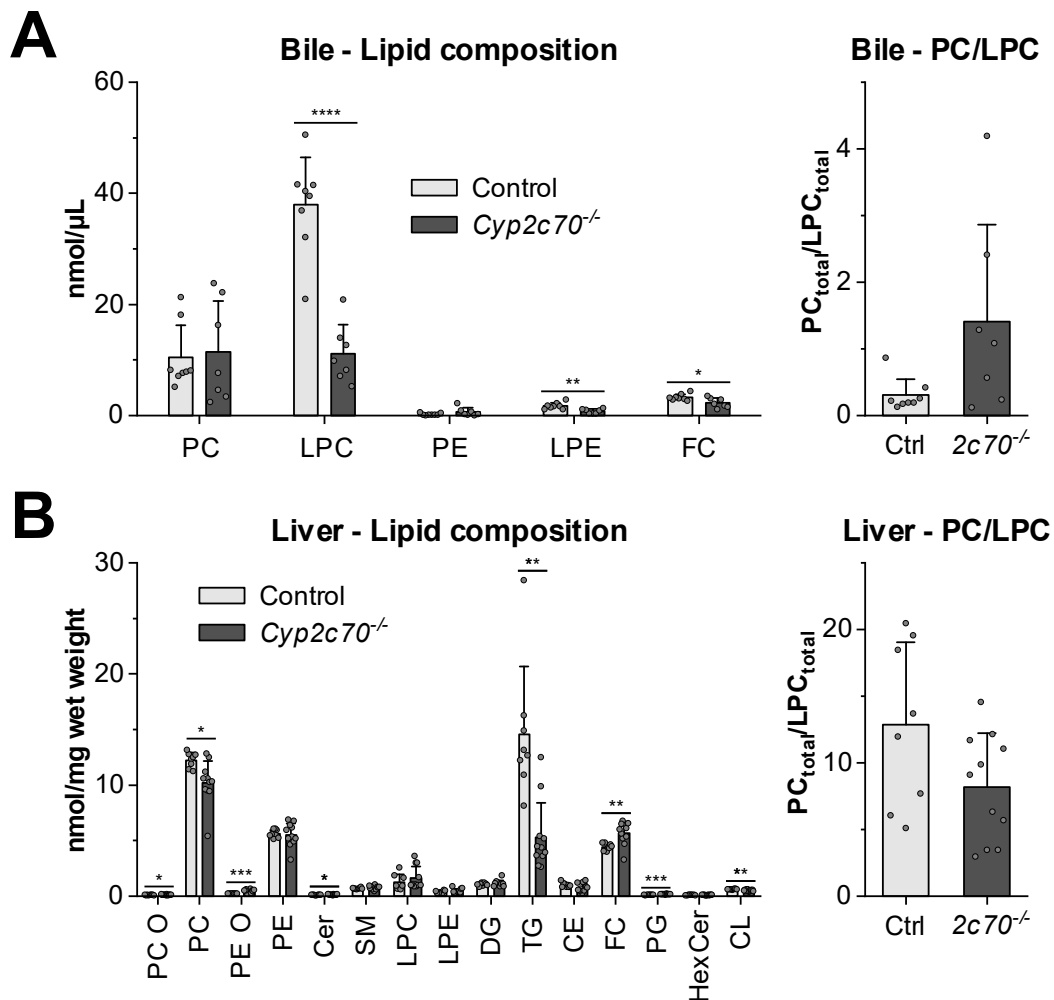
Figure 32. *Cyp2c70^{-/-}* mice have reduced biliary LPC levels and increased PC/LPC which is not reflected in the liver lipidome

(A) Lipid class composition and PC/LPC ratio in bile from *Cyp2c70^{-/-}* and control mice. Data are shown as mean ± SD of n = 7–8. *p < 0.05, **p < 0.01, ***p < 0.001, ****p < 0.0001 after two-sided t-test with unequal variance and Benjamini-Hochberg FDR correction. FDR correction was only applied to the left panel.

(B) Lipid class composition and PC/LPC in liver from *Cyp2c70^{-/-}* and control mice. Data are shown as mean ± SD of n = 8–11. *p < 0.05, **p < 0.01, ***p < 0.001 after two-sided t-test with unequal variance and Benjamini-Hochberg FDR correction. FDR correction was only applied to the left panel.

PC O: Phosphatidylcholine-ether, PC: Phosphatidylcholine, PE O: Phosphatidylethanol-amine-ether, PE: Phosphatidylethanolamine, Cer: Ceramide, SM: Sphingomyelin, LPC: Lysophosphatidylcholine, LPE: Lysophosphatidylethanolamine, DG: Diglyceride, TG: Triglyceride, CE: Cholesteryl Ester, FC: Free Cholesterol, PG: Phosphatidylglycerol, HexCer: Hexosylceramide, CL: Cardiolipin

A lipidomic analysis of the livers in control and KO animals showed no differences in LPC levels or PC/LPC (Figure 32B). This again suggested a difference in biliary PLA_1 activity as the cause for increased bile PC/LPC ratios in the CYP2C70 deficient mice.

To finally confirm that the increased PC/LPC ratio and lower LPC levels in *Cyp2c70^{-/-}* bile were due to attenuated PLA_1 activity, phospholipase activity in control and KO

mouse bile was measured (Figure 33A). Levels of LPC 18:1[D7], representative of biliary PLA$_1$ activity, were reduced by 80–85% in *Cyp2c70*$^{-/-}$ bile.

As observed in GF, OMM[12] and SPF mouse bile (Figure 28C), total LPC concentrations correlated with TCA in the bile (Figure 33B).

Taken together, data from *Cyp2c70*$^{-/-}$ mice support the proposed mechanism of PLA$_1$ induction by TCA.
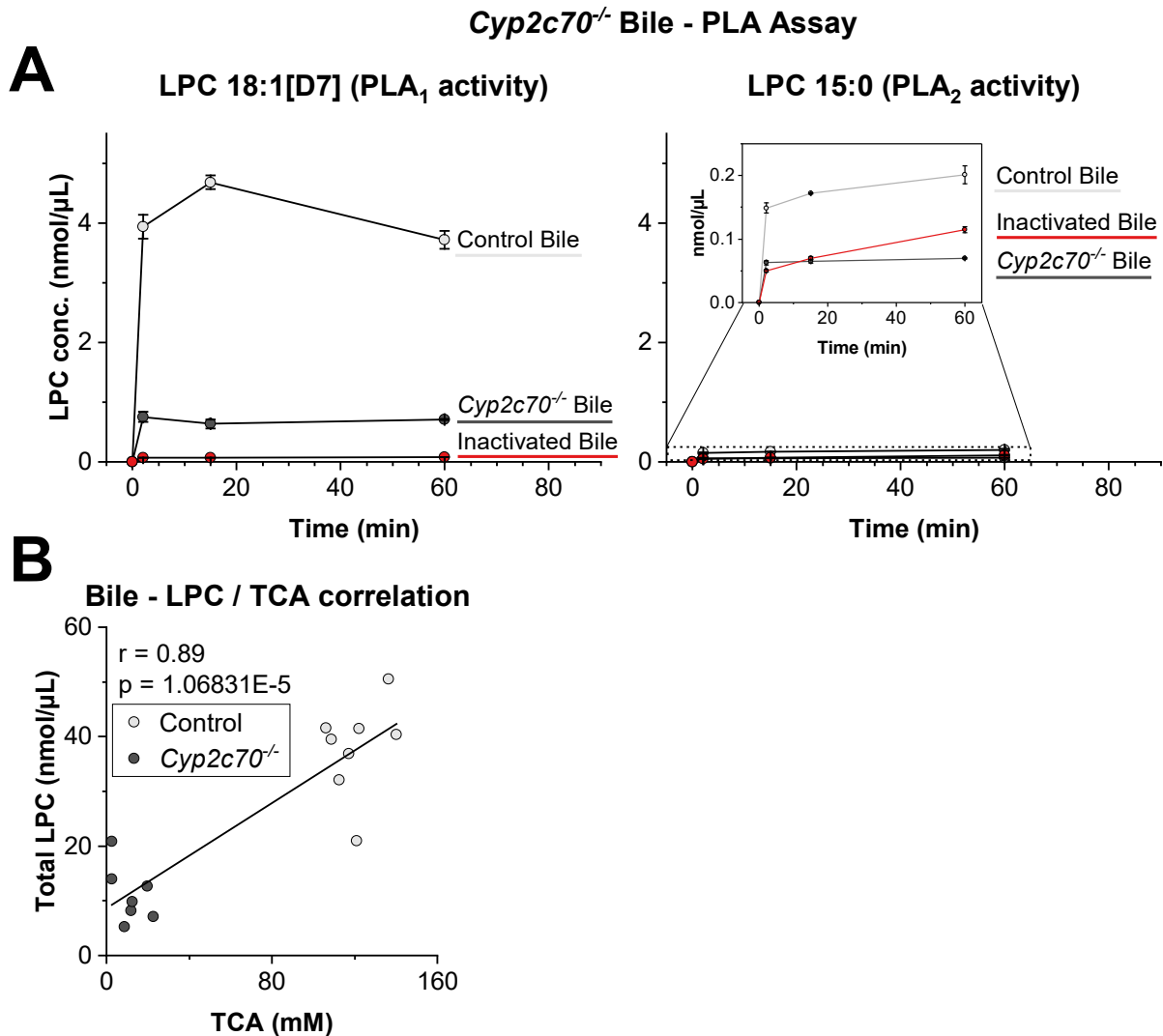
Figure 33. *Cyp2c70*$^{-/-}$ bile shows reduced PLA$_1$ activity and biliary LPC correlates with TCA levels in *Cyp2c70*$^{-/-}$ vs. control mice

(A) LPC 18:1[D7] (PLA$_1$) and LPC 15:0 (PLA$_2$) concentrations after incubation of *Cyp2c70*$^{-/-}$ or control bile with the substrate PC 15:0/18:1[D7] for 2–60 min. Control mouse bile incubated for 15 min at 95 °C with 1% SDS was used as a negative control (Inactivated Bile). Bile from n = 8–9 mice was pooled for each experimental group. Samples were extracted and measured 3 times per time point and condition. Shown as mean ± SD.

(B) Correlation of LPC with TCA concentrations in the bile of *Cyp2c70*$^{-/-}$ mice and controls (n = 7–8). Pearson correlation coefficients r and p-values are indicated.

4. DISCUSSION

The current work has revealed a novel mechanism by which gut microbiota-dependent metabolites regulate the absorption of dietary lipids through host enzyme regulation in the bile. Stable isotope-labeling experiments combined with kinetic multi-compartment modeling showed that the gut microbiota limits uptake of labeled FA from the gut lumen into enterocytes and plasma. This step was dependent on the biliary PC/LPC ratio, which is altered via PLA_1 activity in the bile. Higher TCA levels in colonized mice were shown to increase this enzymatic activity.

4.1. GUT MICROBIOTA REDUCE DIETARY LIPID UPTAKE BY ALTERING BILIARY PC/LPC

The mechanism of how the PC/LPC ratio in bile influences lipid uptake from the lumen to the intestinal tissue is not yet clear. Biliary PC is essential for dietary fat digestion and absorption. $Abcb4^{-/-}$ mice secreting no phospholipids into the bile show an impaired TG absorption into plasma after receiving a lipid bolus (Voshol et al. 2000).

PC aids in emulsifying dietary lipids, enlarging the lipid-water interfacial area by decreasing the size of the emulsified lipid droplets (Tso and Scobey 2018). The emulsification capacity of PC in the SI is magnitudes higher than that of bile salts like TCA, allowing a more efficient digestion of TG by pancreatic lipase (PNLIP) at the surface of the lipid droplets (Linthorst et al. 1977). However, the current work showed that TG hydrolysis by PNLIP was not altered by the microbiota, as the uptake kinetics of FA 16:0[D5] from FFA and FA 16:0[D31] derived from TG were very similar between GF and colonized animals.

A second purpose of biliary PC is to provide phospholipids for the formation of the monolayer membrane of chylomicrons (CM) (Mansbach and Gorelick 2007). Both PC and LPC are absorbed into enterocytes as LPC and subsequently re-esterified before incorporation into CM membranes (Parthasarathy et al. 1974). Therefore, the total amount of phospholipids in the form of PC and LPC, rather than the biliary PC/LPC ratio controls the rate of CM membrane synthesis.

Lastly, luminal PC is required for the formation of mixed micelles with cholesterol and bile salts to efficiently solubilize and transport FFA and 2-MAG across the unstirred water layer to the brush border of enterocytes (Smith and Lough 1976). The biophysical properties of those micelles depend on many different factors such as pH, temperature, the types of BA present, or the ratio of BA to PC and cholesterol (Hofmann and Small 1967). The lower PC fractions in bile from colonized mice compared to GF mice could impact micelle formation and thus reduce lipid uptake into enterocytes. However, PC, but not LPC incorporation into mixed micelles caused them to swell, reducing their coefficient of diffusion across the unstirred water layer and subsequently, lipid absorption. LPC incorporation into micelles did not lower FA uptake as determined in everted sac models of rat jejunum *in vitro* and by infusion into rat intestinal segments *in vivo* (Saunders and Sillery 1976; Rampone and Long

1977; Reynier et al. 1985). These findings could be explained by the different biophysical properties of PC vs. LPC. LPC has an inverted cone shape, which induces micelle formation. PC on the other hand has a more cylindrical shape, which preferably forms lipid bilayers (Negi 2019).

It should be noted that all mentioned studies used *sn*-1 LPC species, as these are the products of PC digestion by pancreatic phospholipase A_2 in the SI. In mouse bile however, the observed PLA_1 activity yielded *sn*-2 LPC species. The difference in the acyl chain position of *sn*-1 vs. *sn*-2 LPC might affect the packing of mixed micelles, leading to different results.

Elucidating the exact mechanism by which the gut microbial changes in bile PC/LPC influence lipid resorption might help to develop new strategies for obesity treatment. For example, dietary supplements containing specific PC or LPC species might be used to balance the emulsifying action of biliary PL in the SI.

4.2. DIRECT METABOLISM OF DIETARY FA BY THE GUT MICROBIOTA

While the main impact of the gut microbiota on dietary lipid absorption was shown to happen indirectly via the manipulation of bile PC and LPC levels, dietary FA could also be directly metabolized by gut bacteria. Labeled FA 18:0[D5/D31] was detected in the SI gut contents (Supplemental Figure 1B), either due to elongation by host FA elongase (ELOVL6) or metabolism by the gut microbiota. The finding that elongation of labeled FA 16:0 was also observed in gut contents of mice without gut microbiota points towards FA metabolism by host enzymes. In any case, the observed levels of FA 18:0[D5/31] were 100-fold lower than those of the labeled FA 16:0 precursors and therefore negligible in influencing lipid uptake.

Gut bacteria might not only elongate, but also hydrolyze or absorb dietary TG, competing with the host for these nutrients. For example, it was shown that certain species of the family of *Coriobacteriaceae,* namely *Collinsella aerofaciens* and *Atopobium parvulum*, exhibit TAG lipase activity *in vitro* (Just 2017). Whether these bacteria also colonize in the SI, the location of dietary lipid absorption, and whether their lipase activities significantly contribute to the already very efficient TG digestion by PNLIP, is unclear. It is likely that their lipase activity rather allows them to metabolize TG in the colon, which have escaped absorption in the SI (Hoyles and Wallace 2010). In any case, bacterial TG lipase activity could not explain the observed differences in lipid uptake, as the uptake of FA 16:0[D5] from FFA and FA 16:0[D31] from TG were similar in all observed matrices.

In vivo in the SI, the gut microbiota does probably not metabolize a significant amount of dietary TG due to their low abundance. Given the average weight of a gut bacterium at 5 pg, the SI bacterial density at 10^8 CFU/mL (Sender et al. 2016) and the average SI volume in mice with around 1 mL (Casteleyn et al. 2010), there are about 0.5 mg of bacteria in the SI. The total weight of the lipids supplied in the oral gavage ($\approx$ 92 mg olive oil + 6 mg labeled lipids) therefore exceeded the total bacterial weight in the SI by more than 190-fold.

In conclusion, direct gut microbial metabolism might occur in the SI but is likely not metabolizing significant amounts of dietary fat to be able to explain lower intestinal lipid absorption in colonized compared to GF animals.

4.3. BILE ENZYMES AS UNEXPECTED REGULATORS OF LIPID ABSORPTION

4.3.1. PLA$_1$ activity converts PC to *sn*-2 LPC in mouse bile

Until now, enzymatic reactions in the bile have not received much attention in the literature. In the current work, a rapid (< 2 min) and very efficient microbiome-dependent enzymatic conversion of PC to LPC was identified in bile. A phospholipase activity assay revealed PLA$_1$ rather than PLA$_2$ activity.

Additional strong support for the general presence of PLA$_1$ activity in bile comes from the measured *in vivo* PC and LPC species profiles of mouse bile (Supplemental Figure 3, Supplemental Figure 6). The bile phospholipid pool is quite different from that of the liver, containing $> 70\%$ PC species with FA 16:0 at the *sn*-1 and unsaturated FA at the *sn*-2 position (Hay et al. 1993). PLA$_1$ activity would therefore mainly cleave FA 16:0 to produce unsaturated LPC species, which is exactly what was observed in mouse bile with $> 80\%$ of all LPC being unsaturated.

4.3.2. Bile proteomics identified phospholipase candidates in bile

The origin and identity of the enzymes which cleaved phospholipids in bile was not initially clear. Previous studies in humans observed increased PLA$_1$ and PLA$_2$ activity of bacterial origin in human bile samples with gallbladder infections (Nakano et al. 1988). The presence of PLA$_1$ and PLA$_2$ in human gallbladder epithelium was also suggested before (Tagesson et al. 1979).

To identify potential proteins with phospholipase activity, the bile proteome was analyzed. To this date, a handful of studies have investigated the bile proteome in humans (Barbhuiya et al. 2011; Farina et al. 2011; Farina et al. 2014; Megger et al. 2017; Son et al. 2020). Only one study was performed in rats (Ciordia et al. 2021) and no mouse proteome data were available.

The proteomic analysis of mouse bile identified ~400–700 murine proteins, but none from bacteria, making a microbial origin of phospholipase activity unlikely. Surprisingly, in the bile proteome datasets, neither mouse/human phospholipase A$_1$ (PLA$_1$) nor phospholipase A$_2$ (PLA$_2$) proteins were detected. However, carboxyl ester lipase (CEL), described to possess a phospholipase activity (Hui and Howles 2002), was detected in all mouse bile samples at very high levels. The hydrolytic activity of CEL requires the presence of bile acids (BA) containing 3α,7α-hydroxy groups such as TCA (3α,7α,12α-OH) (Wang et al. 1997; Fontbonne et al. 2011). TCA binds near the active site, inducing the formation of a hydrophobic pocket which makes the enzyme accessible for substrates (Wang et al. 1997). In SPF mouse bile, almost 60% of all BA is made up of TCA and it positively correlates with bile LPC levels, supporting a microbiota mediated activation of CEL in bile.

Proteomic data indicate that CEL is the sole enzyme explaining the observed PLA$_1$ activity in the bile. Ongoing studies employing GF and SPF $Cel^{-/-}$ mice could experimentally verify the role of CEL in the microbiota-dependent biliary PC metabolism and dietary lipid absorption.

Yet, there is a small chance that unidentified enzymes besides CEL might also contribute to the biliary PC to LPC degradation. They could either be present at concentrations too low to be detected in the proteomic analyses, or their PLA$_1$ activity was not typically observed under most experimental conditions in the literature. For example, it was described that PNLIP was also able to cleave FA at the sn-1 position of phospholipids $in vitro$, but a contamination of the purified PNLIP with other phospholipases could not be ruled out (Haas et al. 1965). In the future, enzymatic assays with raw bile or purified CEL might identify new potent activators of biliary PLA$_1$ activity which could be used to reduce dietary lipid uptake.

4.3.3. The pancreas is likely the source for bile enzymatic activity

Besides identifying candidate PLA$_1$ enzymes, the bile proteomics dataset also provided some clear clues as to the source of the enzymatic activity in mouse bile. Since not only CEL but also other enzymes of pancreatic origin were highly enriched in the mouse bile samples, the reflux of pancreatic juice into the gallbladder was the most plausible source for PLA$_1$ activity in bile.
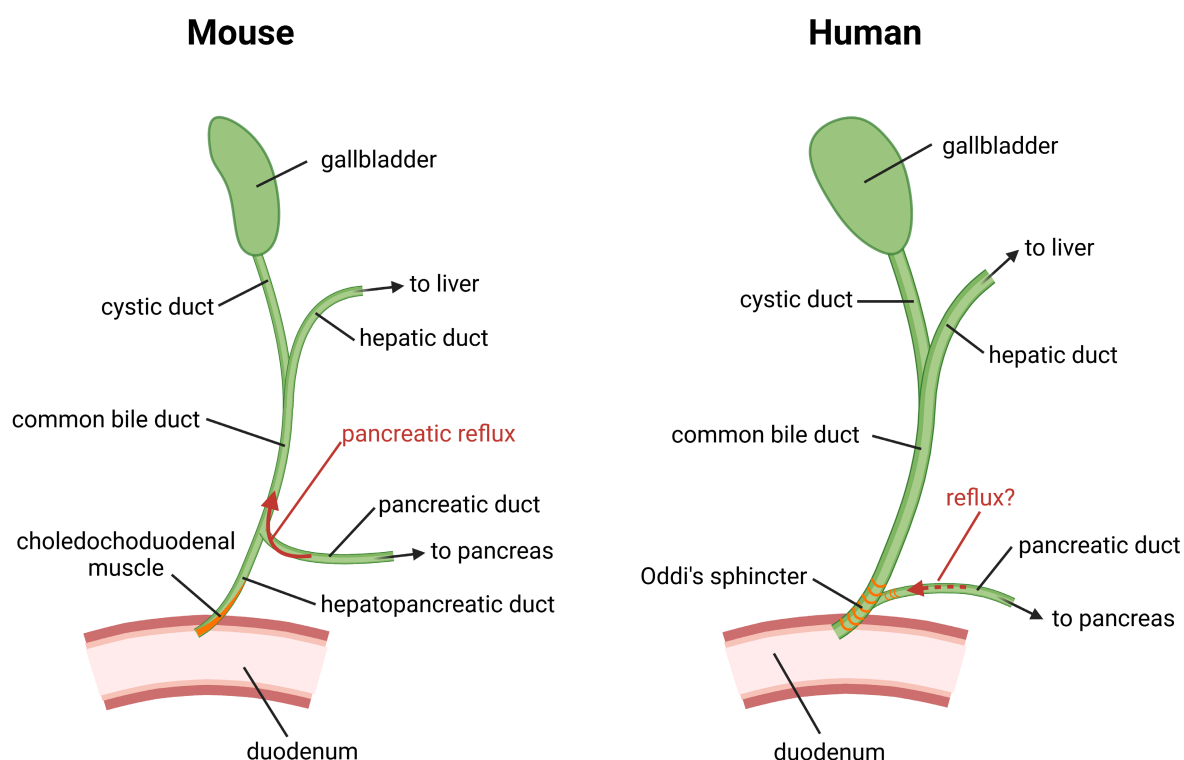
Figure 34. Anatomy and differences of the mouse and human biliary systems
The biliary tract is colored green, the duodenum is colored red, and smooth muscle is colored orange. Illustration based on Higashiyama et al. 2016.

In mice, the branching point of the pancreatic duct is far from the duodenum and not constricted by muscles, allowing the retrograde flow of pancreatic juice into the gallbladder (Figure 34) (Higashiyama et al. 2016). In humans however, the pancreatic duct joins the common bile duct close to the duodenal wall and both ducts are enclosed by Oddi's sphincter (Figure 34). This muscle restricts the secretion of bile and pancreatic juice into the intestine and might reduce pancreatic reflux into the common bile duct and the gallbladder. In line with that, pancreatic enzymes in the analyzed human sample were several orders of magnitude lower than in the mouse samples (Figure 27). Interestingly, patients with anomalous pancreaticobiliary ductal junction (APBDJ) have a similar biliary tract anatomy as mice, with the pancreatic duct junction outside the duodenal wall. In those patients, reflux of pancreatic juice and increased activity of pancreatic enzymes such as PLA_2 and amylase were observed (Shimada et al. 1991).

Investigations with larger human bile cohorts would help to further study the presence of CEL and understand pancreatic reflux in humans. A proteomic analysis of mouse and human gallbladder tissue samples could clarify whether CEL might also originate from gallbladder epithelial cells, which was not investigated here.

Of note, other strategies to manipulate the PC/LPC ratio besides targeting CEL could also be used to modulate dietary lipid uptake.

4.3.4. The *Cyp2c70$^{-/-}$* mouse model supports a PLA$_1$ regulation by TCA

A regulation of PLA_1 activity by the gut microbiome via TCA levels in bile is supported by the increase in phospholipase activity upon stimulation with TCA (Figure 29). The proteomic datasets indicated that PLA_1 activity is not regulated at the protein level as the amount of CEL was similar between GF, OMM^{12} and SPF mice (Figure 27).

Further support for a BA mediated regulation of PLA_1 activity comes from the experiments with *Cyp2c70$^{-/-}$* mice. They harbored 90% lower TCA levels than control animals, leading to around ~80% less *sn*-2 LPC being released by PLA_1 in the *in vitro* phospholipase assay (Figure 31B, Figure 33A). The uptake of stable isotope labeled lipids in *Cyp2c70$^{-/-}$* mice vs. controls was not investigated in this thesis. However, studies showed that despite the lower TCA levels and reduced PC degradation in the bile, *Cyp2c70$^{-/-}$* mice show an impaired lipid and cholesterol absorption. Female KO mice were protected from DIO and liver steatosis on a WTD (Li et al. 2021). In accordance, a reduced accumulation of liver TG in KO mice was also observed in the current work, with TG levels down by more than 50% (Figure 32B).

The seemingly contradictory results can be explained by the fact that not only biliary TCA levels were reduced in *Cyp2c70$^{-/-}$* mice. They possess a highly hydrophobic BA profile compared to the typical hydrophilic profile of WT mice and show certain pathologies such as neonatal cholestasis (Boer et al. 2021). Total BA levels in the gallbladder of *Cyp2c70$^{-/-}$* mice were also reduced by half (Figure 31A), which is not the case comparing GF with SPF bile (Figure 28A).

In sum, the *Cyp2c70*$^{-/-}$ model provides additional evidence for the activation of biliary PLA$_1$ by increased TCA levels.

In the future, it would be helpful to use additional *Cyp* KO models to further evaluate the relationship between TCA levels and PLA$_1$ regulation. *Cyp8b1*$^{-/-}$ mice for example lack the enzyme for hepatic 12α-hydroxylation of the sterol backbone and are devoid of TCA (Bertaggia et al. 2017). Dietary supplementation of TCA might also be used to increase bile TCA levels and study the impact on PLA$_1$ activity.

4.4. MODULATION OF THE GUT MICROBIOTA TO LIMIT FAT UPTAKE

The manipulation of the gut microbiome to reduce intestinal lipid absorption in the context of obesity or other pathologies with excessive fat intake such as intestinal or liver cancer (Sohn et al. 2021; Ocvirk and O'Keefe 2020) may offer new therapeutic perspectives. Especially the promotion of gut microbial diversity seems to be of importance, as adiposity, insulin resistance and dyslipidemia were linked to reduced bacterial richness (Le Chatelier et al. 2013). Indeed, most of the parameters analysed in this thesis (uptake of labeled FA, k_{abs}, PC/LPC ratio, PLA$_1$ activity and TCA levels) changed gradually with the bacterial richness from GF to OMM[11/12] and further in SPF animals. Diet-based approaches such as increasing dietary fiber, or the consumption of fermented foods are therefore promising strategies in reducing long-term weight gain (Makki et al. 2018; Wastyk et al. 2021).

The molecular mechanism regulating intestinal lipid resorption via changes in biliary PC/LPC suggests several targets to decrease dietary fat uptake. PC contents could be reduced by inhibiting ABCB4 mediated PC secretion from the liver. The antimycotic drug itraconazole inhibiting ABCB4 was shown to drastically reduce biliary PL in rats at clinically relevant concentrations (Yoshikado et al. 2011).

Pharmacological inhibitors of lipid digestion and absorption have been investigated for some time now. Famous examples include the PNLIP inhibitor orlistat or the bile acid sequestrant cholestyramine. However, these drugs come with partially severe adverse effects such as steatorrhoea with diarrhoea and fat-soluble vitamin deficiency, constipation and bloating (Ko et al. 2020). Indeed, the ABCB4 inhibitor itraconazole induces cholestasis and the lack of protective PL in the biliary tree leads to cholangiopathy due to the unchecked detergent effects of BA (Yoshikado et al. 2011; Sticova and Jirsa 2020).

Therefore, the newly discovered mechanism of PC to LPC degradation in the bile might offer new, more tolerable treatment options for obesity. PC to LPC conversion could be induced by elevating TCA levels to activate PLA$_1$.

Changing the gut microbial composition and diversity to increase host lipid metabolism and energy expenditure is another promising approach to combat obesity. In a human study, live or pasteurized *A. muciniphila* supplementation improved several metabolic parameters such as insulin sensitivity and plasma cholesterol levels in obese patients (Depommier et al. 2019). In DIO mice, pasteurized

A. muciniphila increased whole-body energy expenditure and fecal energy excretion (Depommier et al. 2020). Fittingly, OMM[11] mice lacking *A. muciniphila* showed slightly higher uptake of the stable isotope labeled lipids compared to OMM[12] mice. Dozens of other clinical studies are investigating the impact of probiotic supplementation for the treatment of overweight and obesity (Wiciński et al. 2020). *Bifidobacterium animalis*, a bacterium frequently used in those studies, is also part of the OMM[12] consortium.

In the future, new OMM consortia lacking *B. animalis* could be used to study the impact on dietary lipid uptake using the stable isotope labeled gavages. Supplementation with specific microbial consortia, e.g. containing *A. muciniphila* and *B. animalis*, to increase microbial richness, might open new venues to reduce intestinal lipid absorption and treat related diseases.

4.5. CONCLUSIONS AND OUTLOOK

The present thesis contributes novel key insights to the yet incomplete picture of gut microbial regulation of dietary fat digestion and absorption. For the first time, a comprehensive lipidomic flux analysis in GF and colonized mice was performed, tracking the uptake of stable isotope labeled dietary lipids from the small intestine. The gut microbiota regulates hepatic BA synthesis important for PL metabolism in bile and dietary lipid emulsification. In colonized mice, TCA levels were increased, promoting biliary PLA_1 activity. CEL, catalyzing PC to *sn-2* LPC degradation, was identified in bile. Further, the proteomic dataset of mouse bile has shed the light on the so far overlooked enzymatic potential of bile to influence host metabolism in health and disease.

In the future, the newly discovered microbial regulation of lipid uptake will be further investigated by employing gnotobiotic *Cel* KO mice. To better understand the principal effect of PC, LPC and BA on the formation of mixed micelles, concentrations of one or several of the constituents could be altered *in vitro* and micelle parameters measured. Especially the influence *sn*-1 vs. *sn*-2 LPC on micelle formation has not been investigated so far.

Because, excessive fat intake is also associated with many other pathologies such as colorectal cancer, the current findings certainly have a relevance in the pathophysiological context. Whether colorectal cancer cells fuel their lipid demand mainly from *de novo* FA synthesis or by taking up those lipids directly from the intestine, is not yet clear. It will be investigated in a follow up project in the framework of the CRC 1371 using the established stable isotope labeling strategies.

5. REFERENCES

Abrams, G. D.; Bishop, J. E. (1967): Effect of the normal microbial flora on gastrointestinal motility. In *Proceedings of the Society for Experimental Biology and Medicine. Society for Experimental Biology and Medicine (New York, N.Y.)* 126 (1), pp. 301–304. DOI: 10.3181/00379727-126-32430.

Aguiar Vallim, T. Q. de; Tarling, E. J.; Edwards, P. A. (2013): Pleiotropic roles of bile acids in metabolism. In *Cell metabolism* 17 (5), pp. 657–669. DOI: 10.1016/j.cmet.2013.03.013.

Altmann, S. W.; Davis, H. R.; Zhu, L.-J.; Yao, X.; Hoos, L. M.; Tetzloff, G. et al. (2004): Niemann-Pick C1 Like 1 protein is critical for intestinal cholesterol absorption. In *Science (New York, N.Y.)* 303 (5661), pp. 1201–1204. DOI: 10.1126/science.1093131.

Araújo, J. R.; Tazi, A.; Burlen-Defranoux, O.; Vichier-Guerre, S.; Nigro, G.; Licandro, H. et al. (2020): Fermentation Products of Commensal Bacteria Alter Enterocyte Lipid Metabolism. In *Cell host & microbe* 27 (3), 358-375.e7. DOI: 10.1016/j.chom.2020.01.028.

Bäckhed, F.; Ding, H.; Wang, T.; Hooper, L. V.; Koh, G. Y.; Nagy, A. et al. (2004): The gut microbiota as an environmental factor that regulates fat storage. In *Proceedings of the National Academy of Sciences of the United States of America* 101 (44), pp. 15718–15723. DOI: 10.1073/pnas.0407076101.

Bäckhed, F.; Manchester, J. K.; Semenkovich, C. F.; Gordon, J. I. (2007): Mechanisms underlying the resistance to diet-induced obesity in germ-free mice. In *Proceedings of the National Academy of Sciences of the United States of America* 104 (3), pp. 979–984. DOI: 10.1073/pnas.0605374104.

Barbhuiya, M. A.; Sahasrabuddhe, N. A.; Pinto, S. M.; Muthusamy, B.; Singh, T. D.; Nanjappa, V. et al. (2011): Comprehensive proteomic analysis of human bile. In *Proteomics* 11 (23), pp. 4443–4453. DOI: 10.1002/pmic.201100197.

Basic, M.; Bolsega, S.; Smoczek, A.; Gläsner, J.; Hiergeist, A.; Eberl, C. et al. (2021): Monitoring and contamination incidence of gnotobiotic experiments performed in microisolator cages. In *International journal of medical microbiology : IJMM* 311 (3), p. 151482. DOI: 10.1016/j.ijmm.2021.151482.

Bertaggia, E.; Jensen, K. K.; Castro-Perez, J.; Xu, Y.; Di Paolo, G.; Chan, R. B. et al. (2017): Cyp8b1 ablation prevents Western diet-induced weight gain and hepatic steatosis because of impaired fat absorption. In *American journal of physiology. Endocrinology and metabolism* 313 (2), E121-E133. DOI: 10.1152/ajpendo.00409.2016.

Besten, G. den; van Eunen, K.; Groen, A. K.; Venema, K.; Reijngoud, D.-J.; Bakker, B. M. (2013): The role of short-chain fatty acids in the interplay between diet, gut microbiota, and host energy metabolism. In *Journal of lipid research* 54 (9), pp. 2325–2340. DOI: 10.1194/jlr.R036012.

Bian, Y.; Zheng, R.; Bayer, F. P.; Wong, C.; Chang, Y.-C.; Meng, C. et al. (2020): Robust, reproducible and quantitative analysis of thousands of proteomes by micro-flow LC-MS/MS. In *Nature communications* 11 (1), p. 157. DOI: 10.1038/s41467-019-13973-x.

Blaut, M. (2018): Composition and Function of the Gut Microbiome. In Dirk Haller (Ed.): The Gut Microbiome in Health and Disease. Cham: Springer International Publishing, pp. 5–30.

Boer, J. F. de; Verkade, E.; Mulder, N. L.; Vries, H. D. de; Huijkman, N.; Koehorst, M. et al. (2020): A human-like bile acid pool induced by deletion of hepatic Cyp2c70 modulates effects of FXR activation in mice. In *Journal of lipid research* 61 (3), pp. 291–305. DOI: 10.1194/jlr.RA119000243.

Boer, J. F. de; Vries, H. D. de; Palmiotti, A.; Li, R.; Doestzada, M.; Hoogerland, J. A. et al. (2021): Cholangiopathy and Biliary Fibrosis in Cyp2c70-Deficient Mice Are Fully Reversed by Ursodeoxycholic Acid. In *Cellular and molecular gastroenterology and hepatology* 11 (4), pp. 1045–1069. DOI: 10.1016/j.jcmgh.2020.12.004.

Brannon, P. M.; Tso, P.; Jandacek R. J. (2018): Digestion and Absorption of Lipids. In Martha H. Stipanuk: Biochemical, physiological, and molecular aspects of human nutrition. Fourth edition. Edited by Martha H. Stipanuk, Marie A. Caudill. Philadelphia: Saunders, pp. 179–193.

Brugiroux, S.; Beutler, M.; Pfann, C.; Garzetti, D.; Ruscheweyh, H.-J.; Ring, D. et al. (2016): Genome-guided design of a defined mouse microbiota that confers colonization resistance against Salmonella enterica serovar Typhimurium. In *Nature microbiology* 2, p. 16215. DOI: 10.1038/NMICROBIOL.2016.215.

Cani, P. D.; Vos, W. M. de (2017): Next-Generation Beneficial Microbes: The Case of Akkermansia muciniphila. In *Frontiers in Microbiology* 8. DOI: 10.3389/fmicb.2017.01765.

Casteleyn, C.; Rekecki, A.; van der Aa, A.; Simoens, P.; van den Broeck, W. (2010): Surface area assessment of the murine intestinal tract as a prerequisite for oral dose translation from mouse to man. In *Laboratory animals* 44 (3), pp. 176–183. DOI: 10.1258/la.2009.009112.

Chen, H. L.; Haack, V. S.; Janecky, C. W.; Vollendorf, N. W.; Marlett, J. A. (1998): Mechanisms by which wheat bran and oat bran increase stool weight in humans. In *The American journal of clinical nutrition* 68 (3), pp. 711–719. DOI: 10.1093/ajcn/68.3.711.

Chow, E. C. Y.; Magomedova, L.; Quach, H. P.; Patel, R.; Durk, M. R.; Fan, J. et al. (2014): Vitamin D receptor activation down-regulates the small heterodimer partner and increases CYP7A1 to lower cholesterol. In *Gastroenterology* 146 (4), pp. 1048–1059. DOI: 10.1053/j.gastro.2013.12.027.

Ciordia, S.; Alvarez-Sola, G.; Rullán, M.; Urman, J. M.; Ávila, M. A.; Corrales, F. J. (2021): Digging deeper into bile proteome. In *Journal of proteomics* 230, p. 103984. DOI: 10.1016/j.jprot.2020.103984.

Claus, S. P.; Ellero, S. L.; Berger, B.; Krause, L.; Bruttin, A.; Molina, J. et al. (2011): Colonization-induced host-gut microbial metabolic interaction. In *mBio* 2 (2), e00271-10. DOI: 10.1128/mBio.00271-10.

Cox, J.; Mann, M. (2008): MaxQuant enables high peptide identification rates, individualized p.p.b.-range mass accuracies and proteome-wide protein quantification. In *Nature biotechnology* 26 (12), pp. 1367–1372. DOI: 10.1038/nbt.1511.

Demenis, C.; McLaughlin, J.; Smith, C. P. (2017): Sulfated Cholecystokinin-8 Promotes CD36-Mediated Fatty Acid Uptake into Primary Mouse Duodenal Enterocytes. In *Frontiers in Physiology* 8, p. 660. DOI: 10.3389/fphys.2017.00660.

Depommier, C.; Everard, A.; Druart, C.; Plovier, H.; van Hul, M.; Vieira-Silva, S. et al. (2019): Supplementation with Akkermansia muciniphila in overweight and obese human volunteers: a proof-of-concept exploratory study. In *Nature medicine* 25 (7), pp. 1096–1103. DOI: 10.1038/s41591-019-0495-2.

Depommier, C.; van Hul, M.; Everard, A.; Delzenne, N. M.; Vos, W. M. de; Cani, P. D. (2020): Pasteurized Akkermansia muciniphila increases whole-body energy expenditure and fecal energy excretion in diet-induced obese mice. In *Gut microbes* 11 (5), pp. 1231–1245. DOI: 10.1080/19490976.2020.1737307.

Donaldson, G. P.; Lee, S. M.; Mazmanian, S. K. (2016): Gut biogeography of the bacterial microbiota. In *Nature reviews. Microbiology* 14 (1), pp. 20–32. DOI: 10.1038/nrmicro3552.

Drover, V. A.; Ajmal, M.; Nassir, F.; Davidson, N. O.; Nauli, A. M.; Sahoo, D. et al. (2005): CD36 deficiency impairs intestinal lipid secretion and clearance of chylomicrons from the blood. In *The Journal of clinical investigation* 115 (5), pp. 1290–1297. DOI: 10.1172/JCI21514.

Ecker, J.; Scherer, M.; Schmitz, G.; Liebisch, G. (2012): A rapid GC-MS method for quantification of positional and geometric isomers of fatty acid methyl esters. In *Journal of chromatography. B, Analytical technologies in the biomedical and life sciences* 897, pp. 98–104. DOI: 10.1016/j.jchromb.2012.04.015.

Ermund, A.; Schütte, A.; Johansson, M. E. V.; Gustafsson, J. K.; Hansson, G. C. (2013): Studies of mucus in mouse stomach, small intestine, and colon. I. Gastrointestinal mucus layers have different properties depending on location as well as over the Peyer's patches. In *American journal of physiology. Gastrointestinal and liver physiology* 305 (5), G341-7. DOI: 10.1152/ajpgi.00046.2013.

Fan, Y.; Pedersen, O. (2021): Gut microbiota in human metabolic health and disease. In *Nature reviews. Microbiology* 19 (1), pp. 55–71. DOI: 10.1038/s41579-020-0433-9.

Farina, A.; Dumonceau, J.-M.; Antinori, P.; Annessi-Ramseyer, I.; Frossard, J.-L.; Hochstrasser, D. F. et al. (2014): Bile carcinoembryonic cell adhesion molecule 6 (CEAM6) as a biomarker of malignant biliary stenoses. In *Biochimica et biophysica acta* 1844 (5), pp. 1018–1025. DOI: 10.1016/j.bbapap.2013.06.010.

Farina, A.; Dumonceau, J.-M.; Delhaye, M.; Frossard, J.-L.; Hadengue, A.; Hochstrasser, D. F.; Lescuyer, P. (2011): A step further in the analysis of human bile proteome. In *Journal of proteome research* 10 (4), pp. 2047–2063. DOI: 10.1021/pr200011b.

Fleissner, C. K.; Huebel, N.; Abd El-Bary, M. M.; Loh, G.; Klaus, S.; Blaut, M. (2010): Absence of intestinal microbiota does not protect mice from diet-induced obesity. In *The British journal of nutrition* 104 (6), pp. 919–929. DOI: 10.1017/S0007114510001303.

Fontbonne, H.; Brisson, L.; Vérine, A.; Puigserver, A.; Lombardo, D.; Ajandouz, E. H. (2011): Human bile salt-dependent lipase efficiency on medium-chain acyl-containing substrates: control by sodium taurocholate. In *Journal of biochemistry* 149 (2), pp. 145–151. DOI: 10.1093/jb/mvq132.

Friedman, E.; Isaksson, P.; Rafter, J.; Marian, B.; Winawer, S.; Newmark, H. (1989): Fecal diglycerides as selective endogenous mitogens for premalignant and malignant human colonic epithelial cells. In *Cancer research* 49 (3), pp. 544–548.

Gåfvels, M.; Olin, M.; Chowdhary, B. P.; Raudsepp, T.; Andersson, U.; Persson, B. et al. (1999): Structure and chromosomal assignment of the sterol 12alpha-hydroxylase gene (CYP8B1) in human and mouse: eukaryotic cytochrome P-450 gene devoid of introns. In *Genomics* 56 (2), pp. 184–196. DOI: 10.1006/geno.1998.5606.

Glatz, J. F. C.; Luiken, J. J. F. P.; Bonen, A. (2010): Membrane fatty acid transporters as regulators of lipid metabolism: implications for metabolic disease. In *Physiological reviews* 90 (1), pp. 367–417. DOI: 10.1152/physrev.00003.2009.

Goodwin, B.; Gauthier, K. C.; Umetani, M.; Watson, M. A.; Lochansky, M. I.; Collins, J. L. et al. (2003): Identification of bile acid precursors as endogenous ligands for the nuclear xenobiotic pregnane X receptor. In *Proceedings of the National Academy of Sciences of the United States of America* 100 (1), pp. 223–228. DOI: 10.1073/pnas.0237082100.

Goodwin, B.; Jones, S. A.; Price, R. R.; Watson, M. A.; McKee, D. D.; Moore, L. B. et al. (2000): A Regulatory Cascade of the Nuclear Receptors FXR, SHP-1, and LRH-1 Represses Bile Acid Biosynthesis. In *Molecular Cell* 6 (3), pp. 517–526. DOI: 10.1016/S1097-2765(00)00051-4.

Gupta, A. (2019): Digestion and Absorption of Lipids. In Anil Gupta (Ed.): Comprehensive biochemistry for dentistry. Textbook for dental students. Singapore: Springer (Springer eBook Collection), pp. 441–450.

Haas, G. H. de; Sarda, L.; Roger, J. (1965): Positional specific hydrolysis of phospholipids by pancreatic lipase. In *Biochimica et biophysica acta* 106 (3), pp. 638–640. DOI: 10.1016/0005-2760(65)90082-2.

Hartmann, D.; Hussain, Y.; Güzelhan, C.; Odink, J. (1993): Effect on dietary fat absorption of orlistat, administered at different times relative to meal intake. In *British journal of clinical pharmacology* 36 (3), pp. 266–270. DOI: 10.1111/j.1365-2125.1993.tb04228.x.

Hay, D. W.; Cahalane, M. J.; Timofeyeva, N.; Carey, M. C. (1993): Molecular species of lecithins in human gallbladder bile. In *Journal of lipid research* 34 (5), pp. 759–768.

He, X.; McClorry, S.; Hernell, O.; Lönnerdal, B.; Slupsky, C. M. (2020): Digestion of human milk fat in healthy infants. In *Nutrition research (New York, N.Y.)* 83, pp. 15–29. DOI: 10.1016/j.nutres.2020.08.002.

Herath, M.; Hosie, S.; Bornstein, J. C.; Franks, A. E.; Hill-Yardin, E. L. (2020): The Role of the Gastrointestinal Mucus System in Intestinal Homeostasis: Implications for Neurological Disorders. In *Frontiers in cellular and infection microbiology* 10, p. 248. DOI: 10.3389/fcimb.2020.00248.

Herp, S.; Brugiroux, S.; Garzetti, D.; Ring, D.; Jochum, L. M.; Beutler, M. et al. (2019): Mucispirillum schaedleri Antagonizes Salmonella Virulence to Protect Mice against Colitis. In *Cell host & microbe* 25 (5), 681-694.e8. DOI: 10.1016/j.chom.2019.03.004.

Higashiyama, H.; Sumitomo, H.; Ozawa, A.; Igarashi, H.; Tsunekawa, N.; Kurohmaru, M.; Kanai, Y. (2016): Anatomy of the Murine Hepatobiliary System: A Whole-Organ-Level Analysis Using a Transparency Method. In *Anatomical record (Hoboken, N.J. : 2007)* 299 (2), pp. 161–172. DOI: 10.1002/ar.23287.

Ho, S. Y.; Storch, J. (2001): Common mechanisms of monoacylglycerol and fatty acid uptake by human intestinal Caco-2 cells. In *American journal of physiology. Cell physiology* 281 (4), C1106-17. DOI: 10.1152/ajpcell.2001.281.4.C1106.

Hoene, M.; Li, J.; Häring, H.-U.; Weigert, C.; Xu, G.; Lehmann, R. (2014): The lipid profile of brown adipose tissue is sex-specific in mice. In *Biochimica et biophysica acta* 1842 (10), pp. 1563–1570. DOI: 10.1016/j.bbalip.2014.08.003.

Hofmann, A. F.; Small, D. M. (1967): Detergent properties of bile salts: correlation with physiological function. In *Annual review of medicine* 18, pp. 333–376. DOI: 10.1146/annurev.me.18.020167.002001.

Honda, A.; Miyazaki, T.; Iwamoto, J.; Hirayama, T.; Morishita, Y.; Monma, T. et al. (2020): Regulation of bile acid metabolism in mouse models with hydrophobic bile acid composition. In *Journal of lipid research* 61 (1), pp. 54–69. DOI: 10.1194/jlr.RA119000395.

Höring, M.; Ejsing, C. S.; Hermansson, M.; Liebisch, G. (2019): Quantification of Cholesterol and Cholesteryl Ester by Direct Flow Injection High-Resolution Fourier Transform Mass Spectrometry Utilizing Species-Specific Response Factors. In *Analytical chemistry* 91 (5), pp. 3459–3466. DOI: 10.1021/acs.analchem.8b05013.

Höring, M.; Ejsing, C. S.; Krautbauer, S.; Ertl, V. M.; Burkhardt, R.; Liebisch, G. (2021): Accurate quantification of lipid species affected by isobaric overlap in Fourier-transform mass spectrometry. In *Journal of lipid research* 62, p. 100050. DOI: 10.1016/j.jlr.2021.100050.

Hoyles, L.; Wallace, R. J. (2010): Gastrointestinal Tract: Fat Metabolism in the Colon. In Kenneth N. Timmis (Ed.): Handbook of Hydrocarbon and Lipid Microbiology. 1. ed., [elektronische Ressource]. Berlin, Heidelberg: Springer, pp. 3111–3118.

Hsieh, J.; Longuet, C.; Maida, A.; Bahrami, J.; Xu, E.; Baker, C. L. et al. (2009): Glucagon-like peptide-2 increases intestinal lipid absorption and chylomicron production via CD36. In *Gastroenterology* 137 (3), 997-1005, 1005.e1-4. DOI: 10.1053/j.gastro.2009.05.051.

Hui, D. Y.; Howles, P. N. (2002): Carboxyl ester lipase: structure-function relationship and physiological role in lipoprotein metabolism and atherosclerosis. In *Journal of lipid research* 43 (12), pp. 2017–2030. DOI: 10.1194/jlr.r200013-jlr200.

Husebye, E.; Hellström, P. M.; Midtvedt, T. (1992): Introduction of conventional microbial flora to germfree rats increases the frequency of migrating myoelectric complexes. In *Neurogastroenterology & Motility* 4 (1), pp. 39–45. DOI: 10.1111/j.1365-2982.1992.tb00077.x.

Husebye, E.; Hellström, P. M.; Midtvedt, T. (1994): Intestinal microflora stimulates myoelectric activity of rat small intestine by promoting cyclic initiation and aboral propagation of migrating myoelectric complex. In *Digestive diseases and sciences* 39 (5), pp. 946–956. DOI: 10.1007/bf02087542.

Hussain, M. M. (2014): Intestinal lipid absorption and lipoprotein formation. In *Current opinion in lipidology* 25 (3), pp. 200–206. DOI: 10.1097/MOL.0000000000000084.

Hussain, Y.; Güzelhan, C.; Odink, J.; van der Beek, E. J.; Hartmann, D. (1994): Comparison of the inhibition of dietary fat absorption by full versus divided doses of orlistat. In *Journal of clinical pharmacology* 34 (11), pp. 1121–1125. DOI: 10.1002/j.1552-4604.1994.tb01990.x.

Inagaki, T.; Choi, M.; Moschetta, A.; Peng, L.; Cummins, C. L.; McDonald, J. G. et al. (2005): Fibroblast growth factor 15 functions as an enterohepatic signal to regulate bile acid homeostasis. In *Cell metabolism* 2 (4), pp. 217–225. DOI: 10.1016/j.cmet.2005.09.001.

Jahan, A.; Chiang, J. Y. L. (2005): Cytokine regulation of human sterol 12alpha-hydroxylase (CYP8B1) gene. In *American journal of physiology. Gastrointestinal and liver physiology* 288 (4), G685-95. DOI: 10.1152/ajpgi.00207.2004.

Jay, A. G.; Simard, J. R.; Huang, N.; Hamilton, J. A. (2020): SSO and other putative inhibitors of FA transport across membranes by CD36 disrupt intracellular metabolism, but do not affect FA translocation. In *Journal of lipid research* 61 (5), pp. 790–807. DOI: 10.1194/jlr.RA120000648.

Johansson, M. E. V.; Jakobsson, H. E.; Holmén-Larsson, J.; Schütte, A.; Ermund, A.; Rodríguez-Piñeiro, A. M. et al. (2015): Normalization of Host Intestinal Mucus Layers Requires Long-Term Microbial Colonization. In *Cell host & microbe* 18 (5), pp. 582–592. DOI: 10.1016/j.chom.2015.10.007.

Jumpertz, R.; Le, D. S.; Turnbaugh, P. J.; Trinidad, C.; Bogardus, C.; Gordon, J. I.; Krakoff, J. (2011): Energy-balance studies reveal associations between gut microbes, caloric load, and nutrient absorption in humans. In *The American journal of clinical nutrition* 94 (1), pp. 58–65. DOI: 10.3945/ajcn.110.010132.

Just, S. (2017): Impact of the interplay between bile acids, lipids, intestinal *Coriobacteriaceae* and diet on host metabolism. Dissertation. Universitätsbibliothek der TU München, München.

Kastl, A. J.; Terry, N. A.; Wu, G. D.; Albenberg, L. G. (2020): The Structure and Function of the Human Small Intestinal Microbiota: Current Understanding and Future Directions. In *Cellular and molecular gastroenterology and hepatology* 9 (1), pp. 33–45. DOI: 10.1016/j.jcmgh.2019.07.006.

Kennelly, J. P.; van der Veen, J. N.; Nelson, R. C.; Leonard, K.-A.; Havinga, R.; Buteau, J. et al. (2018): Intestinal de novo phosphatidylcholine synthesis is required for dietary lipid absorption and metabolic homeostasis. In *Journal of lipid research* 59 (9), pp. 1695–1708. DOI: 10.1194/jlr.M087056.

Kimura, I.; Ozawa, K.; Inoue, D.; Imamura, T.; Kimura, K.; Maeda, T. et al. (2013): The gut microbiota suppresses insulin-mediated fat accumulation via the short-chain fatty acid receptor GPR43. In *Nature communications* 4, p. 1829. DOI: 10.1038/ncomms2852.

Kindt, A.; Liebisch, G.; Clavel, T.; Haller, D.; Hörmannsperger, G.; Yoon, H. et al. (2018): The gut microbiota promotes hepatic fatty acid desaturation and elongation in mice. In *Nature communications* 9 (1), p. 3760. DOI: 10.1038/s41467-018-05767-4.

Kishino, S.; Takeuchi, M.; Park, S.-B.; Hirata, A.; Kitamura, N.; Kunisawa, J. et al. (2013): Polyunsaturated fatty acid saturation by gut lactic acid bacteria affecting host lipid composition. In *Proceedings of the National Academy of Sciences of the United States of America* 110 (44), pp. 17808–17813. DOI: 10.1073/pnas.1312937110.

Ko, C.-W.; Qu, J.; Black, D. D.; Tso, P. (2020): Regulation of intestinal lipid metabolism: current concepts and relevance to disease. In *Nature reviews. Gastroenterology & hepatology* 17 (3), pp. 169–183. DOI: 10.1038/s41575-019-0250-7.

Koh, A.; Bäckhed, F. (2020): From Association to Causality: the Role of the Gut Microbiota and Its Functional Products on Host Metabolism. In *Molecular Cell* 78 (4), pp. 584–596. DOI: 10.1016/j.molcel.2020.03.005.

Krautbauer, S.; Büchler, C.; Liebisch, G. (2016): Relevance in the Use of Appropriate Internal Standards for Accurate Quantification Using LC-MS/MS: Tauro-Conjugated Bile Acids as an Example. In *Analytical chemistry* 88 (22), pp. 10957–10961. DOI: 10.1021/acs.analchem.6b02596.

Kübeck, R.; Bonet-Ripoll, C.; Hoffmann, C.; Walker, A.; Müller, V. M.; Schüppel, V. L. et al. (2016): Dietary fat and gut microbiota interactions determine diet-induced obesity in mice. In *Molecular metabolism* 5 (12), pp. 1162–1174. DOI: 10.1016/j.molmet.2016.10.001.

Langmann, T.; Mauerer, R.; Schmitz, G. (2006): Human ATP-binding cassette transporter TaqMan low-density array: analysis of macrophage differentiation and foam cell formation. In *Clinical chemistry* 52 (2), pp. 310–313. DOI: 10.1373/clinchem.2005.059774.

Le Chatelier, E.; Nielsen, T.; Qin, J.; Prifti, E.; Hildebrand, F.; Falony, G. et al. (2013): Richness of human gut microbiome correlates with metabolic markers. In *Nature* 500 (7464), pp. 541–546. DOI: 10.1038/nature12506.

Li, D.; Chen, H.; Mao, B.; Yang, Q.; Zhao, J.; Gu, Z. et al. (2017): Microbial Biogeography and Core Microbiota of the Rat Digestive Tract. In *Scientific reports* 8, p. 45840. DOI: 10.1038/srep45840.

Li, F.; Jiang, C.; Krausz, K. W.; Li, Y.; Albert, I.; Hao, H. et al. (2013): Microbiome remodelling leads to inhibition of intestinal farnesoid X receptor signalling and decreased obesity. In *Nature communications* 4, p. 2384. DOI: 10.1038/ncomms3384.

Li, H.; Herrmann, T.; Seeßle, J.; Liebisch, G.; Merle, U.; Stremmel, W.; Chamulitrat, W. (2022): Role of fatty acid transport protein 4 in metabolic tissues: insights into obesity and fatty liver disease. In *Bioscience reports* 42 (6). DOI: 10.1042/BSR20211854.

Li, J.; Dawson, P. A. (2019): Animal models to study bile acid metabolism. In *Biochimica et biophysica acta. Molecular basis of disease* 1865 (5), pp. 895–911. DOI: 10.1016/j.bbadis.2018.05.011.

Li, J.; Jia, H.; Cai, X.; Zhong, H.; Feng, Q.; Sunagawa, S. et al. (2014): An integrated catalog of reference genes in the human gut microbiome. In *Nature biotechnology* 32 (8), pp. 834–841. DOI: 10.1038/nbt.2942.

Li, R.; Palmiotti, A.; Vries, H. D. de; Hovingh, M. V.; Koehorst, M.; Mulder, N. L. et al. (2021): Low production of 12α-hydroxylated bile acids prevents hepatic steatosis in Cyp2c70-/- mice by reducing fat absorption. In *Journal of lipid research*, p. 100134. DOI: 10.1016/j.jlr.2021.100134.

Li, T.; Jahan, A.; Chiang, J. Y. L. (2006): Bile acids and cytokines inhibit the human cholesterol 7 alpha-hydroxylase gene via the JNK/c-jun pathway in human liver cells. In *Hepatology (Baltimore, Md.)* 43 (6), pp. 1202–1210. DOI: 10.1002/hep.21183.

Liebisch, G.; Drobnik, W.; Reil, M.; Trümbach, B.; Arnecke, R.; Olgemöller, B. et al. (1999): Quantitative measurement of different ceramide species from crude cellular extracts by electrospray ionization tandem mass spectrometry (ESI-MS/MS). In *Journal of lipid research* 40 (8), pp. 1539–1546. DOI: Study.

Liebisch, G.; Fahy, E.; Aoki, J.; Dennis, E. A.; Durand, T.; Ejsing, C. S. et al. (2020): Update on LIPID MAPS classification, nomenclature, and shorthand notation for MS-derived lipid structures. In *Journal of lipid research* 61 (12), pp. 1539–1555. DOI: 10.1194/jlr.S120001025.

Liebisch, G.; Lieser, B.; Rathenberg, J.; Drobnik, W.; Schmitz, G. (2004): High-throughput quantification of phosphatidylcholine and sphingomyelin by electrospray ionization tandem mass spectrometry coupled with isotope correction algorithm. In *Biochimica et biophysica acta* 1686 (1-2), pp. 108–117. DOI: 10.1016/j.bbalip.2004.09.003.

Linthorst, J. M.; Bennett Clark, S.; Holt, P. R. (1977): Triglyceride emulsification by amphipaths present in the intestinal lumen during digestion of fat. In *Journal of colloid and interface science* 60 (1), pp. 1–10. DOI: 10.1016/0021-9797(77)90250-8.

Livak, K. J.; Schmittgen, T. D. (2001): Analysis of relative gene expression data using real-time quantitative PCR and the 2(-Delta Delta C(T)) Method. In *Methods (San Diego, Calif.)* 25 (4), pp. 402–408. DOI: 10.1006/meth.2001.1262.

Lu, T. T.; Makishima, M.; Repa, J. J.; Schoonjans, K.; Kerr, T. A.; Auwerx, J.; Mangelsdorf, D. J. (2000): Molecular Basis for Feedback Regulation of Bile Acid Synthesis by Nuclear Receptors. In *Molecular Cell* 6 (3), pp. 507–515. DOI: 10.1016/S1097-2765(00)00050-2.

Macierzanka, A.; Rigby, N. M.; Corfield, A. P.; Wellner, N.; Böttger, F.; Mills, E. N. C.; Mackie, A. R. (2011): Adsorption of bile salts to particles allows penetration of intestinal mucus. In *Soft Matter* 7 (18), p. 8077. DOI: 10.1039/c1sm05888f.

Mähler Convenor, M.; Berard, M.; Feinstein, R.; Gallagher, A.; Illgen-Wilcke, B.; Pritchett-Corning, K.; Raspa, M. (2014): FELASA recommendations for the health monitoring of mouse, rat, hamster, guinea pig and rabbit colonies in breeding and experimental units. In *Laboratory animals* 48 (3), pp. 178–192. DOI: 10.1177/0023677213516312.

Makishima, M.; Lu, T. T.; Xie, W.; Whitfield, G. K.; Domoto, H.; Evans, R. M. et al. (2002): Vitamin D receptor as an intestinal bile acid sensor. In *Science (New York, N.Y.)* 296 (5571), pp. 1313–1316. DOI: 10.1126/science.1070477.

Makishima, M.; Okamoto, A. Y.; Repa, J. J.; Tu, H.; Learned, R. M.; Luk, A. et al. (1999): Identification of a nuclear receptor for bile acids. In *Science (New York, N.Y.)* 284 (5418), pp. 1362–1365. DOI: 10.1126/science.284.5418.1362.

Makki, K.; Deehan, E. C.; Walter, J.; Bäckhed, F. (2018): The Impact of Dietary Fiber on Gut Microbiota in Host Health and Disease. In *Cell host & microbe* 23 (6), pp. 705–715. DOI: 10.1016/j.chom.2018.05.012.

Mansbach, C. M.; Gorelick, F. (2007): Development and physiological regulation of intestinal lipid absorption. II. Dietary lipid absorption, complex lipid synthesis, and the intracellular packaging and secretion of chylomicrons. In *American journal of physiology. Gastrointestinal and liver physiology* 293 (4), G645-50. DOI: 10.1152/ajpgi.00299.2007.

Martinez-Guryn, K.; Hubert, N.; Frazier, K.; Urlass, S.; Musch, M. W.; Ojeda, P. et al. (2018): Small Intestine Microbiota Regulate Host Digestive and Absorptive Adaptive Responses to Dietary Lipids. In *Cell host & microbe* 23 (4), 458-469.e5. DOI: 10.1016/j.chom.2018.03.011.

Martinez-Guryn, K.; Leone, V.; Chang, E. B. (2019): Regional Diversity of the Gastrointestinal Microbiome. In *Cell host & microbe* 26 (3), pp. 314–324. DOI: 10.1016/j.chom.2019.08.011.

Maruyama, T.; Tanaka, K.; Suzuki, J.; Miyoshi, H.; Harada, N.; Nakamura, T. et al. (2006): Targeted disruption of G protein-coupled bile acid receptor 1 (Gpbar1/M-Bar) in mice. In *The Journal of endocrinology* 191 (1), pp. 197–205. DOI: 10.1677/joe.1.06546.

Matyash, V.; Liebisch, G.; Kurzchalia, T. V.; Shevchenko, A.; Schwudke, D. (2008): Lipid extraction by methyl-tert-butyl ether for high-throughput lipidomics. In *Journal of lipid research* 49 (5), pp. 1137–1146. DOI: 10.1194/jlr.D700041-JLR200.

Megger, D. A.; Padden, J.; Rosowski, K.; Uszkoreit, J.; Bracht, T.; Eisenacher, M. et al. (2017): One Sample, One Shot - Evaluation of sample preparation protocols for the mass spectrometric proteome analysis of human bile fluid without extensive fractionation. In *Journal of proteomics* 154, pp. 13–21. DOI: 10.1016/j.jprot.2016.11.021.

Milger, K.; Herrmann, T.; Becker, C.; Gotthardt, D.; Zickwolf, J.; Ehehalt, R. et al. (2006): Cellular uptake of fatty acids driven by the ER-localized acyl-CoA synthetase FATP4. In *Journal of cell science* 119 (Pt 22), pp. 4678–4688. DOI: 10.1242/jcs.03280.

Miyake, J. H.; Wang, S. L.; Davis, R. A. (2000): Bile acid induction of cytokine expression by macrophages correlates with repression of hepatic cholesterol 7alpha-hydroxylase. In *The Journal of biological chemistry* 275 (29), pp. 21805–21808. DOI: 10.1074/jbc.c000275200.

Miyamoto, J.; Igarashi, M.; Watanabe, K.; Karaki, S.-I.; Mukouyama, H.; Kishino, S. et al. (2019): Gut microbiota confers host resistance to obesity by metabolizing dietary polyunsaturated fatty acids. In *Nature communications* 10 (1), p. 4007. DOI: 10.1038/s41467-019-11978-0.

Molinaro, A.; Wahlström, A.; Marschall, H.-U. (2018): Role of Bile Acids in Metabolic Control. In *Trends in endocrinology and metabolism: TEM* 29 (1), pp. 31–41. DOI: 10.1016/j.tem.2017.11.002.

Morotomi, M.; Guillem, J. G.; LoGerfo, P.; Weinstein, I. B. (1990): Production of diacylglycerol, an activator of protein kinase C, by human intestinal microflora. In *Cancer research* 50 (12), pp. 3595–3599.

Mueller, M.; Thorell, A.; Claudel, T.; Jha, P.; Koefeler, H.; Lackner, C. et al. (2015): Ursodeoxycholic acid exerts farnesoid X receptor-antagonistic effects on bile acid and lipid metabolism in morbid obesity. In *Journal of hepatology* 62 (6), pp. 1398–1404. DOI: 10.1016/j.jhep.2014.12.034.

Nakano, T.; Yanagisawa, J.; Nakayama, F. (1988): Phospholipase activity in human bile. In *Hepatology (Baltimore, Md.)* 8 (6), pp. 1560–1564. DOI: 10.1002/hep.1840080615.

Nassir, F.; Wilson, B.; Han, X.; Gross, R. W.; Abumrad, N. A. (2007): CD36 is important for fatty acid and cholesterol uptake by the proximal but not distal intestine. In *The Journal of biological chemistry* 282 (27), pp. 19493–19501. DOI: 10.1074/jbc.M703330200.

Nauli, A. M.; Nassir, F.; Zheng, S.; Yang, Q.; Lo, C.-M.; Vonlehmden, S. B. et al. (2006): CD36 is important for chylomicron formation and secretion and may mediate cholesterol uptake in the proximal intestine. In *Gastroenterology* 131 (4), pp. 1197–1207. DOI: 10.1053/j.gastro.2006.08.012.

Negi, J. S. (2019): Nanolipid Materials for Drug Delivery Systems. In : Characterization and Biology of Nanomaterials for Drug Delivery: Elsevier, pp. 137–163.

Ocvirk, S.; O'Keefe, S. J. D. (2020): Dietary fat, bile acid metabolism and colorectal cancer. In *Seminars in cancer biology*. DOI: 10.1016/j.semcancer.2020.10.003.

O'Hara, A. M.; Shanahan, F. (2006): The gut flora as a forgotten organ. In *EMBO reports* 7 (7), pp. 688–693. DOI: 10.1038/sj.embor.7400731.

Pan, Y. H.; Bahnson, B. J. (2007): Structural basis for bile salt inhibition of pancreatic phospholipase A2. In *Journal of Molecular Biology* 369 (2), pp. 439–450. DOI: 10.1016/j.jmb.2007.03.034.

Parks, D. J.; Blanchard, S. G.; Bledsoe, R. K.; Chandra, G.; Consler, T. G.; Kliewer, S. A. et al. (1999): Bile acids: natural ligands for an orphan nuclear receptor. In *Science (New York, N.Y.)* 284 (5418), pp. 1365–1368. DOI: 10.1126/science.284.5418.1365.

Parthasarathy, S.; Subbaiah, P. V.; Ganguly, J. (1974): The mechanism of intestinal absorption of phosphatidylcholine in rats. In *The Biochemical journal* 140 (3), pp. 503–508. DOI: 10.1042/bj1400503.

Petersson, J.; Schreiber, O.; Hansson, G. C.; Gendler, S. J.; Velcich, A.; Lundberg, J. O. et al. (2011): Importance and regulation of the colonic mucus barrier in a mouse model of colitis. In *American journal of physiology. Gastrointestinal and liver physiology* 300 (2), G327-33. DOI: 10.1152/ajpgi.00422.2010.

Prescher, M.; Smits, S. H. J.; Schmitt, L. (2020): Stimulation of ABCB4/MDR3 ATPase activity requires an intact phosphatidylcholine lipid. In *Journal of lipid research* 61 (12), pp. 1605–1616. DOI: 10.1194/jlr.RA120000889.

Qin, J.; Li, R.; Raes, J.; Arumugam, M.; Burgdorf, K. S.; Manichanh, C. et al. (2010): A human gut microbial gene catalogue established by metagenomic sequencing. In *Nature* 464 (7285), pp. 59–65. DOI: 10.1038/nature08821.

Rabot, S.; Membrez, M.; Bruneau, A.; Gérard, P.; Harach, T.; Moser, M. et al. (2010): Germ-free C57BL/6J mice are resistant to high-fat-diet-induced insulin resistance and have altered cholesterol metabolism. In *FASEB journal : official publication of the Federation of American Societies for Experimental Biology* 24 (12), pp. 4948–4959. DOI: 10.1096/fj.10-164921.

Rampone, A. J.; Long, L. W. (1977): The effect of phosphatidylcholine and lysophosphatidylcholine on the absorption and mucosal metabolism of oleic acid and cholesterol in vitro. In *Biochimica et biophysica acta* 486 (3), pp. 500–510. DOI: 10.1016/0005-2760(77)90100-x.

Reynier, M. O.; Lafont, H.; Crotte, C.; Sauve, P.; Gerolami, A. (1985): Intestinal cholesterol uptake: comparison between mixed micelles containing lecithin or lysolecithin. In *Lipids* 20 (3), pp. 145–150. DOI: 10.1007/BF02534246.

Ridlon, J. M.; Kang, D.-J.; Hylemon, P. B. (2006): Bile salt biotransformations by human intestinal bacteria. In *Journal of lipid research* 47 (2), pp. 241–259. DOI: 10.1194/jlr.R500013-JLR200.

Sato, H.; Macchiarulo, A.; Thomas, C.; Gioiello, A.; Une, M.; Hofmann, A. F. et al. (2008): Novel potent and selective bile acid derivatives as TGR5 agonists: biological screening, structure-activity relationships, and molecular modeling studies. In *Journal of medicinal chemistry* 51 (6), pp. 1831–1841. DOI: 10.1021/jm7015864.

Sato, H.; Zhang, L. S.; Martinez, K.; Chang, E. B.; Yang, Q.; Wang, F. et al. (2016): Antibiotics Suppress Activation of Intestinal Mucosal Mast Cells and Reduce Dietary Lipid Absorption in Sprague-Dawley Rats. In *Gastroenterology* 151 (5), pp. 923–932. DOI: 10.1053/j.gastro.2016.07.009.

Saunders, D. R.; Sillery, J. (1976): Lecithin inhibits fatty acid and bile salt absorption from rat small intestine in vivo. In *Lipids* 11 (12), pp. 830–832. DOI: 10.1007/bf02532987.

Sayin, S. I.; Wahlström, A.; Felin, J.; Jäntti, S.; Marschall, H.-U.; Bamberg, K. et al. (2013): Gut microbiota regulates bile acid metabolism by reducing the levels of tauro-beta-muricholic acid, a naturally occurring FXR antagonist. In *Cell metabolism* 17 (2), pp. 225–235. DOI: 10.1016/j.cmet.2013.01.003.

Schmidt, D. R.; Holmstrom, S. R.; Fon Tacer, K.; Bookout, A. L.; Kliewer, S. A.; Mangelsdorf, D. J. (2010): Regulation of bile acid synthesis by fat-soluble vitamins A and D. In *The Journal of biological chemistry* 285 (19), pp. 14486–14494. DOI: 10.1074/jbc.M110.116004.

Schwarz, M.; Lund, E. G.; Setchell, K. D.; Kayden, H. J.; Zerwekh, J. E.; Björkhem, I. et al. (1996): Disruption of cholesterol 7alpha-hydroxylase gene in mice. II. Bile acid deficiency is overcome by induction of oxysterol 7alpha-hydroxylase. In *The Journal of biological chemistry* 271 (30), pp. 18024–18031. DOI: 10.1074/jbc.271.30.18024.

Schwarz, M.; Russell, D. W.; Dietschy, J. M.; Turley, S. D. (2001): Alternate pathways of bile acid synthesis in the cholesterol 7alpha-hydroxylase knockout mouse are not upregulated by either cholesterol or cholestyramine feeding. In *Journal of lipid research* 42 (10), pp. 1594–1603.

Seekatz, A. M.; Schnizlein, M. K.; Koenigsknecht, M. J.; Baker, J. R.; Hasler, W. L.; Bleske, B. E. et al. (2019): Spatial and Temporal Analysis of the Stomach and Small-Intestinal Microbiota in Fasted Healthy Humans. In *mSphere* 4 (2). DOI: 10.1128/mSphere.00126-19.

Sekar, R.; Chow, B. K. C. (2014): Secretin receptor-knockout mice are resistant to high-fat diet-induced obesity and exhibit impaired intestinal lipid absorption. In *FASEB journal : official publication of the Federation of American Societies for Experimental Biology* 28 (8), pp. 3494–3505. DOI: 10.1096/fj.13-247536.

Selwyn, F. P.; Csanaky, I. L.; Zhang, Y.; Klaassen, C. D. (2015): Importance of Large Intestine in Regulating Bile Acids and Glucagon-Like Peptide-1 in Germ-Free Mice. In *Drug metabolism and disposition: the biological fate of chemicals* 43 (10), pp. 1544–1556. DOI: 10.1124/dmd.115.065276.

Semova, I.; Carten, J. D.; Stombaugh, J.; Mackey, L. C.; Knight, R.; Farber, S. A.; Rawls, J. F. (2012): Microbiota regulate intestinal absorption and metabolism of fatty acids in the zebrafish. In *Cell host & microbe* 12 (3), pp. 277–288. DOI: 10.1016/j.chom.2012.08.003.

Sender, R.; Fuchs, S.; Milo, R. (2016): Revised Estimates for the Number of Human and Bacteria Cells in the Body. In *PLOS Biology* 14 (8), e1002533. DOI: 10.1371/journal.pbio.1002533.

Shaffer, E. A. (2000): Review article: control of gall-bladder motor function. In *Alimentary pharmacology & therapeutics* 14 Suppl 2, pp. 2–8. DOI: 10.1046/j.1365-2036.2000.014s2002.x.

Shim, J.; Moulson, C. L.; Newberry, E. P.; Lin, M.-H.; Xie, Y.; Kennedy, S. M. et al. (2009): Fatty acid transport protein 4 is dispensable for intestinal lipid absorption in mice. In *Journal of lipid research* 50 (3), pp. 491–500. DOI: 10.1194/jlr.M800400-JLR200.

Shimada, K.; Yanagisawa, J.; Nakayama, F. (1991): Increased lysophosphatidylcholine and pancreatic enzyme content in bile of patients with anomalous pancreaticobiliary ductal junction. In *Hepatology (Baltimore, Md.)* 13 (3), pp. 438–444.

Shoda, J.; Ueda, T.; Ikegami, T.; Matsuzaki, Y.; Satoh, S.; Kano, M. et al. (1997): Increased biliary group II phospholipase A2 and altered gallbladder bile in patients with multiple cholesterol stones. In *Gastroenterology* 112 (6), pp. 2036–2047. DOI: 10.1053/gast.1997.v112.pm9178697.

Sinal, C. J.; Tohkin, M.; Miyata, M.; Ward, J. M.; Lambert, G.; Gonzalez, F. J. (2000): Targeted Disruption of the Nuclear Receptor FXR/BAR Impairs Bile Acid and Lipid Homeostasis. In *Cell* 102 (6), pp. 731–744. DOI: 10.1016/S0092-8674(00)00062-3.

Smit, J.; Schinkel, A. H.; Elferink, R.; Groen, A. K.; Wagenaar, E.; van Deemter, L. et al. (1993): Homozygous disruption of the murine MDR2 P-glycoprotein gene leads to a complete absence of phospholipid from bile and to liver disease. In *Cell* 75 (3), pp. 451–462. DOI: 10.1016/0092-8674(93)90380-9.

Smith, A.; Lough, A. K. (1976): Micellar solubilization of fatty acids in aqueous media containing bile salts and phospholipids. In *British Journal of Nutrition* 35 (1), pp. 77–87. DOI: 10.1079/bjn19760011.

Sohn, W.; Lee, H. W.; Lee, S.; Lim, J. H.; Lee, M. W.; Park, C. H.; Yoon, S. K. (2021): Obesity and the risk of primary liver cancer: A systematic review and meta-analysis. In *Clinical and molecular hepatology* 27 (1), pp. 157–174. DOI: 10.3350/cmh.2020.0176.

Son, K. H.; Ahn, C. B.; Kim, H. J.; Kim, J. S. (2020): Quantitative proteomic analysis of bile in extrahepatic cholangiocarcinoma patients. In *Journal of Cancer* 11 (14), pp. 4073–4080. DOI: 10.7150/jca.40964.

Sonnenburg, J. L.; Bäckhed, F. (2016): Diet-microbiota interactions as moderators of human metabolism. In *Nature* 535 (7610), pp. 56–64. DOI: 10.1038/nature18846.

Stahl, A.; Hirsch, D. J.; Gimeno, R. E.; Punreddy, S.; Ge, P.; Watson, N. et al. (1999): Identification of the Major Intestinal Fatty Acid Transport Protein. In *Molecular Cell* 4 (3), pp. 299–308. DOI: 10.1016/S1097-2765(00)80332-9.

Staudinger, J. L.; Goodwin, B.; Jones, S. A.; Hawkins-Brown, D.; MacKenzie, K. I.; LaTour, A. et al. (2001): The nuclear receptor PXR is a lithocholic acid sensor that protects against liver toxicity. In *Proceedings of the National Academy of Sciences* 98 (6), pp. 3369–3374. DOI: 10.1073/pnas.051551698.

Sticova, E.; Jirsa, M. (2020): ABCB4 disease: Many faces of one gene deficiency. In *Annals of hepatology* 19 (2), pp. 126–133. DOI: 10.1016/j.aohep.2019.09.010.

Studer, N.; Desharnais, L.; Beutler, M.; Brugiroux, S.; Terrazos, M. A.; Menin, L. et al. (2016): Functional Intestinal Bile Acid 7α-Dehydroxylation by Clostridium scindens Associated with Protection from Clostridium difficile Infection in a Gnotobiotic Mouse Model. In *Frontiers in cellular and infection microbiology* 6, p. 191. DOI: 10.3389/fcimb.2016.00191.

Szarka, L. A.; Camilleri, M. (2012): Methods for the assessment of small-bowel and colonic transit. In *Seminars in nuclear medicine* 42 (2), pp. 113–123. DOI: 10.1053/j.semnuclmed.2011.10.004.

Tagesson, C.; Norrby, S.; Sjödahl, R. (1979): The prerequisites for local lysolecithin formation in the human gallbladder. III. Demonstration of two different phospholipase A activities. In *Scandinavian journal of gastroenterology* 14 (3), pp. 379–384. DOI: 10.3109/00365527909179900.

Takahashi, S.; Fukami, T.; Masuo, Y.; Brocker, C. N.; Xie, C.; Krausz, K. W. et al. (2016): Cyp2c70 is responsible for the species difference in bile acid metabolism between mice and humans. In *Journal of lipid research* 57 (12), pp. 2130–2137. DOI: 10.1194/jlr.M071183.

Tazi, A.; Araujo, J. R.; Mulet, C.; Arena, E. T.; Nigro, G.; Pédron, T.; Sansonetti, P. J. (2018): Disentangling Host-Microbiota Regulation of Lipid Secretion by Enterocytes: Insights from Commensals Lactobacillus paracasei and Escherichia coli. In *mBio* 9 (5). DOI: 10.1128/mBio.01493-18.

Thomas, C.; Gioiello, A.; Noriega, L.; Strehle, A.; Oury, J.; Rizzo, G. et al. (2009): TGR5-mediated bile acid sensing controls glucose homeostasis. In *Cell metabolism* 10 (3), pp. 167–177. DOI: 10.1016/j.cmet.2009.08.001.

Tso, P.; Scobey, M. (2018): The Role of Phosphatidylcholine in the Absorption and Transport of Dietary Fat. In Arnis Kuksis (Ed.): Fat absorption. Boca Raton: CRC Press (CRC revivals).

Tyanova, S.; Temu, T.; Sinitcyn, P.; Carlson, A.; Hein, M. Y.; Geiger, T. et al. (2016): The Perseus computational platform for comprehensive analysis of (prote)omics data. In *Nature methods* 13 (9), pp. 731–740. DOI: 10.1038/nmeth.3901.

Uhlén, M.; Fagerberg, L.; Hallström, B. M.; Lindskog, C.; Oksvold, P.; Mardinoglu, A. et al. (2015): Proteomics. Tissue-based map of the human proteome. In *Science (New York, N.Y.)* 347 (6220), p. 1260419. DOI: 10.1126/science.1260419.

UniProt: the universal protein knowledgebase in 2021 (2021). In *Nucleic acids research* 49 (D1), D480-D489.

Velagapudi, V. R.; Hezaveh, R.; Reigstad, C. S.; Gopalacharyulu, P.; Yetukuri, L.; Islam, S. et al. (2010): The gut microbiota modulates host energy and lipid metabolism in mice. In *Journal of lipid research* 51 (5), pp. 1101–1112. DOI: 10.1194/jlr.m002774.

Voshol, P. J.; Minich, D. M.; Havinga, R.; Elferink, R. P.; Verkade, H. J.; Groen, A. K.; Kuipers, F. (2000): Postprandial chylomicron formation and fat absorption in multidrug resistance gene 2 P-glycoprotein–deficient mice. In *Gastroenterology* 118 (1), pp. 173–182. DOI: 10.1016/S0016-5085(00)70426-4.

Wahlström, A.; Sayin, S. I.; Marschall, H.-U.; Bäckhed, F. (2016): Intestinal Crosstalk between Bile Acids and Microbiota and Its Impact on Host Metabolism. In *Cell metabolism* 24 (1), pp. 41–50. DOI: 10.1016/j.cmet.2016.05.005.

Wang, B.; Rong, X.; Duerr, M. A.; Hermanson, D. J.; Hedde, P. N.; Wong, J. S. et al. (2016): Intestinal Phospholipid Remodeling Is Required for Dietary-Lipid Uptake and Survival on a High-Fat Diet. In *Cell metabolism* 23 (3), pp. 492–504. DOI: 10.1016/j.cmet.2016.01.001.

Wang, H.; Chen, J.; Hollister, K.; Sowers, L. C.; Forman, B. M. (1999): Endogenous Bile Acids Are Ligands for the Nuclear Receptor FXR/BAR. In *Molecular Cell* 3 (5), pp. 543–553. DOI: 10.1016/S1097-2765(00)80348-2.

Wang, X.; Wang, C.; Tang, J.; Dyda, F.; Zhang, X. C. (1997): The crystal structure of bovine bile salt activated lipase: insights into the bile salt activation mechanism. In *Structure* 5 (9), pp. 1209–1218. DOI: 10.1016/s0969-2126(97)00271-2.

Wastyk, H. C.; Fragiadakis, G. K.; Perelman, D.; Dahan, D.; Merrill, B. D.; Yu, F. B. et al. (2021): Gut-microbiota-targeted diets modulate human immune status. In *Cell* 184 (16), 4137-4153.e14. DOI: 10.1016/j.cell.2021.06.019.

Watanabe, M.; Houten, S. M.; Mataki, C.; Christoffolete, M. A.; Kim, B. W.; Sato, H. et al. (2006): Bile acids induce energy expenditure by promoting intracellular thyroid hormone activation. In *Nature* 439 (7075), pp. 484–489. DOI: 10.1038/nature04330.

WHO (Ed.) (2021): Obesity and overweight. Available online at https://www.who.int/news-room/fact-sheets/detail/obesity-and-overweight, checked on 11/10/2022.

Wiciński, M.; Gębalski, J.; Gołębiewski, J.; Malinowski, B. (2020): Probiotics for the Treatment of Overweight and Obesity in Humans-A Review of Clinical Trials. In *Microorganisms* 8 (8). DOI: 10.3390/microorganisms8081148.

Wostmann, B. S. (1973): Intestinal bile acids and cholesterol absorption in the germfree rat. In *The Journal of nutrition* 103 (7), pp. 982–990. DOI: 10.1093/jn/103.7.982.

Wyss, M.; Brown, K.; Thomson, C. A.; Koegler, M.; Terra, F.; Fan, V. et al. (2019): Using Precisely Defined in vivo Microbiotas to Understand Microbial Regulation of IgE. In *Frontiers in immunology* 10, p. 3107. DOI: 10.3389/fimmu.2019.03107.

Yoshikado, T.; Takada, T.; Yamamoto, T.; Yamaji, H.; Ito, K.; Santa, T. et al. (2011): Itraconazole-induced cholestasis: involvement of the inhibition of bile canalicular phospholipid translocator MDR3/ABCB4. In *Molecular pharmacology* 79 (2), pp. 241–250. DOI: 10.1124/mol.110.067256.

Zemski Berry, K. A.; Murphy, R. C. (2004): Electrospray ionization tandem mass spectrometry of glycerophosphoethanolamine plasmalogen phospholipids. In *Journal of the American Society for Mass Spectrometry* 15 (10), pp. 1499–1508. DOI: 10.1016/j.jasms.2004.07.009.

Zimmermann, M.; Zimmermann-Kogadeeva, M.; Wegmann, R.; Goodman, A. L. (2019): Separating host and microbiome contributions to drug pharmacokinetics and toxicity. In *Science (New York, N.Y.)* 363 (6427). DOI: 10.1126/science.aat9931.

Zoetendal, E. G.; Raes, J.; van den Bogert, B.; Arumugam, M.; Booijink, C. C. G. M.; Troost, F. J. et al. (2012): The human small intestinal microbiota is driven by rapid uptake and conversion of simple carbohydrates. In *The ISME journal* 6 (7), pp. 1415–1426. DOI: 10.1038/ismej.2011.212.

6. SUPPLEMENTAL INFORMATION

Supplemental Table 1. Compartment volume estimates for the physiology-based kinetic multi-compartment modeling.

Tissue	GF	OMM[12]	SPF
Duodenum	200	200	100
Jejunum	500	500	300
Ileum	500	500	300
Colon	150	150	150
Plasma	2000	2000	2000
eWAT	5000	5000	5000
iWAT	5000	5000	5000
Liver	1000	1000	1000
Content_duodenum	1	1	1
Content_jejunum	1	1	1
Content_ileum	1	1	1
Content_colon	1	1	1

Supplemental Table 2. Abbreviations for bile acids used in this thesis

Abbreviation	Full Name
αMCA	α-Muricholic acid
β/ωMCA	β/ω-Muricholic acid
TαMCA	Tauro-α-muricholic acid
Tβ/ωMCA	Tauro-β/ω-muricholic acid
GαMCA	Glyco-α-muricholic acid
Gβ/ωMCA	Glyco-β/ω-muricholic acid
UDCA	Ursodeoxycholic acid
HDCA	Hyodeoxycholic acid
GUDCA	Glycoursodeoxycholic acid
GHDCA	Glycohyodeoxycholic acid
TUDCA	Tauroursodeoxycholic acid
THDCA	Taurohyodeoxycholic acid
γMCA	γ-Muricholic acid (Hyocholic acid)
TγMCA	Tauro-γ-muricholic acid (Taurohyocholic acid)
GγMCA	Glyco-γ-muricholic acid (Glycohyocholic acid)
CA	Cholic acid
GCA	Glycocholic acid
TCA	Taurocholic acid
CDCA	Chenodeoxycholic acid
DCA	Deoxycholic acid
GCDCA	Glycochenodeoxycholic acid
GDCA	Glycodeoxycholic acid
TCDCA	Taurochenodeoxycholic acid
TDCA	Taurodeoxycholic acid
GLCA	Glycolithocholic acid
TLCA	Taurolithocholic acid
LCA	Lithocholic acid
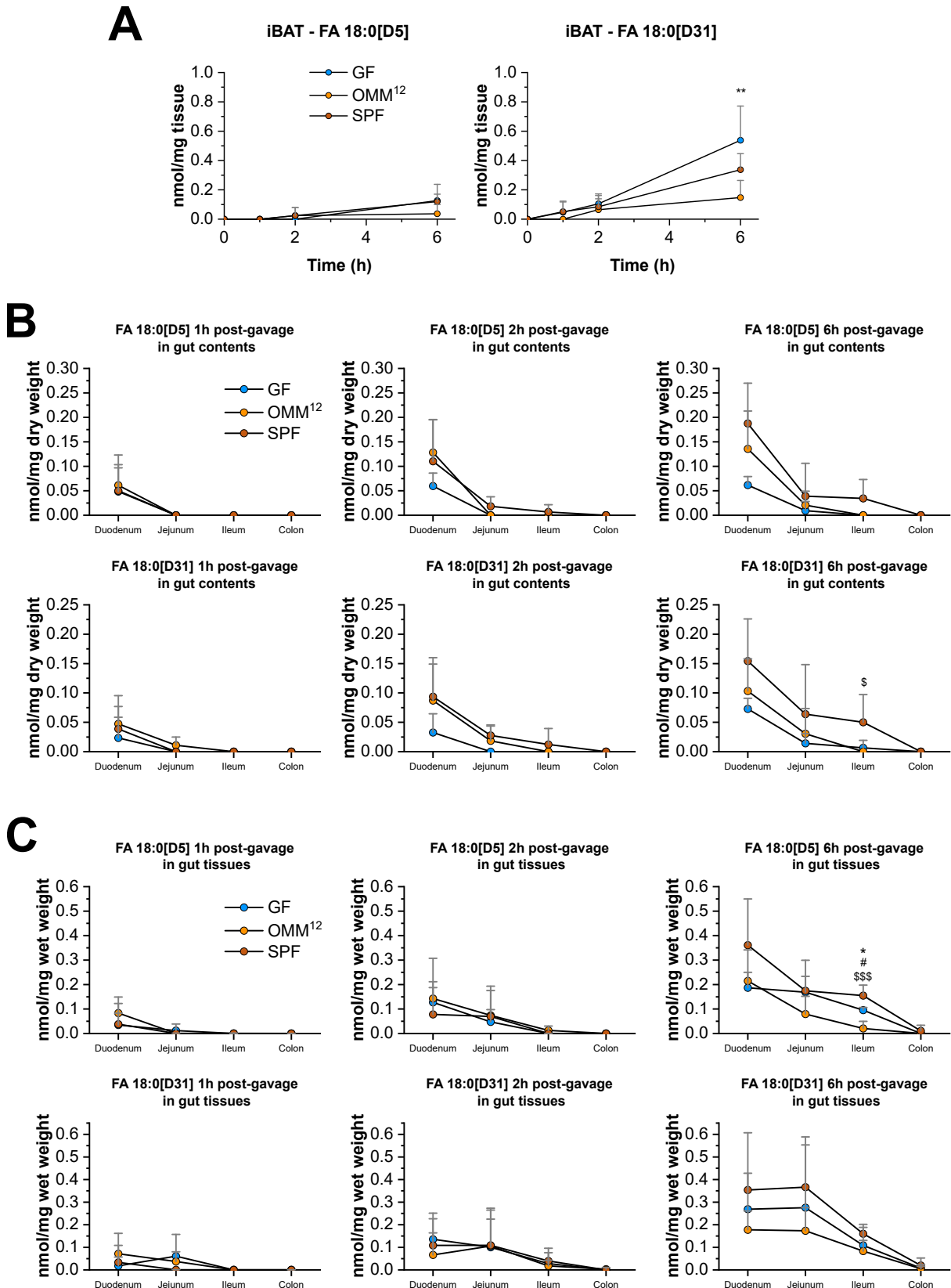
Supplemental Figure 1. Elongated FA 18:0[D5/31] detected in iBAT, intestinal contents and tissues after the oral lipid gavage

Concentrations of FA 18:0[D5] and FA 18:0[D31] in iBAT (A), intestinal contents (B) and intestinal tissues (C) at 1, 2, and 6 h post-gavage. Data are shown as mean ± SD of n = 4–5 per time point or gut section. */#/$$p < 0.05$, **/##/$$$$p < 0.01$, ***/###/$$$$$p < 0.001$ after one-way ANOVA with Tukey post-hoc test. * GF vs. OMM[12], # GF vs. SPF, $ OMM[12] vs. SPF.
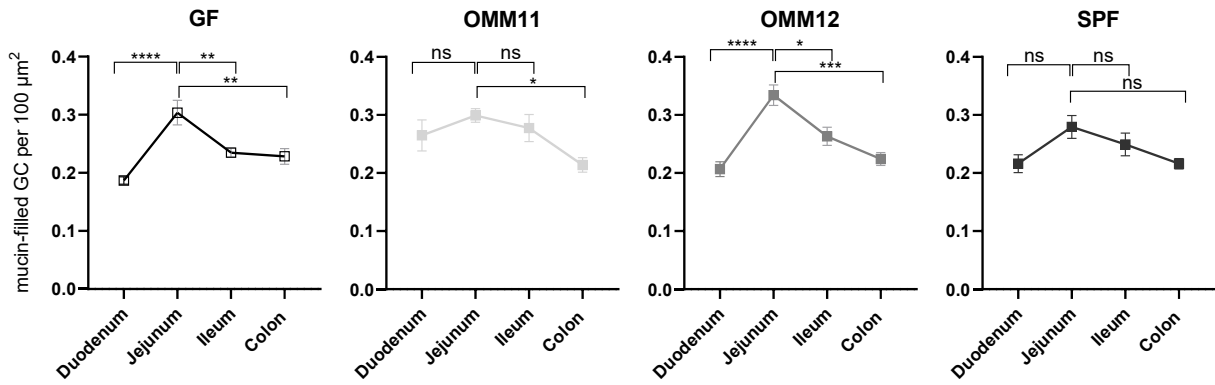
Supplemental Figure 2. Longitudinal analysis of mucin-filled goblet cells along the GIT
Data are shown as mean ± SD of n = 6. ns not significant, $*p < 0.05$, $**p < 0.01$, $***p < 0.001$, $****p < 0.0001$ after one-way ANOVA with Tukey post-hoc test.
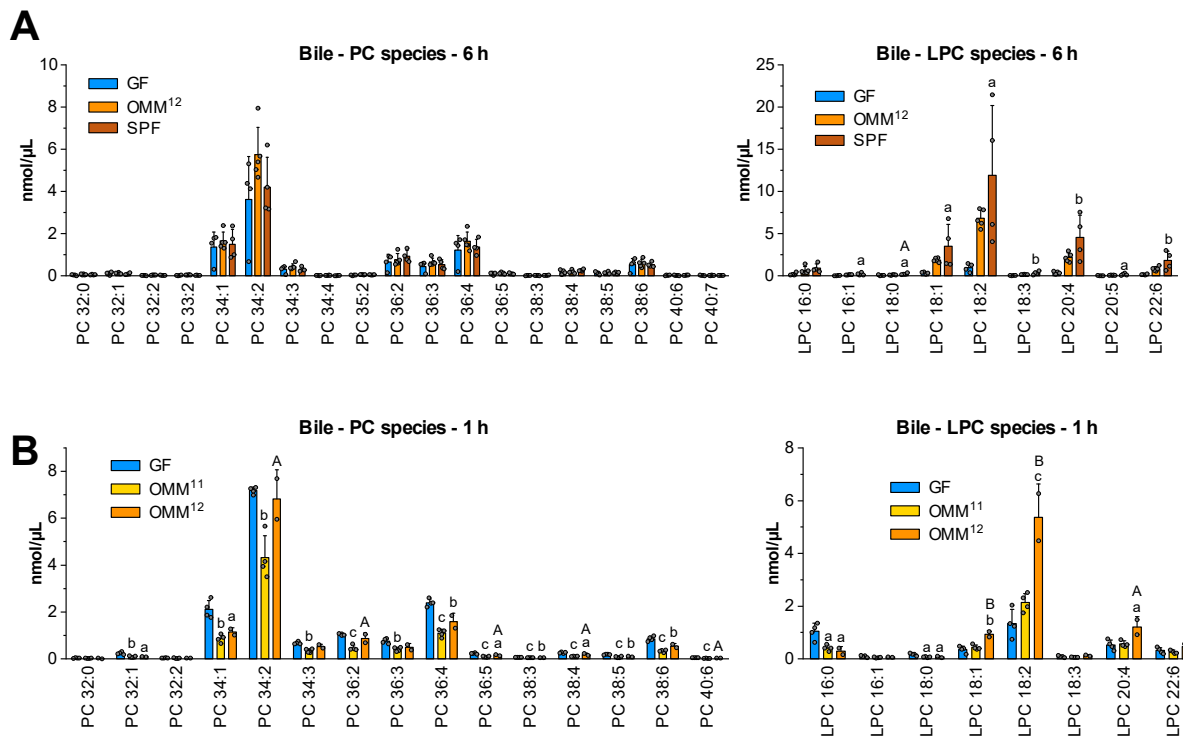
Supplemental Figure 3. PC and LPC species composition of GF, OMM[11], OMM[12] and SPF mouse bile
(A) PC and LPC species in bile of GF, OMM[12] and SPF mice at 6 h post-gavage of the labeled lipids. Data are shown as mean ± SD of n = 4–5. a/A $p < 0.05$, b/B $p < 0.01$ after one-way ANOVA with Tukey post-hoc test and Benjamini-Hochberg FDR correction. a, b significant vs. GF, A, B significant vs. OMM[12].
(B) PC and LPC species in bile of GF, OMM[11] and OMM[12] mice at 1 h post-gavage of the labeled lipids. Data are shown as mean ± SD of n = 2–4. a/A $p < 0.05$, b/B $p < 0.01$, c/C $p < 0.001$ after one-way ANOVA with Tukey post-hoc test and Benjamini-Hochberg FDR correction. a, b, c significant vs. GF, A, B, C significant vs. OMM[11].
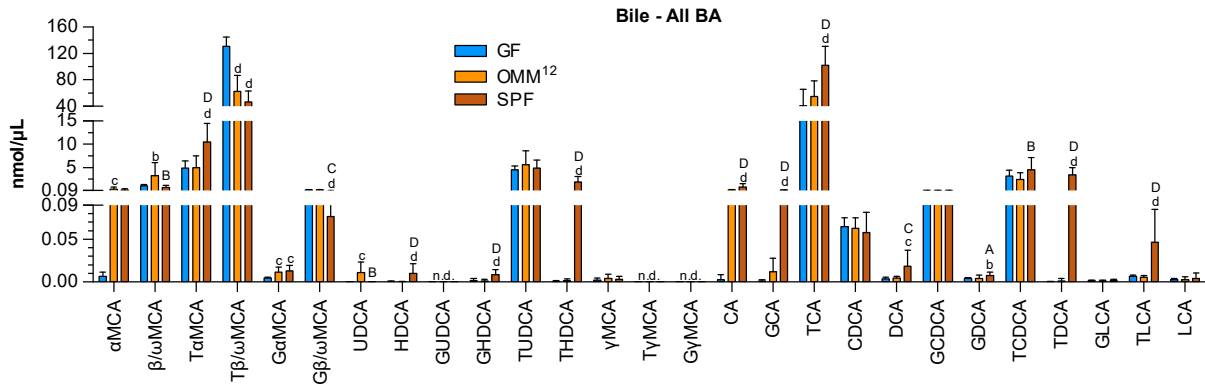
Supplemental Figure 4. All BA detected in bile from GF, OMM12 and SPF mice
Concentrations of all detected bile acids in GF, OMM[12] and SPF mouse bile. Data are shown as mean ± SD of n = 11–20. a/A $p < 0.05$, b/B $p < 0.01$, c/C $p < 0.001$, d/D $p < 0.0001$ after one-way ANOVA with Tukey post-hoc test and Benjamini-Hochberg FDR correction. SPF vs. GF (a, b, c, d) or OMM[12] (A, B, C, D). n.d. = not detected. For full names of BA see Supplemental Table 2.
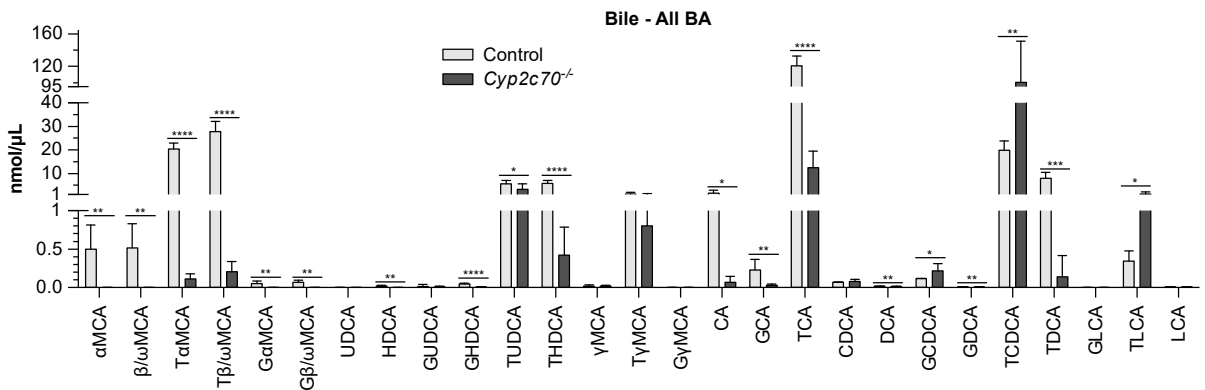
Supplemental Figure 5. All BA detected in bile from *Cyp2c70*^{-/-} and control mice
Concentrations of all detected bile acids in *Cyp2c70*^{-/-} and control mouse bile. Data are shown as mean ± SD of n=8–9. *$p < 0.05$, **$p < 0.01$, ***$p < 0.001$, ****$p < 0.0001$ after two-sided t-test with unequal variance and Benjamini-Hochberg FDR correction. For full names of BA see Supplemental Table 2.
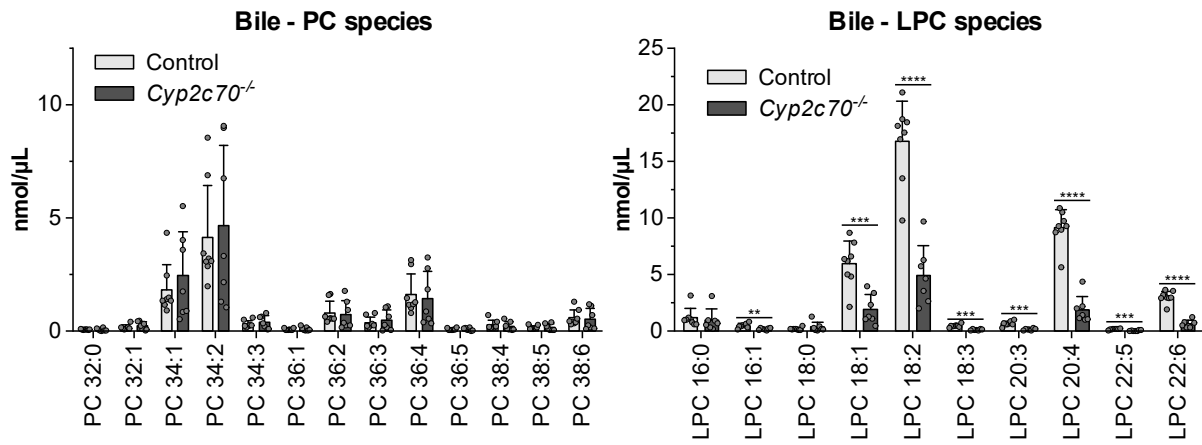
Supplemental Figure 6. PC and LPC species composition of *Cyp2c70*$^{-/-}$ and control bile
PC and LPC species in bile of *Cyp2c70*$^{-/-}$ mice and controls. Data are shown as mean ± SD of n = 7–8. *p < 0.05, **p < 0.01, ***p < 0.001, ****p < 0.0001 after two-sided t-test with unequal variance and Benjamini-Hochberg FDR correction.

7. ACKNOWLEDGEMENTS